Mitochondrial Morphology Dynamics

during Apoptosis

-An integrative modeling approach-

June 2011

Yara Melo Mendes dos Reis

Dissertation
submitted to the
Combined Faculties for the Natural Sciences and Mathematics
of the Ruperto-Carola University of Heidelberg, Germany
for the degree of
Doctor of Natural Sciences

Dissertation Referees:
Prof. Dr. Roland Eils
PD Dr. Anne Régnier-Vigouroux

Written and presented by,
Dipl. Biochem. Yara Melo Mendes dos Reis
born in Maputo, Mozambique
Oral Examination: 27.07.2011

Parts of this thesis have been compiled into a paper submitted to PLoS ONE Journal (positive revision, under re-submission): "**Reis, Y**, Bernardo, M, Richter, D, Wolf, T, Brors, B, Hamacher-Brady, A, Eils, R, Brady, N (2011) Integrative Modeling of Heterogeneous Datasets to Explore Mitochondrial Morphological and Functional Relationships during Apoptosis."

The work presented in this thesis was carried out in the Division of Professor Dr. Roland Eils, Applied Systems Biology at the German Cancer Research Center (DKFZ) in Heidelberg, from September 2007 to March 2011. Professor Dr. Roland Eils and Dr. Nathan Brady closely supervised the establishment and development of the project. This work was supported through the SBCancer within the Helmholtz Alliance on Systems Biology funded by the Initiative and Networking Fund of the Helmholtz Association.

Acknowledgments

For this dissertation I would like to thank my thesis advisor committee members: PD Dr. Anne Régnier-Vigouroux and Dr. Holger Erfle, for their time, interest, and helpful comments. I would also like to thank the other two members of my oral defense committee, Dr. Vytaute Starkuviene-Erfle and PD Dr. Karsten Rippe for their time and insightful questions.

I would like to sincerely thank Prof. Dr. Roland Eils, not only for granting me the opportunity to be part of his research, but also for all the extra and precious opportunities to learn, teach and become a better scientist.

I would like to show my gratitude to Dr. Nathan Brady for all I have learned from him, for his close supervision, constructive criticism and unquestionable availability in every step of the way.

I will always remember Dr. Anne Hamacher-Brady for her significant contributions, of time and ideas, which made my PhD experience productive and stimulating.

I am indebted to my many of my colleagues and friends whose encouragement, guidance and support from the initial to the final level made this PhD possible. Namely, Marti Bernardo Faura, Daniela Richter, Phillip Hundeshagen, Sven Mesecke, Mirjam Dubbert, Ana Stelkic, Johanna Roostalu, Joel Beaudouin, Johanna Berndt, Clarissa Liesche, Thomas Wolf, Manuela Schäfer, Corinna Sprengart, Stephan Hegge, Jürgen Reymann, Michaela Reichenzeller, Leo Neumann, Sabine Aschenbrenner, Juergen Beneke, Nina Beil, Barbara Janssens, Freddy Frischknecht, Markus Meissner, Aina Martin Valls and Eduardo César.

Finally, behind every good thesis stands a strong support network of family, friends and colleagues. I specially thank my family for encouraging me and allowing me to go away and write my own story. I thank all my friends for being there and for listening to my non-problems with the utmost attention. So many people supported me during the last years in so many ways and I thank every single one of them with all my heart. I particularly would like to thank Stefan Hengl, Ana Melo, Monika and Dieter Hengl.

SUMMARY

Mitochondria are central to many important cellular functions. The entire mitochondrial population is in constant flux, driven by continuous fusion and division of mitochondria. Defects in mitochondrial dynamics can cause deficits in mitochondrial respiration, morphology and motility leading to apoptosis under extreme conditions. An important and still unresolved question is how the heterogeneity of mitochondrial morphology, distribution and function are mechanistically realized in the cell. Importantly, to what extent is mitochondrial morphology dependent or affects cell fate decisions. Despite the intense focus on unraveling connections between mitochondrial morphology and severe human pathologies, the analysis and systematic description of mitochondrial phenotypes remains an open challenge. Current approaches to study mitochondrial morphology are limited by low data sampling coupled to manual identification and simplistic classification of complex morphological phenotypes.

The overall goal of this work was to elucidate the nature of the relationship between mitochondria morphology and apoptotic events. Diverse apoptotic triggers were systematically tested and data concerning mitochondrial phenotypes and injury was collected to infer cause and consequence relationships. Therefore, high-resolution fluorescence imaging was employed to extract high-content information essential to identify and quantify spatial and conformational events in the single cell. These included monitoring of mitochondrial membrane permeability and quantification of Bax activation under matched conditions to assess mitochondrial stress.

Experimentally, mitochondrial morphological transitions were followed in human breast carcinoma MCF-7 cells by tagging a mitochondrial inner membrane protein with a fluorescent probe. We made use of apoptotic conditions that have been previously reported to cause mitochondrial fragmentation or swelling. Wide field microscopy allowed for the collection of images containing cells with mostly networked, fragmented or swollen mitochondria. Next, image analysis was performed to extract several mitochondrial features that better characterize each class. These were grouped and used to build a decision tree-based classifier that automatically classifies individual mitochondria into the correspondent phenotypic class. Our population-based classifier accounts for intracellular sub-classes, intermediate mitochondrial stages and reproduces intercellular variances with high accuracy.

Our results show that distinct apoptotic stimuli lead to subtle but significant differences in mitochondrial morphology within cell population that can be specific to a particular insult. Interestingly, there was no direct relation between the induced-mitochondrial classes and the analyzed apoptotic steps. In fact, some apoptotic drugs, which are known to cause similar mitochondrial

damage, showed distinct mitochondrial morphology. Therefore, the observed heterogeneous response of mitochondria to stress strongly suggests that more complex, non-linear interactions exist.

Here, we propose an integrated mechanistic and data-driven modeling approach to analyze heterogeneously quantified datasets and infer hierarchical interactions between mitochondrial morphology and apoptotic events. Our modeling results suggest that Bax activation leads to mitochondrial fragmentation, which is strongly associated with mitochondrial membrane depolarization events. In turn, the loss of mitochondrial membrane potential is closely related to mitochondrial swelling. Our model predictions are in accordance with previous published results and thereby validate our modeling approach that can now be easily extended to include new datasets.

Surprisingly, mitochondrial fragmentation was not the most prominent phenotype, even under conditions where Bax activation was considerably high. Instead, swollen-mitochondria seem to be closer related to mitochondrial-associated death pathways. Next steps include the extension of our pipeline in a time-resolved manner and combined datasets acquisition in order to further investigate this hypothesis.

In summary, we have established and validated a platform for mitochondrial morphological and functional analysis that offers results in an unbiased, systematic and statistically relevant manner. We believe the developed platform is suitable to be extensively used in the investigation of specific molecular targets. Possible applications include RNAi screens (e.g. morphology proteins) or extended compound libraries in a high-throughput mode. Importantly, it can now be further adjusted to other studies relevant to mitochondrial programmed cell death that will hopefully lead into the better understanding of mitochondrial role in physiology and disease progression.

ZUSAMMENFASSUNG

Mitochondrien sind für viele wichtige Zellfunktionen wesentlich. Durch ständige Verschmelzungen und Teilungen der Mitochondrien unterliegt die Gesamtpopulation der Mitochondrien einer andauernden Veränderung. Eine eingeschränkte Dynamik der Mitochondrien kann zu Defiziten bei der Zellatmung, der Morphologie und der Beweglichkeit führen, welche unter Umständen wiederum den Zelltod zur Folge haben können.

Eine wichtige und bisher unbeantwortete Frage ist, wie die Vielfalt und Verschiedenartigkeit der mitochondrialen Morphologie mechanisch in den Zellen verwirklicht wird. Besonders relevant ist die Frage, in welchem Ausmaß die mitochondriale Morphologie abhängig oder sogar ausschlaggebend für das Schicksal der Zelle ist. Neben der Beantwortung der Frage, welche Beziehungen zwischen der Morphologie der Mitochondrien und menschlichen Pathologien bestehen, ist die systematische Erfassung und Analyse der notwendigen Daten eine Herausforderung. Ein Problem aktueller Methoden ist die ungenügende Menge an Daten und somit deren lediglich qualitative Analyse. Auf der anderen Seite ist eine manuelle Klassifizierung und Auswertung komplexer Daten aufwendig und möglicherweise nicht objektiv genug, um aussagekräftige, quantitative Daten zu erhalten.

Das Hauptziel dieser Arbeit ist, die Beziehungen von der mitochondrialen Morphologie zu Apoptose aufzuzeigen. Dazu wurden einerseits Veränderungen in der Morphologie, andereseits Veränderungen der Integrität der Mitochondrien unter verschiedenen Apoptose-auslösenden Substanzen systematisch untersucht. Mit Hilfe von hochauflösender Fluoreszenzmikroskopie konnten quantitative Daten über die räumlichen Lage und Konformation der Mitochondrien in einzelnen Zellen erhalten werden. Um die Integrität der Mitochondrien unter verschiedenen Bedingungen zu bestimmen, wurde deren Permeabilität sowie Aktivierung von Bax gemessen.

Für die Studie wurde die Mammakarzinom-Zellinie MCF-7 verwendet und deren Mitochondrien mit Hilfe eines fluoreszenz-markierten Proteins visualisiert, das in der inneren Mitochondrien-Membran lokalisiert ist. Um die Zellen zu stimulieren, wurden Substanzen verwendet, von denen berichtet ist, dass sie mitochondriale Zertrümmerungen oder Schwellungen verursachen.

Mit Hilfe der Weitfeld-Mikroskopie wurden Zellen aufgenommen, die vernetzte, zertrümmerte oder geschwollenen Mitochondrien aufwiesen. Dann wurden mit Hilfe von Bildverarbeitung Strukturen ermittelt, die eine klare Klassifizierung der verschiedenen Phänotypen ermöglichen. Aus diesen Gruppierungen wurde ein Stammbaum gebildet, der als Sortierwerkzeug automatisch jedes individuelle Mitochondrium dem entsprechenden, korrespondierenden Phänotyp zuweist. Diese Möglichkeit der Sortierung auf der Grundlage der ganzen Mitochondrien-Population bezieht sich

ebenfalls auf interzelluläre Untergruppen sowie mitochondriale Zwischenstadien und reproduziert interzellulare Varianten mit exakter Präzision. Die Ergebnisse zeigen, dass die Morphologie der Mitochondrien in MCF-7 Zellen einen feinen, aber signifikanten Unterschied aufweisen, wenn sie deutlichen apoptischen Stimulationen ausgesetzt sind, und zwar innerhalb einer Zellpopulation, die für bestimmte Substanzen spezifisch sind. Interessanter Weise gibt es keinen direkten Zusammenhang zwischen den induzierten mitochondrialen Klassen und dem Ablauf der Apoptose. Tatsächlich zeigen manche apoptotische Substanzen, die dafür bekannt sind, ähnliche mitochondriale Schäden hervorzurufen, deutlich unterschiedliche Morphologien. Die beobachtete, heterogene Reaktion der Mitochondrien gegenüber Stress lassen auf komplexe nicht-lineare Interaktionen schließen.

Der von uns vorgeschlagene datenorientierte Modellierungsansatz analysiert heterogene Datensätze und leitet daraus hierarchische Interaktionen zwischen der mitochondrialen Morphologie und Apoptose ab. Die Ergebnisse der Modellierung lassen vermuten, dass Bax Aktivität zur Fragmentierung und Depolarisierung von Mitochondrien führt. Der Verlust des mitochondrialen Membran-Potentials ist wiederum eng mit dem Anschwellen der Mitochondrien verknüpft. Die Aussagen unseres Modells stimmen mit den Ergebnissen von anderen, neuen Publikationen überein und bestätigen den Modellierungsansatz, welcher leicht erweitert werden kann, um neue Datensätze auszuwerten.

Überraschenderweise war Fragmentierung von Mitochondrien nicht der bedeutendste Phänotyp, selbst unter Umständen, in denen die Bax Aktivität ausgesprochen hoch waren. Die Ergebnisse zeigen stattdessen einen engen Zusammenhang geschwollener Mitochondrien zum Mitochondrien-abhängigen Zelltod. Weitere Schritte schließen die Aufnahme zeitlich nah aufgelöste Bilder lebender Zellen und deren Strukturen ein und den damit verbundenen Ausbau des Arbeitsablaufs, sowie die Integrierung neuer Datensätze, um die Hypothesen weiter zu untersuchen.

Es wurde eine Methode für die objektive Analyse der mitochondrialen Morphologie entwickelt und getestet, die statistisch aussagekräftige Ergebnisse aus systematisch durchgeführten Experimenten geliefert hat. Wir glauben, dass diese entwickelte Plattform sehr gut dazu geeignet ist, um bei der Erforschung spezifischer sogenannter molekularer targets eingesetzt zu werden. Dabei könnten RNAi-screens oder sogenannte chemical libraries hier Anwendung finden, da unsere Methode die Analyse der Daten im Hochdurchsatzverfahren erlaubt. Somit könnten Studien adaptiert werden, die zum Verständnis der Funktion von Mitochondrien in Krankheitsverläufen beitragen.

Table of Contents

List of Figures

List of Tables

Equations

List of Abbreviations

3D	Three-dimensional (X/Y/Z)
4D	Four-dimensional (X/Y/Z- time)
ADOA	Autosomal-dominant optic atrophy
ADP	Adenosine diphosphate
AIF	Apoptosis inducing factor
AMPK	5' adenosine monophosphate-activated protein kinase
ANT	Adenine nucleotide translocase
Apaf1	Apoptotic protease activator factor 1
ATP	Adenosine triphosphate
BA	Bongkrekic acid
Bad	Bcl-2-associated agonist of cell death
BAK	Bcl-2-antagonist/killer-1
BAX	Bcl-2-associated X protein
Bcl-2	B-cell lymphoma 2
Bcl-XL	B-cell leukemia/lymphoma XL
BD	Binding Domain
BH3	Bcl-2 homology domain 3
BID	BH3-interacting domain death agonist
Bim	Bcl-2-like protein 11
Bok	Bcl-2-related ovarian killer
BOP	BH3-only proteins
BSS	Balanced salt solution (Krebs Henseleit)
Ca^{2+}	Calcium
Caf4	Chromatin assembly factor 4
CaMKIα	Ca^{2+}/calmodulin- dependent protein kinase Iα
CCCP	Carbonyl cyanide m-chlorophenyl hydrazone
CCD	CCD- Charge coupled device
CMT-2A	Charcot-Marie-Tooth syndrome type 2A
COS	CV-1 (simian) in origin and carrying the SV40 genetic material
COXIV	Cytochrome c oxidase IV
CP	CellProfiler
CsA	Cyclosporin A
Cy5	Cyanine 5
Cyclo D	Cyclophilin D
DCF	Dichlorodihydrofluorescein
DEC	Deconvolution
DISC	Death inducing signaling complex
DMEM	Dulbecco's modified eagle medium
Dnm1p	Dynamin-related GTPase 1 protein
DOM	Degree of membership
DR	Death receptor
DRP1	Dynamin related protein 1

DVRT	Deltavision real time
EM	Electron microscopy
ER	Endoplasmic reticulum
ETC	Electron transport chain
`F´	Fragmented
FADD	Fas-associated death domain
FADH2	Flavin adenine dinucleotide H2
FIS1	Mitochondrial fission 1
FL	Fuzzy logic
FLS	Fuzzy logic system
FM	Full medium
FRET	Fluorescence resonance energy transfer
G418	Geneticin 418
GDAP1	Ganglioside-induced differentiation-associated protein
GED	GTPase effector domain
GFP	Green fluorescent protein
GTP	Guanosine triphosphate
H^+	Proton
HeLa	Cervical cancer cells taken from Henrietta Lacks
HL-1	Atrial derived cardiac cell line
HSG	Hyperplasia suppressor gene
HSP60	Heat shock protein 60
kDa	Kilo dalton
LC3	Microtubule-associated protein light chain 3
MARCHV	Membrane-associated RING-CH protein V
MARF	Mitochondrial assembly regulatory factor
MCF-7	Michigan Cancer Foundation - 7
Mcl-1	Myeloid cell leukemia sequence 1
MDA	Mean decrease in accuracy
Mdivi	Mitochondrial division inhibitor
MF	Membership function
MFN2	Mitofusin 2
mito	Mitochondria
mM	mill-molar (mmol/L)
MMP	Mitochondrial membrane permeability
MOMP	Mitochondria outer membrane permeabilization
MPT	Mitochondrial permeability transition
MPTP	Mitochondrial permeability transition pore
mtDNA	Mitochondrial deoxyribonucleic acid
`N´	Networked
N.A.	Numerical aperture
NADH	Nicotinamide adenine dinucleotide H^+
ND	NADH dehydrogenase subunit
NN	Neural network
OOB	Out of the bag error
OPA1	Optic atrophy type
PBS	Phosphate buffered saline
PCA	Principal component analysis

PCD	Programmed cell death
PEG	Polyethylene glycol
PINK1	PTEN-induced putative kinase 1
PKA	Protein kinase A
PLSR	Partial least-squares regression
RF	Random forest
RGB	Red, green and blue
RMSE	Root mean squared error
RNA	Ribonucleic acid
RNAi	RNA interference
ROI	Region of interest
ROS	Reactive oxygen species
RT	Room temperature
`S´	Swollen
s.e.m.	Standard error of the mean
SENP5	Sentrin/SUMO- specific protease
SISO	Single input single output
SOD1	Superoxide dismutase 1
STED	Stimulated emission depletion
SUMO	Small ubiquitin-like modifier
tBid	Truncated Bid
TEM	Transmission electron microscopy
TMRE	Tetramethylrhodamine ethyl ester
TMRM	Tetramethylrhodamine methyl ester
TNFα	Tumor necrosis factor- alpha
TNFR	TNF receptor
TPR	Tetratrico-peptide repeats
TRADD	TNFR-associated death domain
TRAIL	Tumor necrosis factor related apoptosis inducing ligand
Ubc9	Ubiquitin-conjugating enzyme E2I
UCP1	Uncoupling protein1
VDAC	Voltage dependent anion channel
VSMC	Vascular smooth muscle cells
WFM	Widefield microscopy
wt	Wild type
YFP	Yellow fluorescent protein
$\Delta\Psi_m$	Mitochondrial transmembrane potential
µM	micro-molar (µmol/L)

I-INTRODUCTION

I-1. Mitochondria- the versatile cell component.

Mitochondria are dynamic organelles that move, fuse and divide and can appear as a network of elongated and interconnected filaments, as small, fragmented units, or as a combination of both. The length and interconnectivity of mitochondria is a result of the balance between fusion and fission reactions (Sesaki and Jensen 1999; Legros, Lombes et al. 2002). Mitochondria undergo major morphological changes during the cell cycle (Mitra, Wunder et al. 2009), fragment massively in apoptotic cells (Arnoult 2007), become highly elongated in senescent cells and elongate through hyperfusion upon selective stresses (Tondera, Grandemange et al. 2009). Evidence is accumulating that these morphological changes are not merely secondary consequences, but actively participate in cell decisions (Cho, Nakamura et al. 2010; Kane and Youle 2010; Ong and Hausenloy 2010).

I-1.1. Mitochondrial structure.

The number of mitochondria varies widely by organism and tissue type. Many cells have only a single mitochondrion, whereas others can contain several thousand mitochondria (Lodish, Berk et al. 2008). Likewise, mitochondria dimensions change during the cell cycle (Kennady, Ormerod et al. 2004) and vary considerably in shape and size. One mitochondrion can range from 2-10 µm length in different species (Lodish, Berk et al. 2008).

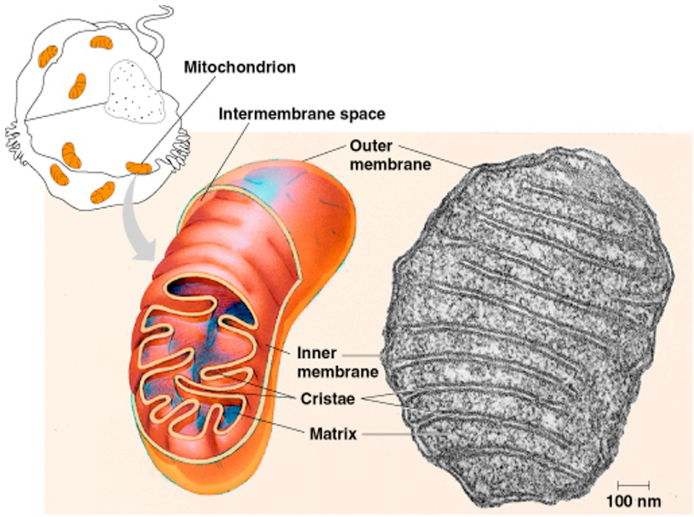

Figure I- 1. **Mitochondrial basic structure.** On the left side, the image shows a cartoon scheme of mitochondria and its compartments and on the right side an electron microscopy (EM) image of a single mitochondrion. (Figure is publically available at: http://www.yellowtang.org/cells.php).

Nevertheless, all mitochondria have a common basic structure (Figure I-1). The organelle is composed of compartments that carry out specialized functions. These compartments or regions include the outer membrane, the intermembrane space, the inner membrane, the cristae and matrix (Figure I- 1). Studies have demonstrated that, in average, the cristae junction diameters are of approximately 28 nm and the distance across the outer membrane and inner boundary membrane is of 20 nm (intermembrane space) (Sjoestrand 1963; Frey and Mannella 2000; Nicastro 2000; Frey, Renken et al. 2002). In contact sites, the space between membranes can be reduced to 14 nm. This corresponds to double the thickness observed for single membranes, with no resolved space between them, making mitochondrial imaging an experimental challenge.

a) Outer membrane.

The outer membrane is smooth unlike the inner membrane and has almost the same amount of phospholipids as proteins. It contains numerous integral proteins called porins, which present a relatively large internal channel (about 2-3 nm) that is permeable to all molecules up to 5000 Da (e.g. nutrient molecules, ions, ATP and ADP molecules). One example is the voltage dependent anion channel (VDAC) that behaves as a general diffusion pore for small hydrophilic molecules (Colombini 1979; Crompton 1999).

b) Inner membrane.

The inner membrane is more complex in structure than the outer membrane. It has numerous invaginations, termed 'cristae' and contains the electron transport chain (ETC) components. ETC complexes are responsible for electron transfer between an electron donor (such as NADH) and an electron acceptor (such as O_2) and for the transfer of protons (H^+ ions) across the membrane. The resulting electrochemical proton gradient is used to generate chemical energy in the form of adenosine triphosphate (ATP). It contains one of the most abundant mitochondrial proteins, the adenine nucleotide translocase (ANT) responsible for the exchange of adenine nucleotide (ADP) across the inner membrane (Halestrap and Brenner 2003).

c) Matrix.

The matrix is a complex mixture of enzymes that are important for the Krebs cycle. A cycle of reactions catalyzed by enzymes in which pyruvate, derived from nutrients and converted to acetyl coenzyme A, is completely oxidized and broken down into carbon dioxide and water to produce high-energy phosphate compounds, the source of cellular energy. It is also where the mitochondrial DNA is

located. Due to their independence from the nuclear DNA and similarities with bacteria, it is believed that mitochondria have originated from bacteria by endosymbiosis (for review see (Gray, Burger et al. 2001)). Among other processes, mitochondria contain their own independent machinery for protein synthesis, including DNA, messenger and transfer RNAs, and ribosomes (McBride, Neuspiel et al. 2006). In particular, it contains cyclophilin D (Cyclo D), a component of the mitochondrial permeability transition pore (MPTP) (Kieffer, Thalhammere et al. 1992).

I-1.2. Multiple functions of mitochondria in the cell.

I-1.2.1. Physiological roles.

a) Oxidative phosphorylation.

The most important function of the mitochondria is to produce energy by a process known as oxidative phosphorylation (for review see (Speakman 2003)). Electrons originating from nutrients are carried to the electron transport chain by NADH and FADH2 and then transferred along a series of carrier molecules in the inner mitochondrial membrane (complexes I to V). This results in the extrusion of protons (H^+) from the matrix across the inner mitochondrial membrane into the mitochondrial intermembrane space. During the redox reactions of complexes I, III, and IV, protons are translocated across the inner mitochondrial membrane to the intermembrane space, generating an electrochemical proton gradient that is expressed largely as a membrane potential of the order of 150-200 mV negative to the cytosol. That potential, usually referred to as $\Delta\Psi_m$ ("delta psi"), provides the driving force for proton influx through the F1F0-ATP synthase. Ultimately, ATP is generated and transported to the cytosol (Saraste 1999; Nicholls 2004).

b) Calcium (Ca^{2+}) signaling at the mitochondria.

Mitochondria not only take up Ca^{2+} at physiological cytosolic Ca^{2+} concentrations but it has also been shown that mitochondrial Ca^{2+} accumulation strictly controls the energetic metabolism of the cells. On one hand by directly modulating the activity of enzymes located in the matrix such as dehydrogenases (liver and heart), metalloproteinases (e.g. in cancer cells) and ATP synthase (in heart and skeletal muscle)(Brown 1992; Das and Byrd 1996; Das 1998; Jouaville, Pinton et al. 1999). On the other hand, Ca^{2+} accumulation contributes to shaping cytosolic Ca^{2+} fluctuation, thus in turn modulating cellular functions regulated by Ca^{2+} variations (Brini 2003).

c) Adaptative thermogenesis.

In the brown fat cells, mitochondria display the additional ability to directly convert this proton gradient into heat (thermogenesis) (Fontanillas, Depraz et al. 2005). The key element of this energy dissipation capacity is the uncoupling protein 1 (UCP1), a mitochondrial inner membrane protein encoded by nuclear genes, which catalyses a highly regulated proton leak under the control of adrenergic receptors activated by noradrenalin (Nedergaard, Golozoubova et al. 2001; Nedergaard, Matthias et al. 2001).

Other functions of mitochondria are related to the cell type in which they are found. Although mitochondria are present in every nucleated cell, they are found in high concentrations in cells with higher energy requirements, such as skeletal muscle cells and brown fat cells (Almind, Manieri et al. 2007). For instance, mitochondria participate in the production of hormones from parts of blood such as estrogen and testosterone. They are required for cholesterol metabolism, neurotransmitter metabolism, and detoxification of ammonia in the urea cycle (Nelson and Cox 2000). Therefore, if mitochondria become dysfunctional, the cell-energy production becomes unbalanced as well as the production of cell-specific components needed for a normal cell functioning (Figure I- 2).

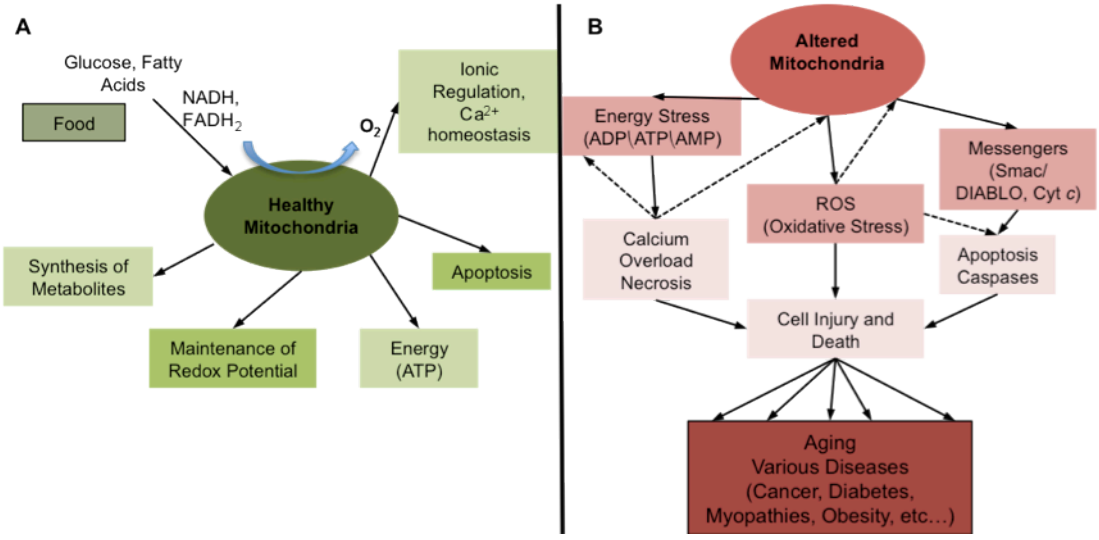

Figure I- 2. Key roles of mitochondria. **(A)** In normal cell function. **(B)** In injury. (Figure adapted from (Kuznetsov and Margreiter 2009)).

I-1.2.2. Pathophysiological roles.

Imbalance between energy production and energy demand, and a disturbance in energy transfer networks, play an important role in various pathologies.

Mitochondria regulate the cellular redox state and play very important roles in ionic regulations (in particular in Ca^{2+} homeostasis) and in apoptosis (Kroemer and Reed 2000; Newmeyer and Ferguson-Miller 2003) and can be considered as an integral part of multiple cellular signaling and a mediator of cell communication and survival (Kuznetsov, Janakiraman et al. 2004; Karbowski, Norris et al. 2006; Youle 2007; Kuznetsov, Smigelskaite et al. 2008). Moreover, mitochondria are directly involved in pathophysiological mechanisms of ischemia-reperfusion injury, oxidative stress, preconditioning, inherited diseases, toxicological injury, and side-effects of pharmacological treatments. Damaged mitochondria cause organ injury also by several mechanisms, including the diminished cellular energy status (energy stress), production of reactive oxygen species (ROS) (oxidative stress), disturbance of ionic balance, cytochrome *c* release and induction of apoptosis (Figure I- 2).

a) Generation of free radicals during oxidative phosphorylation.

In the mitochondrial respiratory chain, Complex IV (cytochrome C oxidase) retains all partially reduced intermediates until full reduction is achieved. Other redox centers in the electron transport chain, however, may leak electrons to oxygen, partially reducing this molecule to superoxide anion (O_2^{-}•). Even though O_2^{-}• is not a strong oxidant, it is a precursor of most other ROS, and it also becomes involved in the propagation of oxidative chain reactions. ROS are highly reactive and uncontrolled increases in the steady-state concentrations of these oxidants lead to free radical-mediated chain reactions, which indiscriminately target proteins, lipids, polysaccharides and DNA (for review see (Turrens 2003)).

b) Calcium.

Mitochondria participate in Ca^{2+} signaling as a result of their close apposition to Ca^{2+} release (endoplasmic reticulum, ER (Rizzuto, Pinton et al. 1998)) and Ca^{2+} entry sites (plasma membrane), where microdomains with high local Ca^{2+} concentrations are formed. In contrast to the beneficial effects of Ca^{2+} (see above), the mitochondrial permeability transition pore (MPTP) embodies the pathological effects of Ca^{2+} on mitochondria by triggering cell death and necrosis (Brini 2003).

Although many mechanisms involved in mitochondrial function and regulation have been studied quite extensively, the interplay among the different roles of mitochondria is still poorly understood.

I-1.3. Programmed cell death.

The term apoptosis, as it is known today, was first used in 1972 by Kerr et al. (Kerr, Wyllie et al. 1972) to describe a novel form of dying which differed in many ways from other modes of programmed cell death. Since then, it has become the main focus of research concerning normal developmental cell death and also too little or too much unwanted cell loss in disorders ranging from cancer to neurodegenerative diseases. The morphological characteristics of apoptosis include cell shrinkage, chromatin degradation and condensation, membrane blebbing and nuclear fragmentation (Kerr, Wyllie et al. 1972). The cell is eventually broken into small membrane-enclosed pieces (apoptotic bodies), which in vivo are removed by macrophages, or taken up by neighboring cells. This prevents the release of cellular compounds and thus ensures that an inflammatory response is not provoked. Traditionally, apoptosis has been classified into caspase-dependent or independent mechanisms and, based on the mode of initiation, arbitrated via two major interconnected pathways, the death receptor (DR)-mediated, or extrinsic, and the mitochondrial or intrinsic cascades.

I-1.3.1. Receptor-mediated/ Extrinsic pathway.

The extrinsic pathway of apoptosis is activated upon interaction of the tumor necrosis family (TNF) members with the cysteine-rich, extracellular sub-domain of their respective DR, which belong to the TNF receptor (TNFR) gene family. The eight-member family of receptors includes CD95 (Fas or APO-1) and TNFR1 (p55 or CD12a). The receptor-mediated pathway is initiated by the binding of a death ligand (e.g. CD95 /Fas ligand, TNF-α) to its cognate cell surface DR (e.g. CD95/Fas, TNF-α receptor) (Ashkenazi and Dixit 1998; Schmitz, Kirchhoff et al. 2000). Consequently, death adapter molecules such as FADD (Fas-associated death domain) and TRADD (TNF receptor-associated death domain) form homotrimers which are recruited to the cytoplasmic tail of the DR through interactions between “death domains” present in both proteins (Tartaglia and Goeddel 1992; Chinnaiyan, Tewari et al. 1995). The ligand-receptor interaction and recruitment of the adaptor molecules result in the formation of signaling complexes that activate caspase-8 and caspase-3. Activation of caspase-8 leads to activation of effector caspases like caspase-3, 6 or 7 (Figure I- 3). This mechanism could directly lead to destruction of the cell or to activation of the, otherwise independent, machinery of mitochondrial pathway.

I-1.3.2. Mitochondrial/ Intrinsic pathway.

Mitochondrial apoptosis can be seen as a magnifying step for caspase activation and other pathways of apoptosis where intrinsic stimuli such as ROS or Ca^{2+} overload cause mitochondrial dysfunction and, eventually, lead to apoptosis (Green, John et al. 1998; Desagher and Martinou 2000). A crucial event in this process is the release of cytochrome *c* and other pro-apoptotic molecules (like apoptosis-inducing factor, AIF and SMAC/Diablo) from the mitochondrial outer membrane. About 90% of the cytochrome *c* is stored in vesicles formed from the mitochondrial inner membrane and 10% is located at the intermembrane space (Mayer and Oberbauer 2003). Cytochrome *c* has a defined role as an electron transfer protein in mitochondrial oxidative phosphorylation. The apoptotic role of cytochrome *c* involves its release into the cytosol and being an essential component in formation of the apoptosome, the structure required for activation of caspase-9 (Figure I- 3).

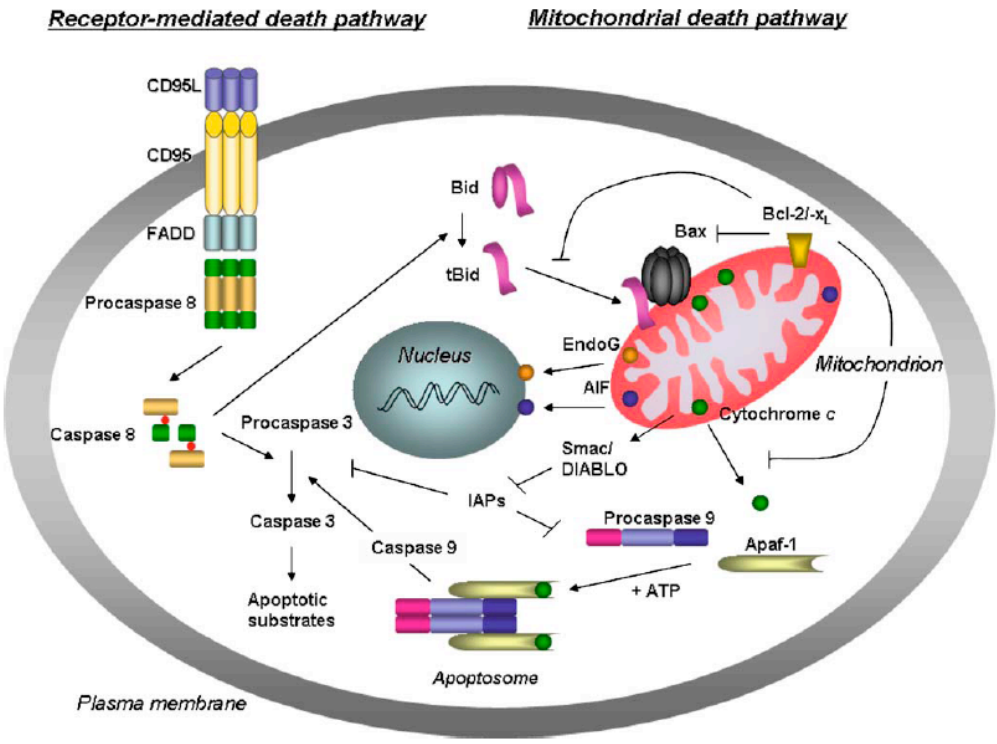

Figure I- 3. Programmed cell death (PCD) pathways. Comprehensive schema of signaling pathways implicated in apoptosis (PCD type I). Depending on the stimuli apoptosis may be initiated extrinsically via the engagement of cell surface death receptors (DRs) or intrinsically via the mitochondrial pathway. The receptor-mediated death pathway is initiated by binding of a death ligand (e.g. CD95L/FasL) to its cognate receptor (e.g. CD95/Fas) in the plasma membrane. The cytoplasmic tail of the DR then engages death adaptor molecules (e.g. FADD), resulting in the recruitment and activation of Procaspase 8. Caspase 8 activates downstream effector caspases such as caspase 3, resulting in the execution of apoptosis. Caspase 8 also activates Bid, thereby linking the two death pathways. The mitochondrial death pathway is regulated by the Bcl-2 family of proteins (see following sections). Cellular stresses are communicated to the mitochondria by pro-apoptotic Bcl-2 family members (e.g. Bid, Bax), leading to the release of pro-apoptotic molecules (e.g. cytochrome *c*, EndoG, AIF, Smac/DIABLO) from the mitochondrial intermembrane space into the cytosol where they initiate the apoptotic cascade. Anti-apoptotic Bcl-2 family members (e.g. Bcl-2 and Bcl-XL) oppose these actions (Figure extracted from (Hamacher-Brady, Brady et al. 2006)).

Although the exact mechanism of the cytochrome *c* release into the cytosol is not known, there are several hypotheses about the structural changes in mitochondrial membrane permeability, due to the interplay of several molecules and mechanisms, with the members of the Bcl-2 family acting as the main regulators of the overall process (Figure I- 3). The changes in the membrane permeability are associated with formation of the mitochondrial permeability transition pore (MPTP) and other membrane channels, involving the members of the Bcl-2 family and the upstream regulatory proteins, such as p53 (Polster and Fiskum 2004).

I-1.4. Death signaling at the mitochondria.

Mitochondria are seen as a central point of convergence and integration of both survival and death signaling pathways. Mitochondria can transmit death signals between each other and to other organelles such as the sarco-/ER and the nucleus. Their ability to cause cell death can be followed by three main factors: increased ROS production, impaired Ca^{2+} homeostasis and MPTP activity.

I-1.4.1. Mitochondrial permeability transition.

The mitochondrial permeability transition (MPT) is a pathophysiological relevant mechanism that leads to increased permeability of the mitochondrial membranes and participates in both necrotic and apoptotic cell death (Kim, Qian et al. 2003). The onset of MPT is initiated by the opening of the nonspecific large-conductance MPTP, whereby the inner mitochondrial membrane is permeable to solutes of up to 1.5 kDa, causing the collapse of the $\Delta\Psi_m$. The multipeptide channel, MPTP, forms at the contact site of the two mitochondrial membranes, consisting of peptides like VADC (outer membrane) and ANT (inner membrane), plus other molecules from the matrix and intermembrane space (Figure I- 4) (Zoratti and Szabb 1995). The Bcl-2-associated X protein (Bax) interacts with individual components of the MPTP (Shimizu and Tsujimoto 1999; Adachi, Higuchi et al. 2004). Binding of the anti-apoptotic members of this family can close the VDAC and inhibit apoptosis (Shimizu, Konishi et al. 2000). Despite these interactions, the permeability transition pores can cause apoptosis on their own and the Bcl-2 family members can regulate release of cytochrome *c* independently of these pores. Therefore, the interaction of members of the Bcl-2 family with VDAC, ANT and other components of the MPTP is only one of the ways these proteins carry on their pro and anti-apoptotic functions.

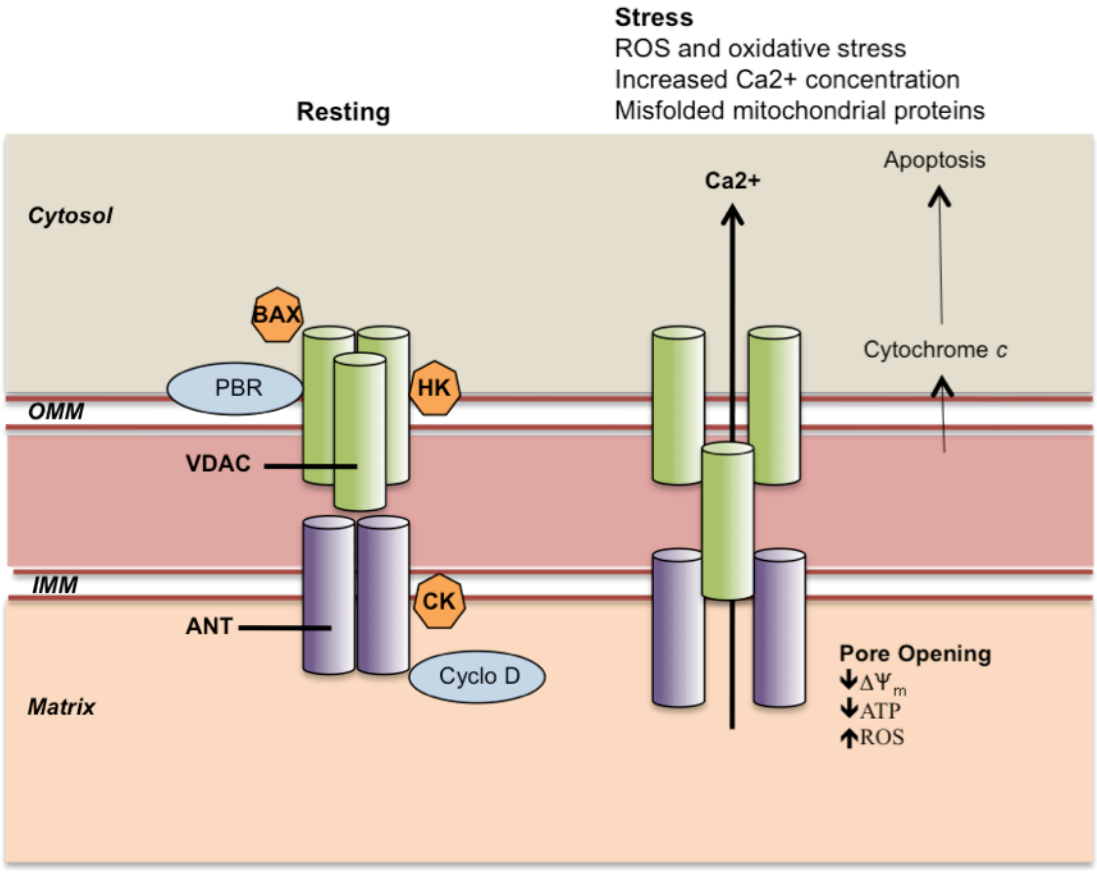

Figure I- 4. Mitochondrial permeability transition pore (MPTP). The MPTP is a conductance pore that spans the inner (IMM) and outer (OMM) mitochondrial membranes. It consists of membranous elements such as the voltage-dependent anion channel (VDAC) on the OMM, the adenine nucleotide translocator (ANT) on the IMM, and cyclophilin D (Cyclo D) in the matrix. Other proteins, such as the peripheral benzodiazepine receptor (PBR), hexokinase (HK) and creatine kinase (CK), might also be associated with the MPTP. It is not clear whether the MPTP has a role in normal mitochondrial physiology. However, under a combination of pathophysiological conditions, such as high Ca^{2+} concentration, increased oxidative stress, low ATP, and mitochondrial depolarization, the complex forms an open pore between the inner and outer membranes, allowing free diffusion of solutes across the membranes. The opening of the MPTP ultimately results in mitochondrial swelling, mitochondrial Ca^{2+} efflux and the release of apoptogenic proteins, such as cytochrome *c* and pro-caspases, from the intermembrane space. ANT-knockout studies suggest that it might not be an essential structural component but might have a role in the regulation of MPTP opening; mitochondrial membrane potential; Bax, ROS. (Figure adapted from (Abou-Sleiman, Muqit et al. 2006)).

I-1.4.2. Bcl-2 family members.

Members of the Bcl-2 family are classified into three groups of pro-apoptotic, anti-apoptotic and BH3-only proteins, sharing at least one conserved Bcl-2 homology (BH) domains. Each of the BH domains is involved in a specific function. BH1 and BH2 are used in formation of the structures necessary for interaction and oligomerization of the members of this family. Therefore, the anti-apoptotic members, including Bcl-2, Bcl-XL, Bcl-w and Mcl-1 have all four domains whereas the BH4 domain is missing from the pro-apoptotic members like Bax and Bcl-2 antagonist/killer-1 (Bak), known as multidomain pro-apoptotic or effector proteins. Other members like Bid, Bnip3, Bok, Bim and Bad only have the

BH3 domain and are known as BH3-only proteins (Huang and Strasser 2000). The BH3 domain is responsible for progression of apoptosis while BH4 domain causes anti-apoptotic activity (Figure I-5).

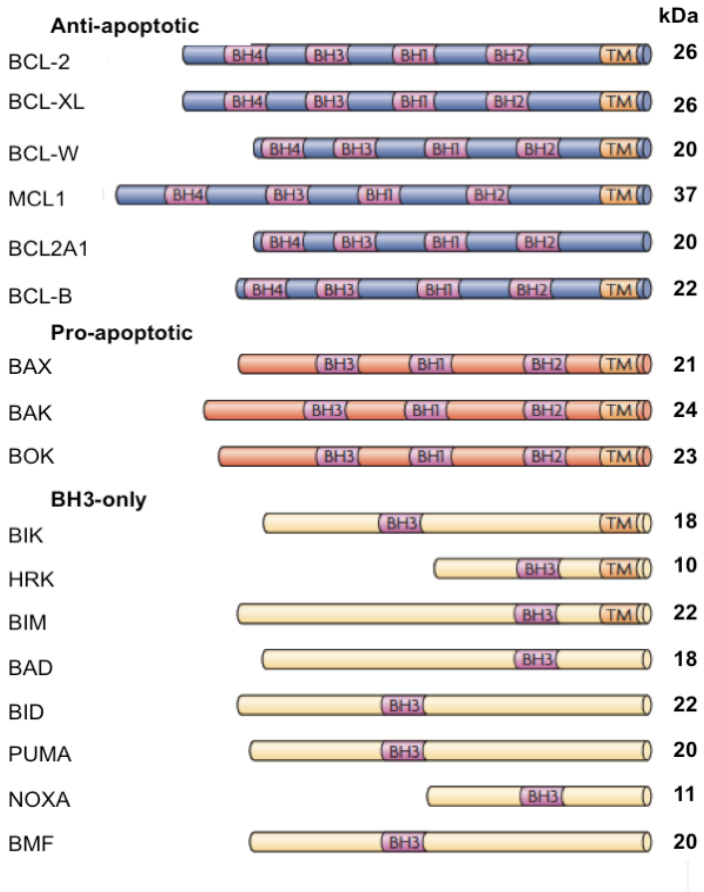

Figure I- 5. B-cell lymphoma-2 (Bcl-2)-family proteins homology domains. Bcl-2 family proteins comprises the anti-apoptotic Bcl-2 family members that contain four Bcl-2 homology domains (BH1-BH4; e.g. Bcl-2, Bcl-XL). Most members of this subfamily also contain transmembrane domains (TM) and are therefore typically associated with membranes. Exceptions are found in the BH3-only subfamily (e.g. Bid). The pro- apoptotic Bcl-2 family can be further subdivided into the multidomain subfamily containing three Bcl-2 homology domains (BH1-BH3; e.g. Bak, Bax) and the BH3-only subfamily (BH3; e.g. Bid, Bnip3). The mammalian BH3-only protein family currently comprises eight members (Bid, BAD, BIM, BIK, BMF, NOXA, PUMA and HRK), all of which promote apoptosis when over-expressed. These proteins share little sequence homology apart from the BH3 motif, and are regulated in distinct ways. (Figure extracted from (Taylor, Cullen et al. 2008)).

In addition to the interactions with the MPTP, the pro-apoptotic members of the Bcl-2 family, can also form new channels and induce membrane lipid alterations (Sharpe, Arnoult et al. 2004). In non-apoptotic cells, Bax exists as an inactive monomer either in the cytosol or loosely bound to the mitochondrial outer membrane. Upon activation by apoptotic stimuli, including interaction with truncated Bid (t-Bid), Bax undergoes a conformational change, which allows the disengagement of its C-terminal anchor domain from the hydrophobic groove and insertion into the mitochondrial outer membrane (Nechushtan, Smith et al. 2001). Studies on the structure of Bcl-XL show that the BH1 and

BH2 domains, along with the BH3 domain, form a hydrophobic groove on the surface of the anti-apoptotic members of the Bcl-2 family to which the alpha helical BH3 domain binds (Muchmore, Sattler et al. 1996; Sattler, Liang et al. 1997). The exact molecular mechanism of protection by the pro-survival members of the Bcl-2 family is not known, but dimerization with their pro-apoptotic relatives is essential to their function.

BH3-only proteins act as upstream sentinels of cellular damage and derangement. They can be activated by many noxious stimuli – including DNA damage, growth-factor withdrawal and oncogene activation – via mechanisms that include transcriptional upregulation, subcellular localization and/or post-translational modifications. For example, p53-upregulated modulator of apoptosis (Puma) and Noxa (the latin word for damage; also known as PMAIP1) are transcriptionally upregulated by p53 in response to DNA damage (Oda 2000; Nakano and Vousden 2001). In some cells, Bim can be sequestered within the cytoskeleton, to be released only in response to certain death stimuli (Puthalakath, Huang et al. 1999). Bid is part of the extrinsic DR pathway, and upon its activation serves to bridge the intrinsic and extrinsic pathways. Following DR-ligand biding (TNFα or Fas), Bid is cleaved by caspase 8 generating the C-terminal product tBid (truncated Bid), which is myristoylated and then translocates to the mitochondria (Li, Zhu et al. 1998; Zha, Weiler et al. 2000). Bid has been proposed to directly participate in the mitochondrial outer membrane permeabilization (MOMP) event (Yuan, Williams et al. 2003), as well as amplify the pro-apoptotic signaling of Bax either through direct interaction with Bax/Bak (Saito, Korsmeyer et al. 2000; Wei, Lindsten et al. 2000), or through scavenging of anti-apoptotic Bcl-2 and Bcl-XL, which oppose Bax activity (Wang, Yin et al. 1996) (Cheng, Wei et al. 2001). Bnip3 is another member of the BH3-only Bcl-2 subfamily which has been described to induce apoptotic (Kubasiak, Hernandez et al. 2002), necrotic (Vande Velde, Cizeau et al. 2000), and autophagic (Daido 2004; Kanzawa, Zhang et al. 2004) cell death. Bnip3 has a C-terminal transmembrane (TM) domain, required for its pro-apoptotic function, including targeting to the mitochondria (Yasuda, Theodorakis et al. 1998). Bnip3 has been shown to contribute to ischemia/reperfusion injury in the *ex vivo* heart via disruption of mitochondrial integrity, leading to enhanced superoxide production and the release of pro-apoptotic factors such as cytochrome *c* and AIF (Hamacher-Brady, Brady et al. 2007).

In summary, the ratio of pro-apoptotic and anti-apoptotic members is essential in the regulation of mitochondrial sensitization and the rate of death via the intrinsic pathway. Likewise, BH3-only proteins can induce apoptosis by direct interaction with the pro-apoptotic members (synergistic and activating effects) or neutralizing the effect of anti-apoptotic members (inhibition of heterodimerization with pro-apoptotic members) (Figure I- 3).

I-1.4.2.1. Bax and Bak as MOMP effectors.

MOMP, which releases numerous pro-apoptotic proteins into the cytosol, is the pivotal event in the intrinsic apoptotic pathway. Bax and Bak double-knockout cells fail to undergo MOMP in response to different death stimuli, including staurosporine, ultraviolet (UV) radiation, growth-factor deprivation, DNA damage and ER stress (Wei 2001). Apoptosis that is caused by BH3-only proteins absolutely requires Bax and Bak (Wei 2001; Kuwana, Bouchier-Hayes et al. 2005; Lindsten and Thompson 2006) (Wei, Lindsten et al. 2000). Bax proteins can be found as monomers in the cytosol or loosely associated with the outer mitochondrial membrane when not activated. Bax translocates to and inserts into the mitochondrial outer membrane during the activation process (Hsu and Youle 1997; Wolter, Hsu et al. 1997; Billen, Kokoski et al. 2008). Bak is inserted into the outer mitochondrial membrane even when not activated (Wei, Lindsten et al. 2000). One of the steps that is involved in the activation of Bax and Bak is a conformational change that exposes the N-terminus of the proteins, which is otherwise hidden in the inactive state (Yethon 2003). Following activation, Bax and Bak form homo-oligomers that can be visualized by microscopy (e.g. GFP-tagged Bax) as they form clusters (Brady, Hamacher-Brady et al. 2006). Bax and Bak oligomers participate in forming pores and cause permeabilization of the outer mitochondrial membrane, leading to the release of the contents of the mitochondrial intermembrane space, including cytochrome *c*, AIF and Smac/Diablo, into the cytosol (Wang 2001). These contents drive the activation of caspases, which cleave and disable crucial proteins throughout the cell. Given the lethal consequences of Bax and Bak activation, understanding how their activation is controlled is key to understanding how a cell makes the decision to undergo apoptosis.

I-1.5. Downstream of the mitochondria.

After the release of cytochrome *c* from the mitochondrial intermembrane space into the cytoplasm, it binds to Apaf1 (apoptotic protease activating factor 1) and, in the presence of dATP, procaspase 9 is recruited to the complex, now termed the apoptosome, leading to the activation of procaspase 9. Activated caspase 9 can then activate downstream effector caspases, and thus determine the cell to death (Li, Nijhawan et al. 1997). Cytochrome *c*-dependent activation of caspase 9 is supported by Smac/DIABLO, which is likewise released from the mitochondrial intermembrane space and removes the anti-apoptotic activity of IAPs (inhibitor of apoptosis proteins). In addition, mitochondria release endonuclease G and AIF that translocate to the nucleus and promote chromatin condensation and large-scale DNA fragmentation (Sharpe, Arnoult et al. 2004). Formation of the activating protein complexes (apoptosome for caspase-9 and DISC for caspase- 8) is a common molecular event in activation of initiator caspases, while the effector caspases are activated through proteolytic cleavage by their respective initiator caspases (Shi 2004). In the same way, activation of caspase-9 mainly leads

to activation of caspase-3, which is also the effector caspase of the DR-mediated apoptosis. Beside the caspase-dependent pathways, mitochondria can be involved in several other apoptotic processes including release of AIF and activation of the caspase-independent pathway (Joza, Susin et al. 2001). The mitochondrial pathway is considered as a magnifying step for the extrinsic apoptosis in certain cell types with low levels of activation of caspase-8 (Scaffidi, Fulda et al. 1998). In such cells, the Bcl-2 family member, Bid, is truncated by caspase-8 and the truncated Bid (tBid) will mediate release of cytochrome *c* and activation of caspases 9 and 3 (Li, Zhu et al. 1998; Luo, Budihardjo et al. 1998). The activation of caspase-3, downstream of caspase-8 and/or caspase-9, leads to cell death due to its cleavage and, therefore, degradation and inactivation of proteins (like the caspase activated DNAse, CAD, or Bcl-2 proteins) and destruction of cellular structures (like lamin) (Jürgensmeier, Xie et al. 1998). This results in many of the morphological characteristics of apoptosis, including condensed nuclei, DNA laddering and exposure of phosphatidylserine to the outer leaflet of the plasma membrane (Thornberry and Lazebnik 1998).

I-1.6. Removing dysfunctional mitochondria from the cell: mitophagy.

Recently, a second mode of programmed cell death (PCD type II), termed autophagic cell death, has been discovered which is morphologically characterized by the presence of numerous autophagic vacuoles (Bursch 2001). Autophagy is a vital process by which macromolecules and organelles are being delivered to lysosomal degradation. Uncontrolled or excessive autophagy is thought to cause cell death via the extensive degradation of cytoplasmic constituents (Bursch 2001). Under these conditions, pharmacological or molecular inhibition of the autophagic components has been shown to prevent cell death. One of the crucial homeostasis events requiring autophagy is the removal of damaged or excessive mitochondria (mitophagy). The term mitophagy refers to the selective removal of mitochondria by autophagy and was coined by Lemasters (Lemasters 2005). Mitophagy prevents the release of pro-apoptotic proteins from permeable-damaged mitochondria.

In mammalian cells, loss of $\Delta\Psi_m$ appears to be a common feature of mitophagy. Lemasters and others have used dyes and confocal techniques to image MPT, $\Delta\Psi_m$ and mitochondrial engulfment by GFP-LC3-positive autophagosomes during starvation (Rodriguez-Enriquez, Kim et al. 2006; Kim, Rodriguezenriquez et al. 2007). When mitochondria were deliberately photo-damaged, GFP-LC3-positive structures appeared in the damage area, suggesting that damaged mitochondria were targets for autophagosomal removal (Scherz-Shouval and Elazar 2007). Mitophagy is observed in starved hepatocytes treated with glucagon (Elmore, Qian et al. 2001) and in serum-starved neurons treated with caspase inhibitor (Xue, Fletcher et al. 2001). Similarly, in reticulocytes, ultrastructural studies indicate that mitophagy is involved in mitochondrial clearance (Gronowicz, Swift et al. 1984). In the past few years, compelling results suggest that removal of mitochondria from cells can be specific, and

the signals that specify mitochondria as targets of the autophagic process have begun to be elucidated (for recent review on mitophagic receptors see (Novak and Dikic 2011)). Recent work demonstrated that an atypical BH3-only protein, Nix, is required for programmed mitochondrial clearance during reticulocyte maturation (Schweers, Zhang et al. 2007; Sandoval, Thiagarajan et al. 2008). Recently, the loss of mitochondrial reticular network has been associated with mitophagic events (Twig, Elorza et al. 2008). However, mitochondrial morphology implication on selective mitophagy remains elusive.

I-2. Mitochondrial morphology.

I-2.1. General heterogeneity of mitochondria.

I-2.1.1. The connectivity of mitochondria.

The connectivity of mitochondria in living cells has been addressed in several studies using a range of imaging techniques (Rizzuto 1998; Collins, Berridge et al. 2002; Collins and Bootman 2003; Kuznetsov, Troppmair et al. 2006; Beraud, Pelloux et al. 2009). In some cell types mitochondria exist as single and randomly dispersed organelles (Collins, Berridge et al. 2002; Kuznetsov, Usson et al. 2004; Kuznetsov, Troppmair et al. 2006). In other cells, mitochondria may also exist as dynamic networks that often change shape and subcellular distribution (Amchenkova, Bakeeva et al. 1998). Application of diverse imaging approaches has revealed electrical connectivity of the mitochondrial network in cells like human skin fibroblasts, COS-7 cells (De Giorgi, Lartigue et al. 2000), and neonatal rat or HL-1 cardiac myocytes (Amchenkova, Bakeeva et al. 1998; Beraud, Pelloux et al. 2009). Mitochondrial imaging and the fluorescence recovery after photobleaching (FRAP) technique have demonstrated the existence of an interconnected branched mitochondrial network also in HeLa cells (Rizzuto, Pinton et al. 1998). In addition, distinct mitochondria (e.g. in HeLa cells) can be consecutively depolarized, indicative of electrically non-connected mitochondria (Collins, Berridge et al. 2002; Collins and Bootman 2003). In these experiments, asynchronous depolarization events induced by laser irradiation clearly indicate the positions of the electrically isolated mitochondria and do not indicate electrical relationships between these organelles (Collins and Bootman 2003). A similar phenomenon of the electrical discontinuity of mitochondria was found in adult cardiomyocytes (Zorov, Filburn et al. 2000; Beraud, Pelloux et al. 2009). Laser irradiation resulted thereby in the $\Delta\Psi_m$ collapse of individual mitochondria due to local ROS production and MPT (Lesnefsky, Tandler et al. 1997; Zorov, Filburn et al. 2000; Knight, Roberts et al. 2003; Cortassa, Aon et al. 2004; Kuznetsov, Troppmair et al. 2006; Wang, Fang et al. 2008; Beraud, Pelloux et al. 2009). This result demonstrates the existence of closely located but differentially energized mitochondria, which enables them to have different functional properties according to cell demand.

I-1.1.2. Functional heterogeneity of mitochondria.

A growing body of evidence has demonstrated that mitochondria not only vary between different types of cells and display dissimilar morphology, but that mitochondria in specific regions of a cell may have different functional properties (Kuznetsov, Mayboroda et al. 1998; Romashko, Marban et al.

1998; Park, Ashby et al. 2001; Collins, Berridge et al. 2002; Kuznetsov, Schneeberger et al. 2004; Kuznetsov, Troppmair et al. 2006). In contrast to biochemical determination, fluorescent confocal imaging provides the unique occasion to directly visualize mitochondrial function separately in various mitochondrial sub-populations, small clusters or even in individual mitochondria (Collins, Berridge et al. 2002; Kuznetsov, Schneeberger et al. 2004; Kuznetsov, Troppmair et al. 2006). Moreover, this technique is a direct approach to resolve the heterogeneity and the complex intracellular spatiotemporal organization of the mitochondria, mitochondrial signals and downstream events. It has been shown that mitochondria localized in different cell regions can have different morphology, biochemical properties and respiratory activities, demonstrating clear intrinsic heterogeneity (Palmer, Tandler et al. 1985). Different mitochondrial sub-populations are present in cells that may be differently involved in physiological (Kuznetsov, Mayboroda et al. 1998) and pathological processes (Lesnefsky, Tandler et al. 1997).

Imaging techniques have recognized the heterogeneity of mitochondrial redox potentials in skeletal muscle (Kuznetsov, Mayboroda et al. 1998) and cardiomyocytes (Romashko, Marban et al. 1998) and also with respect to mitochondrial ROS levels and uncoupling proteins (e.g. UCP-3) (Zorov, Filburn et al. 2000; Jimenez, Yvon et al. 2002; Kuznetsov, Troppmair et al. 2006). The heterogeneity of $\Delta\Psi_m$, which reflects the functional status of mitochondria within cells, was detected in cultures of various cell types under normal growth conditions, cell stresses and apoptosis (Salvioli, Dobrucki et al. 2000; Collins, Berridge et al. 2002; Collins and Bootman 2003; Kuznetsov, Schneeberger et al. 2004; Kuznetsov, Usson et al. 2004; Kuznetsov, Troppmair et al. 2006). Notably, heterogeneous membrane potential has been shown even within individual mitochondrial filaments (Benard and Rossignol 2008). The existence of mitochondrial domains of heterogeneous electrical and redox potentials further supports the existence of a mitochondrial heterogeneity complexity maintained by yet undiscovered processes. In the same manner, mitochondria may consist of sub-populations with differential sensitivity to Ca^{2+}-induced inner membrane permeability transition, indicating that mitochondria are heterogeneous in their response to Ca^{2+} (Bowser, Minamikawa et al. 1998; Kristian, Weatherby et al. 2002). Distinct subsets of mitochondria can thus display different responses to substrates and inhibitors and vary in their sensitivity to pathology, apoptosis and oxidative stress (Romashko, Marban et al. 1998; Kuznetsov, Schneeberger et al. 2004; Chen, Chomyn et al. 2005).

I-2.1.2. Heterogeneity of mitochondrial morphology and organization.

Broad variations in mitochondrial shape and morphology can be observed in various cells, but also within one cell, including small spheres or short rod-like shapes, long filamentous spaghetti-like

mitochondria, together with complex, branched mitochondrial networks found for example in HL-1 cells, human pancreatic cells, etc. (Kuznetsov, Troppmair et al. 2006; Pelloux, Robillard et al. 2006).

In these cells, fusion causes formation of a mitochondrial reticulum, which may play an important role in cell physiology. Several other cell types like adult cardiomyocytes show functionally and structurally distinct mitochondria (Zorov, Filburn et al. 2000; Collins, Berridge et al. 2002; Vendelin, Béraud et al. 2005), which is also very important for the specific functions of these cells (Saks, Kaambre et al. 2001; Saks, Dzeja et al. 2006). Importantly, mitochondrial dynamics (fission/fusion), which controls the shape and organization of these organelles, can be important for their functioning and metabolism regulation (Chen, Chomyn et al. 2005; McBride, Neuspiel et al. 2006; Benard and Rossignol 2008).

Mitochondrial clustering is thought to be a phenotype relevant for mitochondrial function. For instance, mitochondrial clusters surrounding the nuclei in cardiomyocytes may serve to generate ATP directed to the nucleus and may play an important physiological role in nuclear import mechanisms (Park, Ashby et al. 2001; Dzeja, Bortolon et al. 2002). In general, the diversity of mitochondrial shapes and intracellular arrangements can be referred to their highly specialized cellular functions in the cells with different energy requirements.

I-2.2. GTPases, the mitochondrial morphology effectors.

For a long time, mitochondria have been investigated in cell-free isolated systems, creating the impression of a lonely static organelle. Along the past 10 years, this view has changed as new approaches allowed the examination of dynamic mitochondrial function and behavior in response to cellular signals in intact cells. We now understand that mitochondria form a functional reticulum whose steady-state morphology is regulated by dynamic fission, fusion and motility events. Multiple proteins are involved in the re-modeling of mitochondrial membranes (for review see (Chan 2006)).

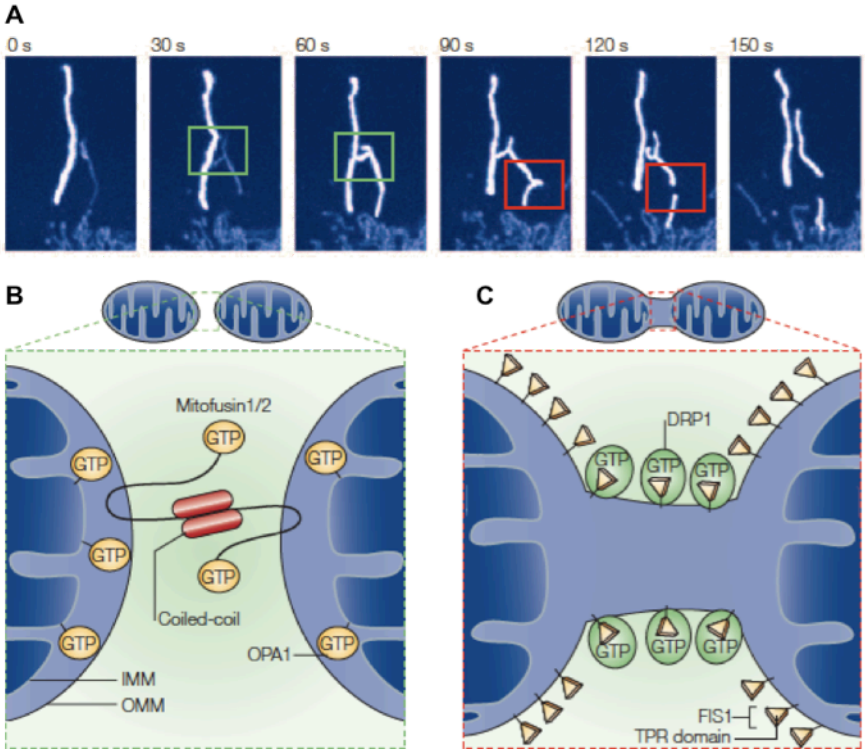

Figure I- 6. GTPases regulating mitochondrial morphology: Fission and Fusion schemes. (A) Confocal time-lapse images of mitochondria labeled with mitochondrial-matrix-targeted photoactivatable GFP. Mitochondrial fusion is shown in the green box and fission is shown in the red box following a single mitochondrion photoactivation. The lower panels show schematic cross-sections through fusing (B) and dividing (C) mitochondria. **(B)** In fusion, two mitochondria dock through coiled-coil-domain interactions between mitofusins that are anchored into the outer mitochondrial membrane (their GTPase domains face the cytosol), whereas Opa1, which is anchored partially on the inner mitochondrial membrane, participates in the membrane fusion process. **(C)** During fission, Fis1 circumscribing the outer mitochondrial membrane recruits the large GTPase and dynamin homologue Drp1 through its tetratrico-peptide repeats (TPR), which subsequently coalesces into foci at mitochondrial scission sites. (Figure extracted from (Youle and Karbowski 2005)).

Mitochondrial fusion is mediated through the action of at least three GTPases. Mitofusin 1 (Mfn1) and Mitofusin 2 (Mfn2) are integrated within the mitochondrial outer membrane, with their GTPase and coiled-coil domains exposed to the cytosol (Chen 2005). Mfn1 and Mfn2 exist as homotypic and heterotypic complexes that can form between adjacent organelles (Chen, Detmer et al. 2003; Koshiba, Detmer et al. 2004). Mechanistically, it has been suggested that the carboxy-terminal coiled coils tether two organelles undergoing fusion, with the GTPase domains probably regulating the fusion reaction (Ishihara, Eura et al. 2004; Neuspiel, Zunino et al. 2005; Griffin and Chan 2006). Another dynamin-like GTPase, Opa1, resides in the intermembrane space, where it is associated with the inner membrane (Alexander, Votruba et al. 2000; Olichon, Baricault et al. 2003; Satoh, Hamamoto et al. 2003). Opa1 exists as multiple splice and cleavage variants and its function in mitochondrial fusion has been linked genetically to that of Mfn1 (Delettre, Griffoin et al. 2001; Cipolat, Martins de Brito et al. 2004). Mitochondrial fission relies on another GTPase from the dynamin family, Drp1 (Pitts, Yoon

et al. 1999; Smirnova, Griparic et al. 2001; Yoon, Pitts et al. 2001). By analogy with dynamins, it has been suggested that Drp1 oligomerizes into ring-like structures around the fission sites, to constrict the organelle in a GTP-dependent manner. In fact, Drp1 forms punctae on the mitochondrial membrane, some of which mark future fission sites (Figure I- 6).

Because Drp1 does not have a TM domain, for it to bind to the outer mitochondrial membrane, it either binds directly to Fis1 or induces fission independently of Fis1 (Yoon, Krueger et al. 2003). Alternatively, in a similar manner to its yeast homologue, Dnm1p, adaptor proteins such as Mdv1 and Caf4 mediate its binding to Fis1, although the mammalian homologous proteins have yet to be identified (Griffin, Graumann et al. 2005) (Tieu, Okreglak et al. 2002). Mammalian Fis1 was first identified in 2001 by its homology with Fis1p, the yeast ortholog (James, Parone et al. 2003; Yoon, Krueger et al. 2003). It is a small protein of 17 kDa and 152 amino acids whose primary function is to promote fission of mitochondria and peroxisomes (Figure I- 5). It is ubiquitously expressed and is detected throughout the mitochondrial network, where it is inserted into the outer mitochondrial membrane. Over-expression of Fis1 in cells induces mitochondrial fragmentation, which can result in Drp1-dependant cytochrome *c* release and apoptosis (Jofuku, Ishihara et al. 2005). In contrast, inhibiting Fis1 can protect against apoptotic cell death (Jofuku, Ishihara et al. 2005). Fis1 can also induce apoptotic cell death independent of Drp1 and can promote mitochondrial fragmentation without inducing apoptotic cell death (Alirol, James et al. 2006). Finally, Fis1 is required to induce mitochondrial fission in senescent-long mitochondria to facilitate their removal by mitophagy (Yoon, Yoon et al. 2006).

I-2.2.1. Processes regulating mitochondrial GTPases.

Recent work suggests that Drp1 activation and translocation to the mitochondria may be post-translationally regulated by sumoylation, ubiquitination, S-nitrosylation or phosphorylation of serine residues within the GTPase Effector Domain (GED). For instance, mitochondrial E3 ubiquitin ligase, MARCH-V, is known to promote mitochondrial fission by facilitating Drp1 translocation to the mitochondria without affecting its stability (Karbowski, Neutzner et al. 2007). The small ubiquitin-like modifier (SUMO) proteins are also involved in regulating Drp1 activity (Harder, Zunino et al. 2004). Sumoylation can alter subcellular localization of protein substrates or protect proteins from ubiquitination. SUMO-1 and its conjugating enzyme Ubc9 have been associated with mitochondrial fission events by stabilizing Drp1 (Harder, Zunino et al. 2004). In contrast, the sentrin/SUMO-specific protease, SENP5, reduces Drp1 levels, thereby preventing mitochondrial fission (Zunino, Schauss et al. 2007). S-nitrosylation, a post- translational modification, has been suggested to also enhance Drp1 pro-fission activity, by inducing dimerization and GTPase activity (Cho, Nakamura et

al. 2009). However, these results have been recently contested by the finding that nitric oxide leads to mitochondrial fission by phosphorylating Ser616 on Drp1 (Bossy, Petrilli et al. 2010). Interestingly, PKA activation also increased Drp1 phosphorylation at Ser656 in adult murine hearts, suggesting Drp1 regulation by phosphorylation in cardiac tissue (Cribbs and Strack 2007). Finally, a recent report has shown that the phosphorylation of Ser600 of Drp1 isoform 3 (equivalent to Ser637 on human Drp1 splice variant 1) by the Ca^{2+}/calmodulin- dependent protein kinase Iα (CaMKIα) resulted in mitochondrial fission, likely due to an increase in hFis1 affinity (Han, Lu et al. 2008).

The pro-apoptotic effect of Mfn2, independent of its mitochondrial morphology role, was found to be mediated through the down-regulation of the PI3K-Akt pathway and executed through the mitochondrial pathway of apoptosis (Guo, Chen et al. 2007). Most recently, the same researchers have implicated PKA in the regulation of Mfn2 in its anti-proliferative actions on vascular smooth muscle cells (VSMCs) in culture, neointimal hyperplasia and restenosis in a rat carotid artery balloon-injury model (Zhou, Chen et al. 2010).

I-2.2.2. Mitochondrial GTPases in healthy cells.

It is known that the dynamic mitochondrial network serves as a means of distribution of mitochondrial DNA (mtDNA) to the progeny of both yeast and mammalian cells (Nunnari, Marshall et al. 1997; Margineantu, Gregory Cox et al. 2002). This function of the fission/fusion processes is highlighted by experiments demonstrating that a loss or dysfunction of these proteins can result in the decrease or total loss of mtDNA from cells (Jones and Fangman 1992; Hermann, Thatcher et al. 1998; Herlan, Vogel et al. 2003; Chen, Vermulst et al. 2010). The dynamic network may also act as a distribution system for other molecules and participate in the process of mitochondrial quality control (Detmer and Chan 2007; Tatsuta and Langer 2008). As the centers of oxygen consumption in the cell, mitochondria sustain a remarkable amount of oxidative damage to the molecules of mtDNA, lipids, and proteins over the course of their lifetimes. It is thought that a dynamic network of circulating mitochondria will be able to help repairing and replenishing damaged mitochondria, their DNA, lipids and proteins from the healthy pool (Detmer and Chan 2007; Tatsuta and Langer 2008). This hypothesis is supported by the fact that blocking fission results in the accumulation of oxidized proteins and that the absence of Opa1 in flies increases ROS production (Yarosh, Monserrate et al. 2008; Tang, Le et al. 2009). Furthermore, extremely damaged mitochondria that lost their $\Delta\Psi_m$ and pH gradient necessary for normal mitochondrial fusion, are degraded by autophagy (Legros, Lombes et al. 2002; Meeusen, McCaffery et al. 2004; Twig, Elorza et al. 2008).

Several studies suggest that mitochondrial fusion frequency indeed plays an important role in vertebrate cells (Enriquez, Cabezas-Herrera et al. 2000). For example, the mitochondria of rat cardiac

muscle and diaphragm skeletal muscle appear as isolated ellipses or tubules in embryonic stages but then reorganize into reticular networks in the adult (Bakeeva, Chentsov et al. 1978; Bakeeva, Chentsov Yu et al. 1983). Secondly, time-lapse fluorescence microscopy of cultured HeLa cells showed mitochondria organized into extensive tubular networks undergoing fusion and fission (Rizzuto, Pinton et al. 1998). Finally, fusion proteins, Mfn1 and Mfn2, have been shown to be essential for mice embryonic development and by enabling fusion, have been suggested to support cooperation between mitochondria, thereby protecting mitochondria from respiratory dysfunction (Chen, Detmer et al. 2003). Independent of this discovery, Mfn2 has also been identified as mitochondrial assembly regulatory factor (MARF) in muscle cells from obese Zucker rats (Bach, Pich et al. 2003), and hyperplasia suppressor gene (HSG) in VSMCs (Chen, Guo et al. 2004), which in part may explain some of the observed non-fusion related effects of Mfn2. Most recently, Mfn2 has been reported to be present in the ER, tethering mitochondria to the ER (De Brito and Scorrano 2008), and allowing the communication of Ca^{2+} between these two organelles. In addition, there are studies suggesting that Mfn2 can protect cerebellar neurons against apoptotic cell death induced by DNA damage, oxidative stress or potassium deprivation (Jahani-Asl, Cheung et al. 2007).

All together, maintaining a healthy mitochondrial population through fission and fusion of the network seems to allow for a tight regulation and modulation of the system and might explain why the proteins that govern these processes are so important for cellular survival.

I-2.2.3. GTPases in cell dysfunction and disease.

Emerging data suggest that changes in mitochondrial morphology may actually be relevant to apoptosis, embryonic development, metabolism, diabetes mellitus, autophagy and various aspects of cardiovascular biology: these include cardiac development, the response to ischemia-reperfusion injury and heart failure.

Under conditions that compromise mitochondrial function, such as mtDNA depletions (Gilkerson, Margineantu et al. 2000) or treatment with mitochondrial toxins (Legros, Lombes et al. 2002), mitochondria often loose connectivity and become short and round. As expected, inhibition of both fusion and fission does not affect mitochondrial morphology whereas genetic inactivation of the fission mechanism leads to an increase of mitochondrial connectivity and genetic inactivation of fusion results in an increase in mitochondrial fragmentation (Otsuga, Keegan et al. 1998; Sesaki and Jensen 1999).

Table I- 1. Disorders associated with mitochondrial perturbations.

Disease	Gene	Mitochondrial Function	Description
CMT2A	*Mfn2*	Fusion	Autosomal dominant peripheral neuropathy
ADOA	*Opa1*	Fusion	Autosomal dominant optic atrophy
Unnamed	*Drp1*	Fission	Neonatal lethality

In fact, the inability to properly regulate mitochondrial morphology has been shown to cause several human diseases. Mutations in Mfn2 (Santel and Fuller 2001) lead to the peripheral neuropathy Charcot-Marie-Tooth syndrome type 2A (CMT-2A; (Zuechner, Mersiyanova et al. 2004)) while mutations in the human profusion gene Opa1 cause autosomal-dominant optic atrophy (ADOA; (Olichon, Emorine et al. 2002)), a disease characterized by progressive blindness due to the loss of retinal ganglion cells and optic nerve atrophy (Delettre, Lenaers et al. 2000) (Table I- 1). However, it is not currently understood how the loss of Opa1 or Mfn2 activity in these diseases is causally linked to cell dysfunction and/or death or why the damage is restricted to particular neuronal tissues despite the ubiquitous expression of both proteins.

I-2.3. Mitochondrial morphology and apoptosis.

Changes in mitochondrial morphology have been linked to apoptotic cell death (Martinou, Desagher et al. 1999). It has been demonstrated that cells undergo mitochondrial fission generating fragmented mitochondria, in response to an apoptotic stimulus. However, the presence of mitochondrial fragmentation does not necessarily indicate that the cell is undergoing apoptosis. Frank and colleagues first demonstrated that the mitochondria of COS cells changed from a reticulo-tubular interconnected network to a fragmented discrete punctiform phenotype in response to the apoptotic inducer, staurosporine. A process which was dependant on the activation and mitochondrial translocation of Drp1 (Frank, Gaume et al. 2001). In turn, transgenic over-expression of the Drp1 dominant negative (Drp1K38A) prevented mitochondrial cytochrome *c* release and apoptotic cell death (Frank, Gaume et al. 2001).

Subsequently, it has been demonstrated that the process of outer mitochondrial membrane rupture (or MOMP), a key step in mitochondrial-induced apoptosis, is actually mediated by a complex interplay between Drp1, the pro-apoptotic protein Bax and Mfn2 which form foci on the outer membrane (Figure I- 7) (Karbowski, Lee et al. 2002). It has been suggested that the formation of Drp1-induced mitochondrial fission sites are required for Bax translocation to the mitochondria, as the over-expression of the anti-apoptotic protein Bcl-XL prevented apoptosis but not mitochondrial

fragmentation (Sheridan, Delivani et al. 2008). Under normal conditions it has been suggested that 20% of Drp1 is associated with mitochondria, and the presence of Bax mediates an increase in mitochondrial Drp1 translocation prior to mitochondrial cytochrome *c* release. The translocation of Drp1 is also regulated by phosphorylation and sumoylation (see section 2.2.1). In addition, it has been proposed that accumulation of Mfn2 at these foci mediates Bax-induced MOMP (Karbowski, Lee et al. 2002). There is the intriguing possibility that these three proteins may form functional units at sites where ER-tethers to mitochondria, thereby introducing Ca^{2+} from the ER into the equation (De Brito and Scorrano 2008). However, it must be appreciated that this pro-apoptotic effect of Mfn2 appears to be independent of its ability to induce mitochondrial fusion. Finally, although Drp1 may dock with hFis1 to induce mitochondrial fission, the latter induces apoptotic cell death independent of both Drp1 and Bax, and does so via the ER apoptosis pathway (Alirol, James et al. 2006) (James, Parone et al. 2003).

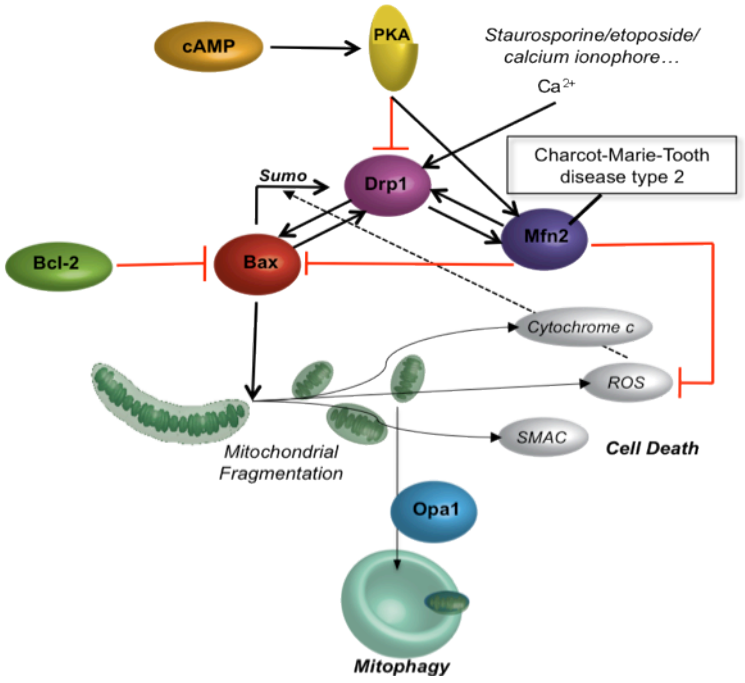

Figure I- 7. Scheme of known interactions between GTPases and apoptotic proteins. Bax is a BH3-only pro-apoptotic effector protein that has been shown to be involved in mitochondrial fragmentation and its action can be counteracted by Bcl-2 anti-apoptotic protein. Recent studies have shown Bax activity is strongly connected to the pro-fission protein Drp1. Fission and Fusion (Mnf2) proteins are present in the cell in a delicate balance that can be disrupted by multiple factors. For example, protein kinase A (PKA) through the cAMP pathway leads to the phos- phorylation of Drp1 and inhibition of mitochondrial fission, leading to a more connected mitochondrial reticulum (networked). In opposition, calcium (Ca^{2+}) levels have been shown to induce Drp1 and Bax promotes Drp1 association with mitochondria in apoptosis trough sumoylation (Sumo). In addition, Mfn2 has been shown to reduce ROS levels, which are associated with sumoylation events. Finally, Opa1 expression was detected in mitophagy, an event that once again is related with mitochondrial morphology and clearance of dysfunctional mitochondria. (For detailed description and literature references please see I- 2.2. section).

In contrast to fission, mitochondrial fusion plays a protective role in apoptosis. Inhibition of mitochondrial fusion facilitates cell death in response to some apoptotic signals (Olichon, Baricault et al. 2003; Sugioka, Shimizu et al. 2004). Mitochondrial fusion is reduced following induction of apoptosis (Karbowski, Arnoult et al. 2004) and over-expression of mitofusins can reduce the level of apoptosis (Sugioka, Shimizu et al. 2004). Depletion of Opa1 or mitofusins results in poor cell growth (Chen, Chomyn et al. 2005) and enhances susceptibility to apoptotic stimuli (Olichon, Baricault et al. 2003; Lee, others et al. 2004; Sugioka, Shimizu et al. 2004).

All together, fission and fusion-related proteins seem to be involved in life and death decisions. Further studies are necessary to elucidate the underlying mechanisms.

I-2.4. Mitochondrial morphology and autophagy.

Emerging studies suggest mitochondrial morphology to be essential in the selection of damaged depolarized mitochondria for removal by autophagosomes (mitophagy) (Twig, Elorza et al. 2008; Mouli, Twig et al. 2009). It is now accepted that mitochondrial fusion enables the transfer of soluble and membranous components (including mtDNA) between neighboring mitochondria, thereby providing a mechanism for renewing function in damaged mitochondria (Detmer and Chan 2007; Tatsuta and Langer 2008). Specifically, selective mitochondrial fusion between two polarized mitochondria occurs along with mitochondrial fission (division) that results in one polarized daughter mitochondria and one depolarized mitochondria to be degraded (Twig, Elorza et al. 2008). This mechanism further supports the theory that the frequency and selectivity of fusion is required to maintain healthy mitochondrial function and allow mitophagy to take place (Sheridan, Delivani et al. 2008).

I-2.5. Mitochondrial morphology and metabolism.

The idea that changes in mitochondrial morphology influence mitochondrial metabolism was introduced in 1988, even before the identification of the first mitochondrial shaping proteins (GTPases). Amchenkova and co-workers noted that mitochondrial clusters in cardiomyocytes and long mitochondrial filaments in fibroblasts were electrically interconnected, allowing the movement of energy from the cell to the periphery (Amchenkova, Bakeeva et al. 1998). The mitochondrial fusion proteins, Mfn2 and Opa1, play relevant roles in mitochondrial metabolism. Knock-down of Mfn2 has been demonstrated to reduce $\Delta\Psi_m$, lower oxygen consumption, and reduce substrate oxidation, resulting in less oxidative phosphorylation and increased dependency on anaerobic glycolysis, with a higher rate of glucose uptake and a lower rate of glycogen synthesis (Bach, Pich et al. 2003; Pich,

Bach et al. 2005). Furthermore, the lack of Mfn2, may reduce Ca^{2+}-dependent increases in mitochondrial respiration due to a loss of tethering between the ER and mitochondria (De Brito and Scorrano 2008). Oppositely, mitochondrial metabolism and oxidative phosphorylation are increased under Mfn2 over-expression (Pich, Bach et al. 2005). Knock-down of Opa1 results in similar effects with lower $\Delta\Psi_m$ and decreased respiration rates via reduced activity of complex I, II and III of the electron transport chain (Olichon, Baricault et al. 2003; Chen, Chomyn et al. 2005). However, the over-expression of Opa1 does not improve mitochondrial respiration (Chen, Chomyn et al. 2005). In the same manner, the knock-down of the mitochondrial fission protein, Drp1, shows similar effects (Benard, Bellance et al. 2007), suggesting that any shift in the mitochondrial network has a negative impact on metabolism. Nevertheless, it is not yet clear if the effects on mitochondrial metabolism are caused by the pleiotropic actions of these proteins or are instead a result of mitochondrial morphologic changes.

I-2.6. Mitochondrial morphology and heart disorders.

The process of mitochondrial fission has been implicated in the pathogenesis of adult skeletal muscle atrophy, a condition that is executed by the autophagy-lysosomal and ubiquitin–proteasomal systems. Namely, inhibition of Drp1 and hFis1 prevented the development of skeletal muscle atrophy while over-expression of the pro-fission machinery induced skeletal muscle wasting via AMPK activation (Romanello, Guadagnin et al. 2010).

Parra and co-workers found that, in primary neonatal cardiomyocytes, ceramide-induced mitochondrial fragmentation was co-occurring with elevated levels and co-localization of Drp1 and hFis1 and increased cell death (Parra, Eisner et al. 2008).

Brady and co-workers were the first to show extensive fragmentation of mitochondria in HL-1 cells (a murine atrial derived cardiac cell line) as a response to simulated ischemia-reperfusion (Brady, Hamacher-Brady et al. 2006). Ong and colleagues identified Drp1 activation in the same experimental setup and demonstrated that the fragmentation process can be largely prevented by expression of the Drp1 dominant negative version (Drp1K38A) (Ong, Subrayan et al. 2010). Nevertheless, the actual interplay between mitochondrial fragmentation, ROS production and mitochondrial respiration requires further investigation. Importantly, the pre-treatment of HL-1 cells with mdivi-1 (a recently described small molecule Drp1 inhibitor), was beneficial in a similar manner, confirming the cardio-protective effects of inhibiting mitochondrial fission (Ong, Subrayan et al. 2010).

I-2.7. Mitochondrial morphology and neurodegenerative disorders.

Different cells and tissues have distinct sensitivities and responses to mitochondrial dysfunction. These differences are probably due to the cell-type specializations that rely on particular functions of mitochondria.

Table I- 2. Mitochondrial proteins mutated in neurodegenerative diseases.

Disease	Gene	Function
Charcot-Marie-Tooth type 2A	MFN2	Mitochondrial fusion
Charcot-Marie-Tooth type 4A	GDAP1	Mitochondrial dynamics/fission?
Dominant optic atrophy	OPA1	Mitochondrial fusion and cristae structure
Recessive optic atrophy	OPA3	Unknown
Leber's hereditary optic neuropathy	ND genes in mtDNA	Oxidative phosphorylation
Hereditary spastic paraplegia	Paraplegin	Mitochondrial ATPase/protease
Hereditary spastic paraplegia	HSP60	Mitochondrial heat shock protein
Familial amyotrophic lateral sclerosis	SOD1	Superoxide dismutase
Familial Parkinson's disease	PINK1	Mitochondrial serine/threonine kinase
Friedreich's ataxia	Frataxin	Formation of iron-sulphur clusters in mitochondria

(ND- NADH dehydrogenase subunit. Please see Abbreviations list)

Neurons appear particularly vulnerable to mitochondrial dysfunction, and many mitochondrial dysfunctions result in neurodegeneration (Table I- 2). In part, this vulnerability may be due to their extreme physical dimensions and the need to actively recruit mitochondria to nerve terminals. Classic mitochondrial encephalomyopathies caused by mtDNA mutations are often characterized by neurological symptoms (Dimauro and Davidzon 2005; Taylor and Turnbull 2005). Prominent are those associated with movement, such as ataxia, dysarthria and peripheral neuropathy. Mutations in mitochondrial proteins that are encoded in the nucleus have also been linked to neurodegenerative diseases (Beal 2005).

I-3. Mitochondrial morphology analysis.

Phenotypic heterogeneity in cellular populations has been widely observed and is the source of innumerous speculations. However, finding the possible explanations for cellular heterogeneity in mammalian biology and disease is an exceptionally challenging problem due to the intricacy of cellular phenotypes, the large possibilities of perturbations, and the lack of methods for separating meaningful biological information from noise. In particular, given the large variability of mitochondrial shapes and position, the standardization of a method to correctly classify mitochondrial morphology has been proven challenging.

Recently, high-throughput image-based assay technologies and high-content analysis, have become a useful tool for drug discovery (Gerlich, Beaudouin et al. 2001; Jones, Carpenter et al. 2009; Held, Schmitz et al. 2010), small molecule screening (Tanaka, Bateman et al. 2005), subcellular localization (Huang and Murphy 2004; Lin, Tsai et al. 2007), etc. These methodologies allow for visualization, tracing and quantification of cellular and morphological changes in high resolution and play an increasingly important task in understanding biological processes.

Over the past years, the cost of acquiring a large number of microscopic cell images has been decreasing and thus the range and power of analysis tools must increase (for a recent example see (Neumann, Walter et al. 2010)). Correlating drug influences to morphological changes of mitochondria has become increasingly important mainly due to its connection to apoptosis, disease and aging process.

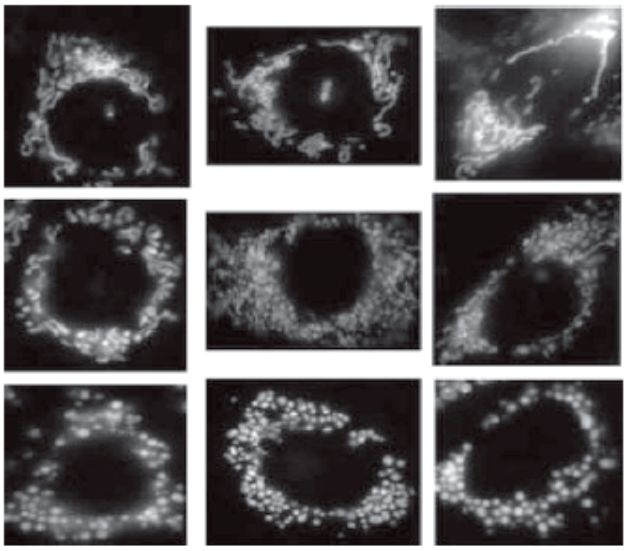

Figure I- 8. Representative microscopic fluorescent images of single cells with different levels of mitochondrial fragmentation. Intact mitochondria form filamentous networks (top row), completely fragmented mitochondria have round shape (bottom row) and partially fragmented mitochondria (middle row). (Figure extracted from (Lin, Lin et al. 2010)).

Figure I- 8 shows representative cell images with different levels of mitochondrial fragmentation (Lin, Lin et al. 2010). It becomes clear that intact or completely fragmented mitochondria are relatively easy to recognize, but it is difficult to quantify partial fragmentation. In fact, in addition to fragmentation, mitochondria may become tubular, shortened, elongated or swollen. All these morphological changes are important biological indicators as discussed in section I-2. Nonetheless, off-the-shelf analysis software is only able to distinguish morphological patterns at cellular level and no partial modification or mixture of patterns at subcellular level can be readily detected. In addition, quantification requires human inspection, which is infeasible for high-throughput screening (Taguchi, Ishihara et al. 2007).

I-3.1. The challenge in mitochondrial image analysis.

Given the emerging importance of mitochondrial plasticity in cell signaling pathways and metabolism, it is essential to develop tools for quantitative analysis of mitochondrial morphology in a cell population-based manner. In some cells like neurons, a highly dynamic organization of mitochondrial networks can be achieved by these organelles moving along the cytoskeleton and attaching to the cytoskeleton using specific motor and connector proteins (Huang, Fowler et al. 2004). Alternatively, in adult cardiomyocytes mitochondria are organized in a "lattice" of parallel rows surrounding the contractile myofilaments and are rather fixed in their positions (Figure I- 9) (Vendelin, Béraud et al. 2005; Beraud, Pelloux et al. 2009).

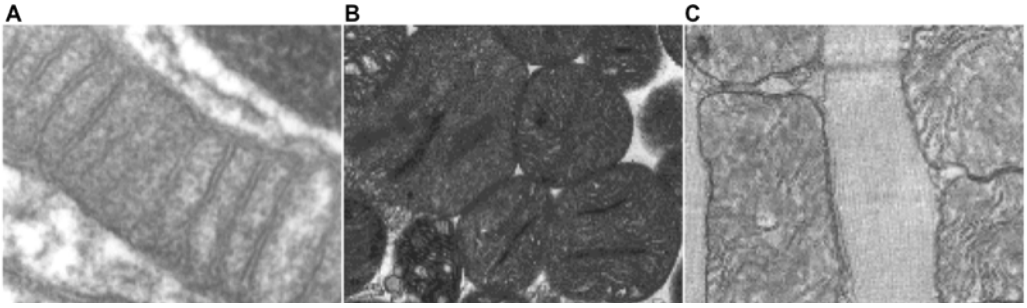

Figure I- 9. Three examples of mitochondrial distinct arrangements in different cell types. (A) Human lung cells. **(B)** Human muscle cells. **(C)** Cardiac muscle cells. (TEM images can be publically accessed at http://cellimages.ascb.org/cdm4/terms.php).

I-3.2. Current status.

Mitochondrial imaging has been used intensively to analyze functional and morphological characteristics of mitochondria in living cells, as well as their intracellular distribution and arrangement (McConnell, Stewart et al. 1990; Dimmer, Fritz et al. 2002; Altmann and Westermann 2005; Meeusen, DeVay et al. 2006; Soubannier and McBride 2009). Recently developed methods include: fluorescence resonance energy transfer (FRET) for imaging protein-protein interactions and conformational changes; recording the image data in three spatial dimensions over time (i.e. 4D imaging), as well as 4Pi and STED microscopy (for review see (Jakobs 2006)). Various EM imaging techniques permit both spatial and temporal study of mitochondrial morphology and function. Several mitochondria-specific markers or fluorescent proteins specifically targeted at mitochondria are now widely used in combination with high-resolution imaging techniques. These imaging approaches are the most direct means of visualizing the intracellular heterogeneity of mitochondria and mitochondrial function.

However, the clear disadvantage of EM is that it offers only a snapshot in time and space, which does not provide direct information of mitochondrial dynamics or mitochondrial morphology. For example, the detection of elongated mitochondria in the adult heart can be due to an increased rate of mitochondrial fusion, but can also result from reduced mitochondrial fission. In fact, several groups have invested on the establishment of experimental methods for assessing the process of mitochondrial fusion. *In vitro*, these are based on a polyethylene glycol (PEG) assay, in which the mitochondrial fusion events are followed by the combination of mitochondrial red and green fluorescent proteins (Legros, Lombes et al. 2002). More recently, an *in vitro* quantitative assay for mitochondrial fusion based on Renilla Luciferase complementation has been described (Huang, Choi et al. 2010). *In vivo*, the process of mitochondrial fusion can be tracked using photo-activatable mitochondrial green fluorescent protein (PA-GFP) (Twig, Graf et al. 2006). However, these two methods suffer from a

number of technical problems and are not very robust. For example, the PEG-fusion alone is likely to affect the natural kinetics of mitochondrial fusion and the required addition of cyclohexamide can be problematic. On the other hand, the PA-GFP approach is time consuming (several hours) and refers to one single cell at a time, making statistical analysis very tedious.

I-3.3. Limitations in current methods.

One of the basic limitations in the study of mitochondrial dynamics has been the dependence on semi-quantitative analysis of mitochondrial phenotypes within cell, which are labor-intensive, low-throughput, require complex imaging techniques and therefore are of low statistical significance.

The majority of the mitochondrial studies reports mitochondrial changes between two subjective classes: 'Fragmented' or 'Fused'. These classifications cannot distinguish whether the observed phenotypes are the result of an increase in fusion rates or decrease in fission. In addition, mitochondrial phenotypes are not limited to this classical binary state of fragmented/fused. Researchers have also reported donut-shape, swollen or disk-shaped mitochondria (Benard and Rossignol 2008; Sauvanet, Duvezin-Caubet et al. 2010). For example, upon over-expression of PINK1 in neuronal cells, mitochondrial become donut-shaped (Cui, Tang et al. 2010) and in human skin fibroblast, swollen-mitochondria can occur as a result of bioenergetics perturbation and along with mitochondrial membrane permeabilization (Pham, Richardson et al. 2004). Furthermore, the classification methods to date are greatly based on human interpretation, which does not allow for identifying mitochondria in an intermediate stage. Finally, most approaches do not conceal intracellular variability as well as whole cell-population heterogeneity (intercellular variability).

It is clear that mitochondrial dynamics play an important role in many diseases, most notably Parkinson's Disease and other neurodegenerative conditions (Chan 2006), as well as metabolic disorders such as diabetes (Chen and Chan 2009). The integration of scientists from these fields into the study of mitochondrial dynamics will depend upon the availability of robust and transferable assay systems to quantify mitochondrial fusion.

I-4. Data-driven modeling: integration of heterogeneous datasets.

Modeling techniques are largely data-driven and aim to discover correlations among signals or between signals and cellular phenotypes (Figure I- 10). These methods include principal component analysis (PCA) and partial least-squares regression (PLSR) (Friedman 2004; Janes and Yaffe 2006; Harder, Mora-Bermudez et al. 2009). In contrast, differential equation-based models are highly specified and dependent on prior knowledge about the players and their interactions, while having the advantage to capture temporal and spatial dynamics at the level of individual reactions (Levchenko, Bruck et al. 2000; Chakraborty, Dustin et al. 2003; Wiley, Shvartsman et al. 2003; Hlavacek, Faeder et al. 2006). Between these extremes, modeling methods such as Bayesian statistics, hidden Markov models, and logic-based models have been used to construct graph-based representations of influences and dependencies among signals and phenotypes based on experimental data (Weng, Bhalla et al. 1999; Said, Oppenheim et al. 2003; Bulashevska and Eils 2005; Sachs, Perez et al. 2005; Margolin, Wang et al. 2006; Price, Trent et al. 2007). An advantage of the latter methods is that they can be applied to situations where the mechanistic information is missing (incomplete or fragmentary) but there is a general notion of the interacting biochemical species network.

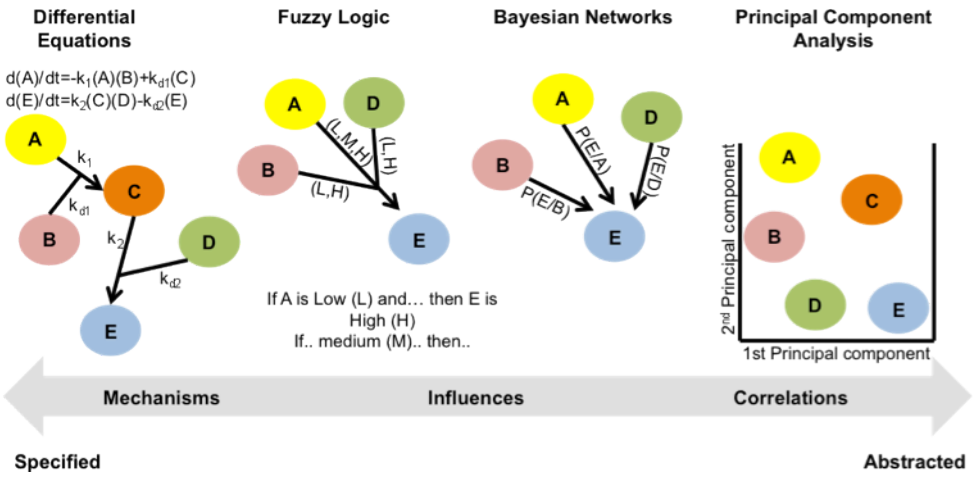

Figure I- 10. Spectrum of modeling methods. Modeling techniques balance specificity and complexity. Principal component analysis (PCA) elucidates correlations among network components (A–E) by a linear transformation of the data, resulting in orthogonal principal components. Bayesian networks use conditional probabilities to associate correlations and influences between network components. Fuzzy logic (FL) uses rule-based gates and probabilistic representation of input variables to quantify influences and mechanism that regulate network species. Differential-equations models using mass-action kinetics are highly specified defining regulatory mechanism by defining rates of change in network species concentrations. (Figure adapted from (Aldridge, Saez-Rodriguez et al. 2009)).

In order to choose a modeling method, it is first necessary to evaluate the type of question being posed (e.g., mechanistic or phenotypic), the prior knowledge about the network (interaction map or detailed biochemical pathway) and finally, the quality and type of experimental data (quantitative or qualitative). In our study, multivariate, heterogeneous datasets were produced concerning mitochondrial morphology and apoptotic steps. Thus, it was necessary to establish a modeling approach that could combine heterogeneous datasets and infer linear and non-linear relations between the relevant players.

I-4.1. Fuzzy logic approach.

The concept of fuzzy logic (FL) was conceived by Lotfi Zadeh (Zadeh 1965) and presented as a way of processing data by allowing partial-set membership rather than crisp-set membership or non-membership. This set theory-based approach was first applied to control systems in the 70´s, once there was sufficient small-computer capability (Wang and Tan 1997; Cabrera, Cordero et al. 2009). FL deals with imprecise inputs, is inherently robust, and can process any reasonable number of inputs. Simple, plain-language "IF X AND Y, THEN Z" rules are used to describe the desired system response in terms of linguistic variables rather than mathematical formulas (Banks 2003). The number of rules is of course dependent on the number of inputs, outputs, and the creator's control response interests. FL's approach to control problems mimics how a person would make decisions, only much faster. Thereby, it offers a simple way to obtain a definite conclusion based upon vague, ambiguous, imprecise, noisy, or missing input information. In addition, it conveys the possibility to integrate heterogeneous datasets, originated from different experimental protocols. Unlike the above referred methods, FL is able to identify linear, as well as non-linear relations within the data (Cabrera, Cordero et al. 2009).

II- OBJECTIVES

Given that mitochondrial morphology is dramatically altered during apoptosis and proteins controlling morphological states influence cell death, the overall goal of this project was to determine the relationship between changes in mitochondrial morphology during various modes of programmed cell death. To that end, the following four aims were proposed.

Aim 1. Establish an experimental approach for detection of mitochondrial morphology in living cells.

Aim 2. Implement a computational platform that enables automated classification of mitochondrial morphology in response to diverse apoptotic stimuli.

Aim 3. Perform single cell-based quantitative measurements of mitochondrial function and dysfunction.

Aim 4. Integrate and relate mitochondrial morphology and cell death datasets to infer causalities among the relevant players.

Aim 1- We aimed to establish standards for imaging acquisition, feature extraction, data handling and image processing. This included the selection of control conditions for the main phenotypes: Networked/Fragmented/Swollen. Therefore, high-content microscopy was used to image GFP-tagged mitochondria under established pro-apoptotic insults and rich-feature extraction was performed.

Aim 2- We aimed at developing a process to resolve mitochondrial morphology classification in an unbiased and statistically significant manner. Therefore, we built a supervised learned algorithm based on the initially extracted mitochondrial features. For the first time, it is possible to distinguish intermediate states of mitochondria in a subcellular level while capturing whole cell population variations.

Aim 3- Next we wanted to relate mitochondrial morphology with cell death mechanisms. For that purpose, we have acquired diverse data-types in matching conditions that are directly related to mitochondrial injury, such as Bax activation and mitochondrial membrane permeability assays. In addition, we assessed mitochondrial cell death events by monitoring cytochrome *c* release, ROS production and ultimately, total cell death.

Aim 4- In order to combine and correlate mitochondrial morphology with cell death-related mitochondrial injury, we have established a fuzzy logic modeling approach. This allowed for the integration of all the heterogeneously acquired datasets, the easy inference of hierarchical relations and the unraveling of non-linear interactions.

General Conclusions and Perspectives- Our approach established and validated for human breast cancer cells can now be extended to include new phenotypic classes of mitochondrial morphology and new cell death datasets according to future studies interests. Importantly, our predicative modeling-results are in accordance with published data, thereby sustaining the utility of our approach in future work aimed at determining the importance and role of mitochondrial network maintenance in the regulation of apoptotic cell death.

III- MATERIALS AND METHODS

III-1. MATERIALS

III-1.1. Laboratory equipment.

8-well imaging µ-slide	IBidi
Balance	KERN- ALJ 220-4
Centrifuges	Beckman Coulter
Culture Flasks	TPP, Techno Plastic Products AG
DeltaVision Deconvolution Microscope	Olympus IX71, Applied Precision
Flow cytometer	B FC500 MPL , Beckman Coulter
Freezer (-80°C, -20°C, 4°C)	LIEBHERR
Glass bottom plates (6, 24 and 96 wells)	PerkinElmer
Incubator	NUAIRE™ DHD Auto Flow (CO2 air injecter)
Inverted Microscope	Olympus CKX41, Applied Precision
Pipettes, adjustable	Eppendorf AG, Hamburg
Plate Reader	Infinite M200, Tecan Austria GmbH
Sterile Hood	NUAIRE™ Class II
Thermo-shaker	Eppendorf
Vortex	Heidolph Reax
Water Bath	GFL, Labsource

III-1.2. Chemicals and antibodies.

Alexa Fluor 546	Invitrogen
Alexa Fluor 647	Invitrogen
Anti- COXIV	Cell Signalling
Anti- cytochrome *c*	BD Pharmingen
Artesunate	Saokim Ltd
Bongkrekic acid	Santa Cruz Biotechnology
Bovine serum albumin, BSA	Sigma
C-6 ceramide	Biozol

Calcium chloride, $CaCl_2$	Applichem
Camptothecin	BioVision
CCCP	Calbiochem
CellMask™ Deep Red	Invitrogen
Cyclosporin A, CsA	Calbiochem
DMEM, culture medium	Invitrogen
DMSO	Sigma-Aldrich
Ethidium Bromide	Applichem
FBS, serum	Invitrogen
Glucose	Applichem
Glutamax	Invitrogen
Glutamax	Invitrogen
H_2DCF- DA	Invitrogen
HEPES	GENAXXON Bioscience
Hoechst 33342	Sigma
Hoechst 33342	GENAXXON Bioscience
Immersion Oil	Applied Precision
Immersion Oil (N=1.516)	Applied Precision
Krebs- Henseleit	Sigma
Magnesium sulfate, $MgSO_4$	Applichem
NAA solution	PAA laboratories
Neomycin, G418	Carl Roth GmbH
Oligomycin	Sigma
Paraformaldehyde, PFA	EMS- Electron Microscopy Science
Penicilin/Streptomycin	MERCK
Potassium chloride, KCl	AnalaR NORMAPUR
Potassium dihydrogen phosphate, KH_2PO_4	Applichem

Propidium Iodide, PI	Invitrogen
Sodium chloride, NaCl	AnalaR NORMAPUR
Sodium hydrogen carbonate, $NaHCO_3$	Applichem
Thapsigargin	Calbiochem
TMRM	Invitrogen
TNFα	BASF
TRAIL	R&D Systems
Triton X-100	Sigma
Trypsin	GIBCO, Tryple™ Express

III-1.3. Kits.

DNA purification	Qiagen
Effectene transfection	Qiagen

III-1.4. Software.

Figure Preparation	PowerPoint (V 12.2.9), Illustrator CS3 (V 13.0.0) and Photoshop CS3 (V 10.0)
Flow Cytometer	MXP Cytometer (V 2.2)
Fuzzy Logic Modeling	Matlab (R2009a)
Image Processing	ImageJ (V 1.44o)
Microscope Deconvolution	Softworks (V 3.5.1)
Mitochondrial Morphology Analysis	CellProfiler (V 1.0.5811)
Random Forest Classifier	R (V 2.10)
Tecan Plate Reader	Magellan (V 6.3)

III-2. METHODS

Standard molecular biology methods were used according to Sambrook and colleagues and are not described in detail (Sambrook and Russell 2001). All centrifugations were performed at 4°C.

III-2.1. Cell culture techniques.

Human breast carcinoma MCF-7 cells (Cell Lines Services, Heidelberg) were cultured in DMEM medium supplemented with 10% FBS, 1% penicillin/streptomyci, 1% glutamax and 1% nonessential amino acids in a 37°C, 5% CO_2 incubator. For microscope imaging procedures, cells were incubated in basic salt solution (BSS; Krebs- Henseleit supplemented with- in mM: 110 NaCl, 4.7 KCl, 1.2 KH_2PO_4, 1.25 $MgSO_4$, 1.2 $CaCl_2$, 25 $NaHCO_3$, 15 glucose, 20 HEPES, pH 7.4) or phenol red-free DMEM. Cells were seeded overnight before transfection or a specific treatment in the following densities:

a) 6 well plate- 30 x 10^5 cells per well or 15 x 10^5 cells per well (for transfection);

b) 8-well imaging µ-slide- 5 x 10^5 cells per well or 2.5 x 10^5 cells (for transfection)

c) 24 well plate- 4 x 10^5 cells per well or 2.5 x 10^5 cells per well (for transfection);

d) 96 well plate- 1.5 x 10^5 cells per well.

III-2.1.1. Transfection and expression plasmids.

Cells seeded overnight were transfected with Effectene transfection kit according to manufacturer description. Final reagent concentrations have been previously optimized in the lab for adherent MCF-7 cells achieving on average ~40% and ~60% transfection efficiency, respectively, without detectable toxicity (Table III- 1).

Table III- 1. Effectene Transfection Reagents- adjusted for the different cell culture formats.

Culture format	DNA (µg)	Enhancer (µl)	Final volume of DNA in buffer EC (µl)	Effectene reagent (µl)	Volume of medium to add to cells (µl)	Volume of medium to add to complexes (µl)
iBidi	0.15	1.2	50	4	150	100
96-well	0.1	0.8	30	2.5	100	0
24-well	0.2	1.6	60	5	350	350
6-well	0.4	3.2	100	10	1600	600

(for detailed protocol please see Qiagen product-sheet)

Briefly, the DNA of interest was diluted in EC buffer and incubated for 5 minutes at room temperature (RT) following addition of Enhancer. Then, the non-liposomal lipid reagent Effectene was added and the mixture was incubated for an additional 10 minutes. Fully supplemented (containing serum and antibiotics) DMEM medium was added and the transfection complexes were immediately added to cells. Medium was exchanged after 16-24 hours.

a) Mitochondrial imaging.

In order to visualize individual mitochondria, MCF-7 wild type (wt) cells were transfected with plasmids encoding proteins from the inner and outer mitochondrial membrane tagged with a fluorescent probe:

- Inner Membrane: mito-GFP and mito-mCherry- fusion of the localization tag of Cytochrome c oxidase IV (COXIV) (Rizzuto, Dsandona et al. 1990);

- Outer Membrane: mitoNEET-GFP- fusion of the localization tag of mitoNEET (kindly provided by Professor Jack E. Dixon (Wiley, Murphy et al. 2007)).

Positive clones were selected using G418 (1mg/mL). Stable cell lines were generated from single colonies in order to minimize genetic background.

b) Mitochondrial morphology.

Regulation of fission machinery was achieved by over-expression of Drp1-pcDNA3.1. (pro-fission) or its dominant negative Drp1K38A-pcDNA3.1. (constructs were kindly provided by Dr. Alexander M. van der Bliek (van der Bliek 2000)). MCF-7 wt cells were transiently co-transfected with mito-mCherry or mCherry-pcDNA3.1 in a 1:2 proportion and analyzed 24 hours after transfection.

c) Apoptosis imaging.

For cell death analysis, we made use of constructs previously established in the lab (by Dr. Anne Hamacher-Brady and Dr. Nathan Brady). Namely, tBid-mCherry, Bnip3-mCherry, GFP-Bax, mCherry-Bax and mCherry-Bak were transfected and data was collected 24 or 48 hours after transfection. MCF-7 cells stably expressing GFP-Bax were achieved by G418 (1mg/mL) selection. Stable cell lines were generated from single colonies in order to minimize genetic background.

Finally, MCF-7 wt cells were transiently transfected AIF-GFP construct (kindly provided by Dr. Ruth Slack (Cheung 2005)) to monitor its release from the mitochondrial after mitochondrial membrane permeabilization induction.

III-2.2. Survival assay by flow cytometry.

Flow cytometric measurements were carried out with a modified flow cytometer FC500 MPL (Beckman Coulter). Modification enabled the simultaneous detection of GFP, mCherry and YFP fluorescence. To this end, the standard argon-Ion laser (488 nm; 20 mW; Cyonics) was exchanged with a Sapphire 488 nm; 20 mW and a Compass 561 nm; 40 mW laser. Furthermore, the Radius 635 nm laser was exchanged with a Radius 405 nm; 25 mW laser. All three lasers (405 nm, 488 nm and 561 nm) were aligned collinearly. Additionally, the FC500 MLP is equipped with a multi-plate-loader (MLP), allowing automatic sampling of multi-well plates (6 to 96 wells format). MCF-7 cells were plated in 24 well plates and transfected with constructs of interest labeled with mCherry fluorescent protein. As an index of cell viability we measured the percentage of mCherry-positive cells by flow cytometry every 24 hours, for up to 144 hours after transfection. At least 1000 events were collected for each well. To minimize non-specific compound effects, each experiment was carried out in parallel with the respective fluorescent protein alone (mCherry). For each sample, cell number and mean fluorescence intensity were reported by the bundled software (MXP V 2.2). All measurements were first normalized to control conditions inside each plate (to allow comparison between 24-well plates) and then corrected for unspecific changes by normalization to the mean of the respective constructs, measured under identical conditions (of at least 3 independent experiments). The mean of all normalized experiments was then expressed as %-changes to the control, as indicated.

III-2.3. Widefield fluorescence microscopy (WFM).

Cells were plated in glass-bottom 8-well µ-slides (iBidi) and imaged with a DeltaVision deconvolution microscope, Olympus IX71-WFM (Applied Precision, USA). The microscope is equipped with a 20x lens (air 0.3 N.A., Hoffman), a 40x (air 1.2 N.A, Hoffman) and a 63x objective (1.4 N.A. oil immersion lens, Hoffman), a Z-motor and Peltier cooled CCD camera (Photometrics). Automated excitation and emission filter wheels are controlled by an Applied Precision nanochassis that also drives the stage motor (Hewlett Packard Vectra), the filter wheel, the neutral density and the shutters. It is linked to a 100 watts mercury lamp for illumination and contains a polychroic filter providing excitation and emission wavelengths for DAPI or Hoechst (blue), FITC or GFP (green), rhodamine (red) and Cy-5 (far red). Life-cell imaging was performed with a temperature and CO_2 controller (CROMAPHOR). When mentioned, Z-stacks were acquired with 0.22 um increments and images

were deconvolved to maximize spatial resolution by Softworxs software (version 3.5.1). After deconvolution, images were further processed by the ImageJ software or CellProfiler (CP) modules.

III-2.4. Cell death assays.

Drugs were selected which initiate mitochondrial apoptosis in a spatially heterogeneous manner. Death receptor (DR) ligands TNFα (43 ng/mL) and TRAIL (20 ng/mL) activate the mitochondrial death pathway via caspase 8-mediated cleavage of Bid (Li, Zhu et al. 1998). The endoplasmic reticulum (ER) calcium (Ca^{2+}) pump inhibitor thapsigargin (1 μM) induces ER stress, cytosolic Ca^{2+}, and subsequent activation of BH3-only proteins (Puthalakath, O'Reilly et al. 2007). Camptothecin (2 μM), a DNA topoisomerase I inhibitor, induces mitochondrial apoptosis (Shimizu and Pommier 1997). The pro-apoptotic lipid second messenger ceramide (300 μM) is known to induce mitochondrial fragmentation (Parra, Eisner et al. 2008). Bioenergetic perturbations were induced with oligomycin (10 μM), which inhibits oxidative phosphorylation at the mitochondrial ATP synthase (Penefsky 1984) and CCCP (carbonyl cyanide mchlorophenylhydrazone; 20 μM) a known mitochondrial membrane uncoupler (Ganote and Armstrong 2003).

Drug stocks were prepared according to manufacturer instructions. Drugs were diluted in basic salt solution (BSS) before application and cells were incubated for 6 hours at 37°C prior to all measurements unless stated otherwise.

III-2.4.1. Assessment of mitochondrial morphology.

MCF-7 cells stably expressing mito-GFP were seeded overnight in an 8-well imaging μ-slide (iBidi) and treated with the above-described apoptotic drugs. Nuclei were stained with Hoechst (100 ng/mL) for 1 minute prior to imaging. Live cells were imaged using a 63x oil objective (NA 1.40) and Z-stacks with 0.22 μm step sizes were collected and subsequently deconvolved using the bundled SoftworX software. The estimated middle slice of the Z-stack was most representative of cellular mitochondrial content under all conditions, and was chosen for following analysis.

III-2.4.2. Quantification of mitochondrial injury.

III-2.4.2.1. Bax activation.

GFP-Bax redistribution was used as a parameter to quantify irreversible cellular injury (Wolter, Hsu et al. 1997). MCF-7 cells stably expressing GFP-Bax were incubated for 6 hours with the respective compounds or transfected with constructs of interest (e.g. tBid, Drp1) and nuclei were stained with

Hoechst (100 ng/mL) before imaging (40x air objective, NA 1.20). 10 Z-stacks were acquired per condition and Z-maximum projections were performed prior to analysis. 3D rendering was performed for representative images. Cells were scored as cells with (i) diffuse or (ii) punctate mitochondrial GFP-Bax fluorescence. For each drug treatment, approximately 500 cells were classified in at least 5 independent experiments.

III-2.4.2.2. Mitochondrial membrane potential ($\Delta\Psi_m$).

Rhodamine-based dyes are commonly used probes for $\Delta\Psi_m$ detection. Tetramethylrhodamine methyl ester (TMRM) accumulates electrophoretically in the matrix of actively respiring mitochondria and is released once $\Delta\Psi_m$ is impaired (Métivier, Dallaporta et al. 1998; Bernardi, Petronilli et al. 2001). TMRM is arguably the preferable $\Delta\Psi_m$ indicator, as it exhibits the least amount of matrix binding and inhibition of respiration, compared to tetramethylrhodamine ethyl ester (TMRE) and Rhodamine 123 (R123), two other commonly employed $\Delta\Psi_m$ indicators (Hüser, Rechenmacher et al. 1998).

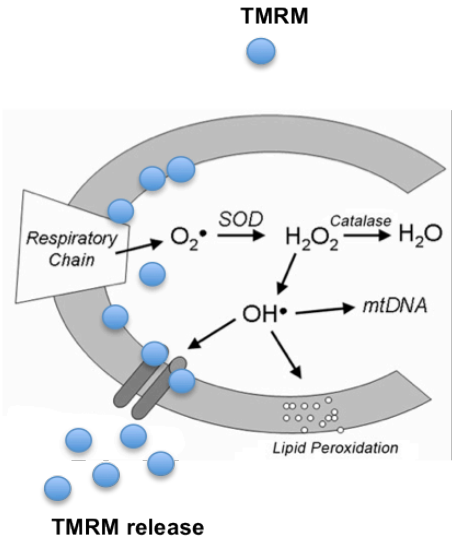

Figure III- 1. Schematic cartoon illustrating the TMRM assay. Upon photon-illumination, reactive oxygen species (ROS) are formed (e.g. $OH^{\bullet}$, $O_2^{\bullet}$) that lead to mitochondria membrane permeabilization and TMRM dye release from the intermembranar space to the cytosol. (Figure adapted from (Szeto 2006)).

We found that 25 minutes incubation of 25 nM TMRM at 37°C resulted in photo-oxidatively activated local fluctuations in $\Delta\Psi_m$ signal that were apparent as localized decreases in TMRM mitochondrial fluorescence. Thereby, after 6 hours treatment with respective drug, TMRM was added and sequential images were acquired every second, over a period of 5 minutes to induce photo-toxicity (Figure III-1).

For inhibition of the mitochondrial permeability transition pore (MPTP), MCF-7 wt cells were pre-incubated in cyclosporine A (CsA, 5 μM) for 30 minutes at 37°C or pre-treated with bongkrekic acid (BA, 50 μM) for 1 hour at 37°C. Imaging was performed using a 40x air objective (NA 1.20) and exposure times were identical for each condition. The estimated middle Z-stack was followed for this time period.

$$StDev\_decay(t/2) = \frac{(\max imum + \min imum)}{2}$$

Equation III- 1. Equation employed in MATLAB script to extract $t_{1/2}$_decay parameter from StDev curves of TMRM signal.

The release kinetics of the dye is here reported by measure of the standard deviation (StDev) of the signal intensity throughout each individual cell. Under normal conditions, mitochondrial TMRM is highly localized (high StDev) and upon $\Delta\Psi_m$ loss, redistribution of the probe throughout the cell occurs and the overall signal decreases per cell, so does the StDev. From the StDev curves plotted for each condition, three parameters were extracted by using an automated MATLAB script: (i) $t_{1/2}$_decay: time for the signal to reach half of its initial value; (ii) Y_spread: total signal decrease over time; (iii) MAX: initial signal maximum value. The median of the first and last 10 points of each data set were used to calculate the maximum and minimum intensity. The $t_{1/2}$_decay is defined as the timepoint at which the StDev of the signal reaches half of its initial starting value (see Equation III- 1).

III-2.4.3. Quantification of cell injury.

III-2.4.3.1. ROS detection.

Intracellular ROS levels were assessed using dichlorodihydrofluorescein diacetate ($DCFH_2$-DA) via the fluorescent nature of its oxidized product DCF (Presley, Fuller et al. 2003). $DCFH_2$-DA (10 μM) was added to the MCF-7 wt cells (96 well plate) after 6 and 24 hours of treatment with pro-apoptotic drugs and incubated for 30 minutes at 37°C to ensure mitochondrial loading of DCFH2-DA. Dye fluorescence was measured with a Tecan Infinite M200 plate reader by means of the bundled software Magellan V 6.3 (excitation: 480 nm; emission: 530 nm) and according to manufacturer's instructions.

III-2.4.3.2. Propidium Iodide (PI) viability assay.

The fluorescent probe, PI, intercalates into the DNA of non-viable cells but cannot enter viable cells because it is excluded by the plasma membrane. MCF-7 wt cells were grown in flat-bottomed, 96-well microtiter plates to approximately 80% confluency. Cells were treated with the different drugs for 6 hours or for 24 hours at 37°C and stained with PI (1.0 ug/ml) for 30 minutes at 37°C. Fluorescence was measured with a Tecan plate reader in bottom-read mode using Magellan V 6.3 software (excitation: 530 nm; emission: 620 nm) and according to manufacturer's instructions.

III-2.4.2.3. Cytochrome c release.

MCF-7 cells stably expressing GFP-Bax were grown overnight in 8-well microscopy chambers and subjected to the indicated treatments for 6 hours at 37°C. Cells were then fixed with 4% paraformaldehyde (PFA) in PBS, permeabilized with 0.3% Triton X-100/PBS, and blocked with 3% BSA. Next, PFA-fixed cells were incubated with primary antibodies against cytochrome *c* (mouse) and COXIV (rabbit) overnight at 4°C. After washing, the cells were incubated with Alexa Fluor 546 goat anti-mouse and Alexa Fluor 647 goat anti-rabbit to visualize cytochrome *c* and COXIV, respectively, for 1 hour at room temperature. Z- stacks of 5 fields-of-view per condition were imaged at 63x magnification (approx. 60 cells per condition).

III-3. Mitochondrial morphology classification.

Image analysis consists of several steps, starting from image loading to the extraction of the results (Figure III- 2). The processes of loading an image as well as extracting results and writing them to a database require a flexible input/output interface to handle data formats. Inherent image preprocessing predominantly deals with compensating acquisition artifacts. There is an abundance of preprocessing strategies. They include pixel brightness transformations (histogram-based equalization, contrast stretching) and local preprocessing (smoothing, convolution operations, noise reduction filtering), to name just a few of the more commonly used methods. Preprocessing methods are well described in the literature (Gonzalez and Woods 2001); (Seul, O´Gorman et al. 2000; Huang, Choi et al. 2010) and are essential for preventing artifacts. Next, image segmentation is the process of partitioning an image into objects, and image classification is the process of naming these objects.

Figure III- 2. General steps inherent to image processing and segmentation.

III-3.1. Mitochondrial image analysis.

Mitochondrial morphology analysis was performed with CP software by combining available modules and submodules (*www.cellprofiler.org*), and configured to automatically (i) perform image preprocessing, (ii) segment and identify objects within the image and (iii) measure several mitochondrial and cellular features. CP has been validated for a wide variety of biological applications (Vokes and Carpenter 2008) that include the analysis of fluorescence staining levels, microscopic images for cell size and morphology studies, cell cycle distributions and other features of individual cells in images (Carpenter, Jones et al. 2006). Our challenge was to apply CP analysis to a small organelle (mitochondrion) and extract relevant features within single cells. Here we show a detailed description of the assembled pipeline.

CP MODULES:

1. Load Images
2. Rescale Intensity (nuclei)
3. Rescale Intensity (mitochondria)
4. Apply Threshold (mitochondria)
5. Correct Illumination_Calculate (nuclei)
6. Correct Illumination_Apply (nuclei)
7. Smooth or Enhance (mitochondria)
8. Identify Primary Automatic (nuclei)
9. Identify Secondary (cells)
10. Convert to Image (cells)
11. Save Images (cells)
12. Identify Primary Automatic (mitochondria)
13. Convert to Image (mitochondria)
14. Save Images (mitochondria)
15. Measure Object Area Shape (mitochondria)
16. Measure Object Neighbors (mitochondria)
17. Measure Texture (cell)
18. Relate (mitochondria to the cell)
19. Export to Excel
20. Export to Database

1. Load images.

Deconvolved image stacks were loaded into CP. The module assigns the respective acquisition channels to each image.

2. and 3. Rescale intensity.

We applied rescaling `Method E´ on individual images by entering a minimum and a maximum intensity value. Pixels range were kept between (0;1), while the highest value and the lowest value of the rescaled image were adjusted to: ´Nuclei´ (0;0.6) and for ´Mitochondria´ image (0.009;1.67).

4. Apply threshold.

In order to clearly define the boundaries of mitochondria, we applied a binary threshold to the ´mitochondria´ image (0.28). All other settings were kept at standard settings and the original intensity values were retained.

5. Correct illumination_calculate.

The background intensity was calculated per each image by setting a pixel box size of 150 pixels to the ´nuclei´ images.

6. Correct illumination_apply.

The previous calculated background image was subtracted from the image after module 2 (´rescaled nuclei´).

7. Smooth or enhance.

To derive the cytoplasmic region from the ´mitochondria´ channel we applied a Gaussian Filter smoothing method on mitochondria images (50 pixels box).

8. Identify primary automatic.

This module identifies primary objects (nuclei) in the grayscale images obtained from module 6. To identify and segment the nuclei, we chose a) to discard the objects outside the diameter range (100; 300) pixels; b) to merge small objects that are close to larger ones, as they are likely to belong to the nucleus and were mistakenly separated; c) to discard objects (nuclei) touching the image border because part of its cell will be out of the image. We applied Otsu Adaptative for segmentation with a correction factor of 1.2. In order to distinguish and divide clumped objects we selected the `Intensity´ feature and decided on a second step to have filled holes in the identified objects,

9. Identify secondary.

We applied CP Propagation method based on the mitochondria smoothed images from module 7 to identify the cell borders, (0.05 regularization factor) and Otsu Adaptative threshold (no correction and full range).

12. Identify primary automatic.

Individual mitochondria were segmented by CP Otsu Adaptative (1.2 correction factor). In this case, we have only discarded object lying outside the diameter range (5; 300).

15. Measure object area and shape.

This module extracts area and shape features of each individual object (mitochondrion) of images from module 14.

16. Measure object neighbors.

We considered all objects within 15 pixels distance to be neighbors.

17. Measure texture.

This module extracts texture features of each individual object (cell). We chose a scale of texture of 3.

18. Relate objects.

This module allows for the association of "children" objects (mitochondria) with "parents" objects (cell). In this case, we can quantify how many mitochondria are present per cell as well as obtain a mean value for all measures performed above, averaged per cell.

20. Export to database.

Measurements described above (modules 15 and 16) were automatically exported to a SQL database. Data is given for all segmented objects (nuclei, cell and mitochondria) containing their related features. Mean mitochondria features per cell were used for classification (Table III- 2 to 4).

Table III- 2. List of Features extracted per cell and related to the nucleus

C_Texture_AngularSecondMoment_N_3
C_Texture_Contrast_N_3
C_Texture_Correlation_N_3
C_Texture_Variance_N_3
C_Texture_InverseDifferenceMom_N_3
C_Texture_SumAverage_N_3
C_Texture_SumVariance_N_3
C_Texture_SumEntropy_N_3
C_Texture_Entropy_N_3
C_Texture_DifferenceVariance_N_3
C_Texture_DifferenceEntropy_N_3
C_Texture_InfoMeas1_N_3
C_Texture_InfoMeas2_N_3
C_Texture_GaborX_N_3
C_Texture_GaborY_N_3

(C- Cell, N-Nuclei)

Table III- 3. List of Features extracted per cell and related to the cell.

C_Children_M_Count
Means_M_per_C_Location_Center_X
Means_M_per_C_Location_Center_Y
Means_M_per_C_AreaShape_Area
Means_M_per_C_AreaShape_Eccentricity
Means_M_per_C_AreaShape_Solidity
Means_M_per_C_AreaShape_Extent
Means_M_per_C_AreaShape_EulerNumber
Means_M_per_C_AreaShape_Perimeter
Means_M_per_C_AreaShape_FormFactor
Means_M_per_C_AreaShape_MajorAxisLength
Means_M_per_C_AreaShape_MinorAxisLength
Means_M_per_C_AreaShape_Orientation

(C- Cell, M-Mitochondria)

Table III- 4. List of Features extracted per cell and related to each mitochondrion.

Means_M_per_C_Zernike_0_0
Means_M_per_C_Zernike_1_1
Means_M_per_C_Zernike_2_0
Means_M_per_C_Zernike_2_2
Means_M_per_C_Zernike_3_1
Means_M_per_C_Zernike_3_3
Means_M_per_C_Zernike_4_0
Means_M_per_C_Zernike_4_2
Means_M_per_C_Zernike_4_4
Means_M_per_C_Zernike_5_1
Means_M_per_C_Zernike_5_3
Means_M_per_C_Zernike_5_5
Means_M_per_C_Zernike_6_0
Means_M_per_C_Zernike_6_2
Means_M_per_C_Zernike_6_4
Means_M_per_C_Zernike_6_6
Means_M_per_C_Zernike_7_1
Means_M_per_C_Zernike_7_3
Means_M_per_C_Zernike_7_5
Means_M_per_C_Zernike_7_7
Means_M_per_C_Zernike_8_0
Means_M_per_C_Zernike_8_2
Means_M_per_C_Zernike_8_4
Means_M_per_C_Zernike_8_6
Means_M_per_C_Zernike_8_8
Means_M_per_C_Zernike_9_1
Means_M_per_C_Zernike_9_3
Means_M_per_C_Zernike_9_5
Means_M_per_C_Zernike_9_7
Means_M_per_C_Zernike_9_9
Means_M_per_C_Neighbors_NumberOfNeighbors_15
Means_M_per_C_Neighbors_PercentTouching_15
Means_M_per_C_Neighbors_FirstClosestObjectNu_15
Means_M_per_C_Neighbors_FirstClosestXVector_15
Means_M_per_C_Neighbors_FirstClosestYVector_15
Means_M_per_C_Neighbors_SecondClosestObjectN_15
Means_M_per_C_Neighbors_SecondClosestXVector_15

Means_M_per_C_Neighbors_SecondClosestYVector_15
Means_M_per_C_Neighbors_AngleBetweenNeighbor_15
Means_M_per_C_Parent_C
Means_M_per_C_Distance_C

(M- Mitochondria, C- Cell)

In this work, we have established an unbiased method that allows for automated segmentation, feature extraction and subsequent classification. These steps were tested and optimized for MCF-7 stably expressing mito-GFP, imaged with a 63x objective and therefore might need re-adjustment when applied to different experimental systems.

The above-described CP pipeline allowed us to extract numerous features concerning mitochondria size, texture, signal intensity, and spatial distribution in the cell that varied among the three classes (Table III- 2 to 4). Having more than 60 features extracted per cell and single mitochondrion, there are too many parameters to be manually adjusted (Table III- 2 to 4). To overcome this limitation, we made use of a machine learning approach.

III-3.2. Machine learning.

Machine learning is an area of artificial intelligence that deals with finding an optimal algorithm to solve a complex problem. Obviously, our specific problem is analyzing a set of images. Learning is achieved by presenting the machine learning method with training data. There are two main types of learning approaches, unsupervised learning, and supervised learning. Unsupervised learning is based on the purely statistical analysis of the training data and does not entail a user input. It is commonly used when there is no, or very limited, prior knowledge about the problem space. By opposition, we have applied supervised learning, which requires user feedback. Here, learning is accomplished by comparing machine-produced with user-produced results on the training data.

III-3.2.1. Random forest classifier.

The Random Forest (RF) algorithm was developed by Leo Breiman and is a meta-learner comprised of many individual trees, designed to operate quickly over large datasets and, more importantly, to be diverse by using random samples to build each tree in the forest (Breiman 2001; Liaw and Wiener 2002). Figure III- 2 shows how the training data is sampled to create an in-bag portion to construct the tree, and a smaller out-of-bag portion to test the completed tree to asses its performance. This performance measure is known as the out-of-bag (ooB) error estimate (Figure III- 3) (Pater 2005).

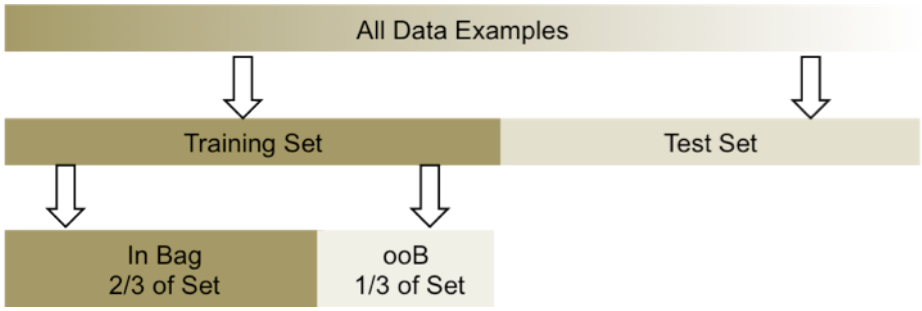

Figure III- 3. Breakdown of data used to build trees. Collected data is split into a training set used to build the model and a test set, used to validate the model. `In bag´ corresponds to the data that was correctly classified and `ooB´ (out of bag error) corresponds to the misclassified data. A good classifier performance should not result in more than 1/3 of misclassified data. (Adapted from (Pater 2005)).

The features exported by the CP (Table III- 2 to 4) were provided to a RF model, which performed multidimensional data exploration and supervised machine learning-based image classification. The algorithm consists of an ensemble of classification trees that vote for a final outcome. The percentage of trees voting for a specific class is referred to as RF score. At each iteration of the RF construction, the data not in the training subsample (ooB) is used to estimate the error rate (Figure III-3). Peak importance is estimated by the mean decrease in accuracy (MDA). This score is the increase in the ooB error when the ooB data for that peak is permuted while all others are left unchanged. A specific class can be assigned by RF score major votes, but this was only used for the 10 x 10 fold cross validation and validation purposes (comparison with manual classification). All effective data analysis steps used "raw" percentages given by the RF score, i.e. plotted results correspond to the mean value of each class assigned per cell, reflecting mitochondrial population distribution under a specific treatment. Thus, the RF predictor assigns a degree of belonging between 0% and 100% to each class (networked/fragmented/swollen=N/F/S) per cell.

The following packages were combined to built the classifier (in R language, version 2.10):

Random Forest package: ***randomForest***

Decision tree package: ***rpart***

Cross validation package: **mlbench**

III-4. Fuzzy logic (FL) modeling approach.

III-4.1. Why fuzzy logic?

FL offers several unique features that make it a particularly good choice for our work (Cabrera, Cordero et al. 2009).

1) It is intrinsically robust because it does not require precise, noise-free inputs and therefore can be set to fail safely if a feedback parameter quits or is destroyed over time. Despite a wide range of input variation, the output control is always a smooth function.

2) It is based on user-defined rules and thus it can be easily modified and significantly adjusted to improve or change the system performance. Additionally, it can easily incorporate new events by generating appropriate governing rules.

3) FL reduces the system complexity while maintaining its relative costs and relations. This is possible because it is not limited to a few feedback inputs and one or two control outputs, nor is it necessary to measure or compute rate-of-change parameters in order for it to be implemented. In fact, any sensor data that provides some indication of a system's actions and reactions is sufficient.

4) Since it is built on a rule-based operation, any reasonable number of inputs can be processed and numerous outputs can be generated. However, introducing too many inputs and outputs quickly increases complexity, since the user must also implement rules for all single inter-relation. In this work, we broke the model into smaller steps and used several smaller FL controllers distributed on the system, each with more limited, but clearer responsibilities.

5) Importantly, FL can control nonlinear systems that would be difficult or impossible to model mathematically. This opens doors for control systems that would normally be deemed unfeasible for automation.

III-4.2. FL model assembly.

The FL toolbox (MATLAB R2009a) was used to establish a modeling pipeline to perform exhaustive searches for relative correlations between measured events. Single input-single output (SISO) FL models were assembled using the Sugeno inference method (Sugeno 1985). As a parameter reduction strategy, input membership functions (MF) were fixed to Gaussian functions, and thereby the number of input parameters was excluded from the model training. In FL, a Gaussian function has the form shown in Equation III- 2, where the height of the peak is fixed to 1, i.e. the maximum degree of belonging to a fuzzy set (degree of membership, DOM).

$$\mu_{low}(x) = e^{-\frac{(x-a)^2}{2b^2}}$$

Equation III- 2. Gaussian equation as a membership function to establish the degree of membership (DOM) of a measurement x to the set *low*.

Model assembly to explore the relationship between multiple events and a single functional feature was performed according to the following steps:

1. Data processing.

Raw data from the various experimental procedures was scaled to each maximal-observed value in order to make datasets comparable.

2. Assembly of a Sugeno FLS.

The FL Toolbox was used to generate a fuzzy logic system (FLS) automatically with the existing function genfis1, thereby creating a grid of rules to relate one input MF to exclusively one output MF. 2 gaussian functions were used to fuzzify one input. In genfis1, the number of rules is *`m to the power of n´*, where *`m´* is the number of input-MFs and *`n´* is the number of inputs; hence in our single-input case, the number of rules was 2 per model. Upon exploration of the MF parameter space we observed slightly better performance using other non-linear functions. However, the above-mentioned setting was used due to its smaller number of parameters. Linear MFs were chosen as output with standard settings previous to training. Genfis1 requires the experimental data as a matrix. In the case of multiple events and a single functional feature, all columns in the matrix, except the last one, are considered causative events and the last column is accepted as a functional feature.

3. Training of the FLS.

Once generated, the FLS was trained using adaptative neuro-fuzzy inference systems (ANFIS)(Cabrera, Cordero et al. 2009). As a learning algorithm, a hybrid of backpropagation coupled to least-squares was employed.

4. Simulation of the FLS.

Simulink, the simulation platform coupled to Matlab, was used to create a simulink model to simulate the trained FLS. This model was then run for each experimental datapoint to estimate the value of the desired phenotype (Figure III- 4). The resulting estimated values were saved in an excel sheet together with the experimental dataset, which were used to calculate the root mean squared error (RMSE) between the predicative and experimental result.

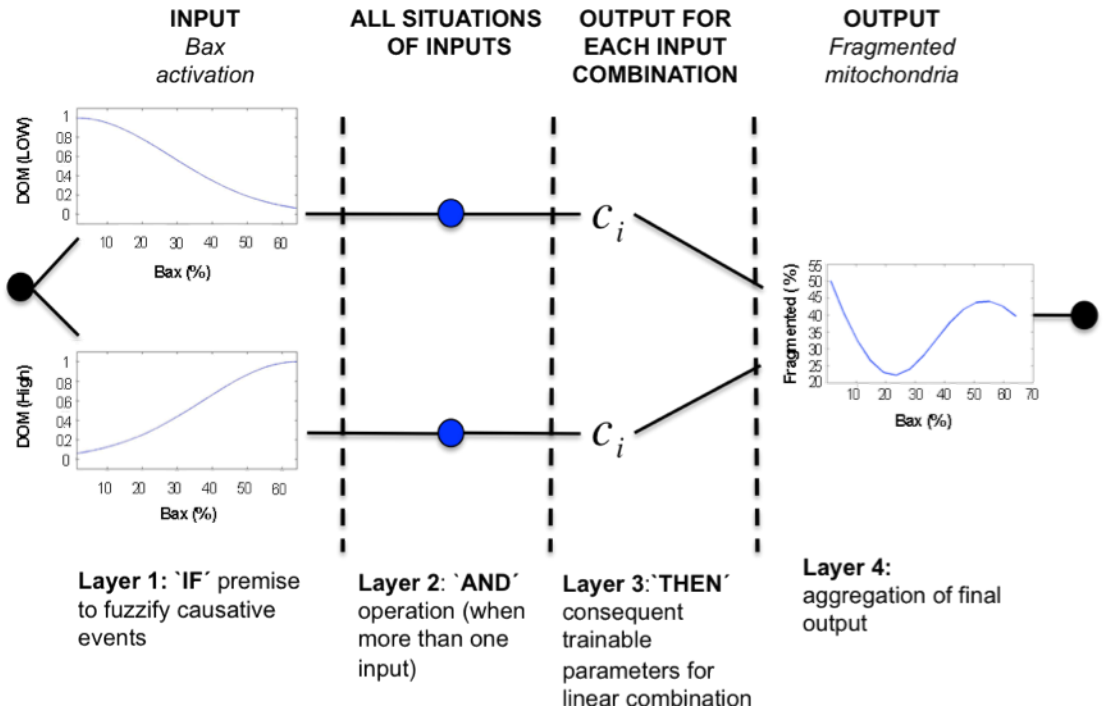

Figure III- 4. Representative single input-single output (SISO) model. Example of one model built upon the hypothesis that Bax activation leads to mitochondrial fragmentation. The parameters of the model are distributed following a neural network (NN) structure. In the first layer are shown the parameters of the membership functions (MFs) that fuzzified Bax activation, mapping the degree of membership (DOM) of its measurements into 2 fuzzy sets. These fuzzy sets represent "low" and "high" levels of Bax activation. The second layer has scalability purposes: it would contain the rules to combine all the inputs if the model had more than 1 input. The third layer contains parameters (c) to linearly combine the *i* input MFs. Input and output MF parameters were fitted to the data. The forth layer aggregates the values from layer 3 to finally model the behavior of `Fragmented´mitochondria as a function of `Bax´.

5. Exhaustive search.

The process stated in steps 1, 2 and 3 was then iterated to create the FLS for a total of 35 models representing all logical interactions. For example, Bax activation influencing each one of the three morphological classes (3 models) and the correspondent mirror-models (3 models).

6. Model selection.

For follow-up analysis of the least-RMSE models, see results sections.

III-5. Data analysis and statistics.

Plotted data is given as mean ± standard error of the mean (s.e.m) of at least 3 independent experiments unless stated otherwise. Statistical significance of differences was determined using a two-tailed Student's t-test. P values ≤ 0.05 were considered to be statistically significant.

IV- RESULTS

IV-1. Mitochondrial morphological changes are integrated with apoptosis.

Mitochondrial participation in programmed cell death is a contributing factor to many diseases, including neurodegeneration (e.g. Alzheimer or Parkinson disease), cardiac ischemia/reperfusion injury and cancer (for review see (Fosslien 2001)). The activation of BH3-only proteins by various stress stimuli triggers mitochondrial membrane permeability and leads to the release of pro-apoptotic intermembrane space proteins into the cytosol and consequent activation of caspase-mediated cell death (Figure IV- 1).

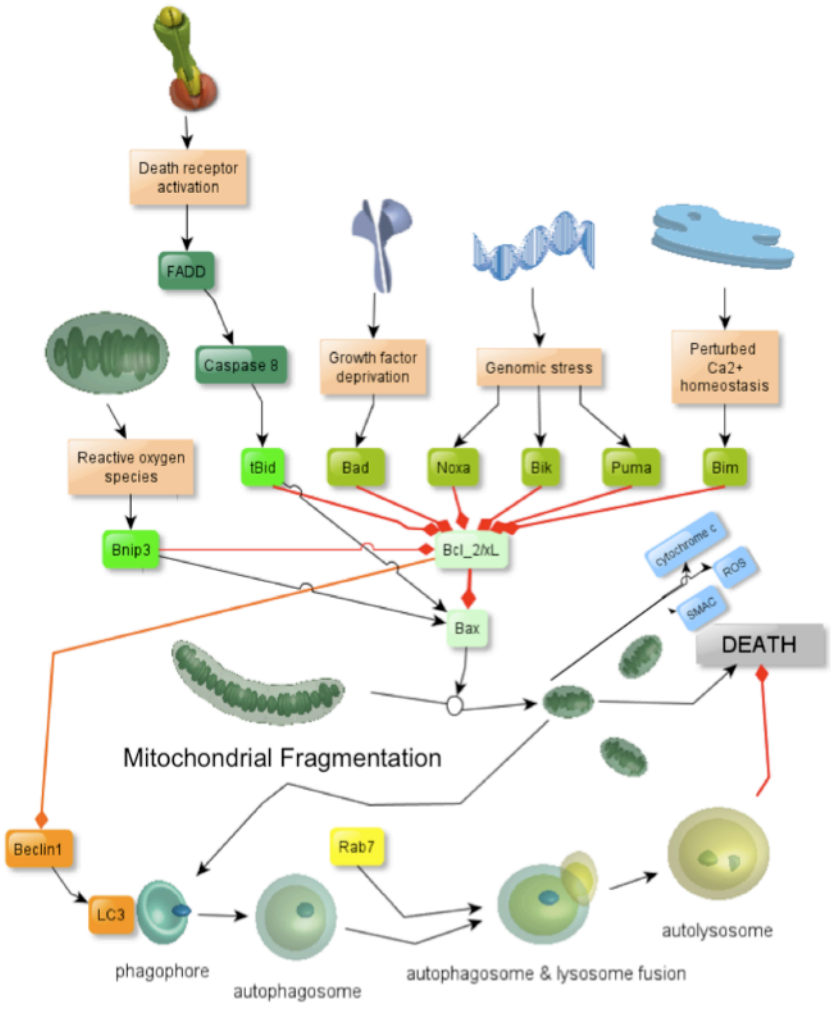

Figure IV- 1. Cell death at the mitochondria. Bcl-2 family members act as signal transmitters from the cytosol to the mitochondria by inhibiting anti-apoptotic proteins Bcl-2/XL or directly activate Bax translocation to the mitochondria (tBid and Bnip3). Dysfunctional mitochondria release pro-apoptotic proteins that lead to cell death. Fragmented mitochondria can be engulfed by a autophagosome and targeted to lysosomal degradation by mitophagy.

IV-1.1. BH3-only proteins impact mitochondrial morphology changes and lead to cell death.

Our initial aim was to investigate mitochondrial morphology under genetic expression of pro-apoptotic BH3-only proteins (chronic stimuli). Precisely, we were interested in those BH3-only proteins that are able to directly activate Bax translocation to the mitochondria (Figure IV- 1). Therefore, we first analyzed mitochondrial morphology phenotypes under expression of tBid and Bnip3 proteins. Bid has been proposed to directly participate in the mitochondrial outer membrane permeabilization (MOMP) event (Yuan, Williams et al. 2003) by direct interaction with Bax/Bak (Saito, Korsmeyer et al. 2000; Wei, Lindsten et al. 2000), or through scavenging of anti-apoptotic Bcl-2 and Bcl-XL, which oppose Bax activity (Wang, Yin et al. 1996) (Cheng, Wei et al. 2001). Bnip3 is another member of the 'BH3-only' Bcl-2 subfamily which has been described to induce apoptotic (Kubasiak, Hernandez et al. 2002), necrotic (Vande Velde, Cizeau et al. 2000), and autophagic (Daido 2004; Kanzawa, Zhang et al. 2004) cell death. Bnip3 possesses a C-terminal transmembrane (TM) domain, which is required for its pro-apoptotic function, including targeting to the mitochondria (Yasuda, Theodorakis et al. 1998).

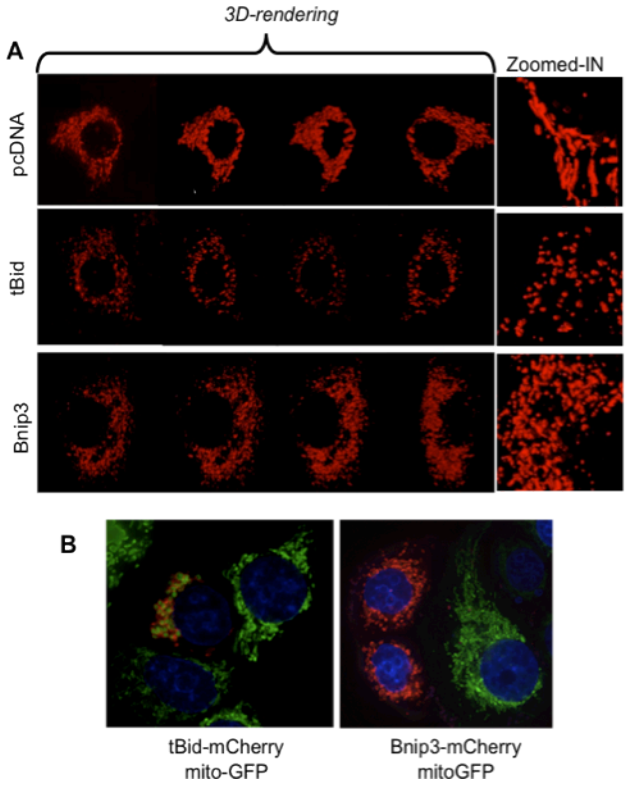

Figure IV- 2. Mitochondrial fragmentation upon BH3-only proteins expression. (A) MCF-7 cells were co-transfected with mito-mCherry and BH3-only proteins (tBid or Bnip3). Images show mitochondrial signal in cells expressing tBid, Bnip3 or control (mCherry alone). **(B)** MCF-7 stably expressing mito-GFP were transiently transfected with tBid-mCherry or Bnip3-mCherry.

In order to investigate mitochondrial morphology under tBid and Bnip3 expression, we made use of the mCherry fluorescent protein fused to the COXIV mitochondrial inner membrane targeting sequence (Rizzuto, Dsandona et al. 2010). As shown in Figure IV- 2, cells transfected with vector alone (mCherry) displayed an elongated network of mitochondria. Both tBid and Bnip3 expression resulted in loss of the elongated mitochondria, and widespread fragmentation (Figure IV- 2A). The fragmentation of mitochondria under these conditions was quite generalized, although there were different states between tBid and Bnip3-induced fragmentation. Whereas tBid seemed to induce a more acute fragmented phenotype and some swollen mitochondria, Bnip3 presented mostly fragmented mitochondria, but some networked mitochondria 24 hours post transfection. This realization, although clear to the eye, was merely qualitative and we show in the following sections how we proceeded to obtain a quantitative measure.

IV-1.1.1. Mitochondrial integration of Bnip3 and tBid in the outer membrane.

The mitochondrion is composed of two membranes with different functions and signaling properties (Lodish, Berk et al. 2008). The inner membrane defines the mitochondrial matrix and contains the components of the respiratory chain confined and folded into cristae. The outer membrane serves to control exchange of proteins, substrates and ions between cytosol and intermembrane space, where cytochrome *c*, AIF (apoptosis inducing factor) and SMAC/diablo reside (Wang 2001).

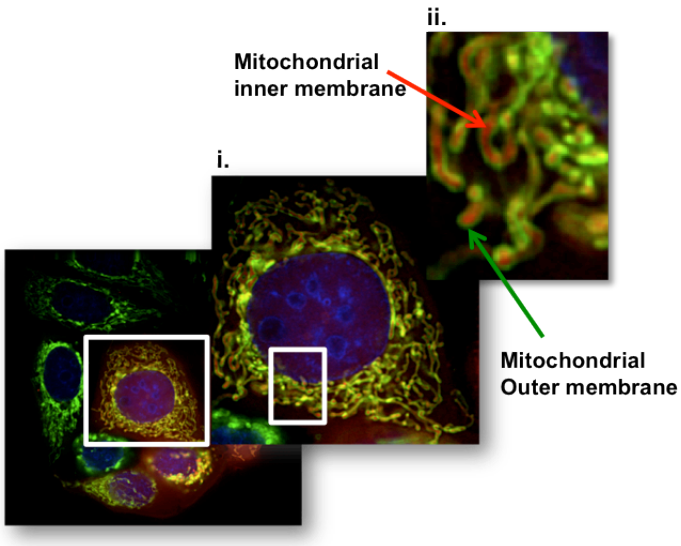

Figure IV- 3. Mitochondrial inner and outer membranes. Illustrative example of MCF-7 cells stably expressing mitoNEET-GFP (green, outer membrane) and transfected with mito-mCherry (red. inner membrane). **(i)** Zoomed ROI for one cell example. **(ii)** Zoomed mitochondrial region.

In order to image these distinct components, we established MCF-7 cells stably expressing mitoNEET-GFP, a mitochondrial outer membrane protein (Colca, McDonald et al. 2004) and transiently transfected mito-mCherry to, simultaneously, visualize the inner membrane (Figure IV- 3). Cells that expressed both inner and outer membrane proteins revealed a dynamic and interconnected network of mitochondrial population (movie not shown). Next, we were interested in characterizing tBid and Bnip3 proteins at the mitochondrial membrane.

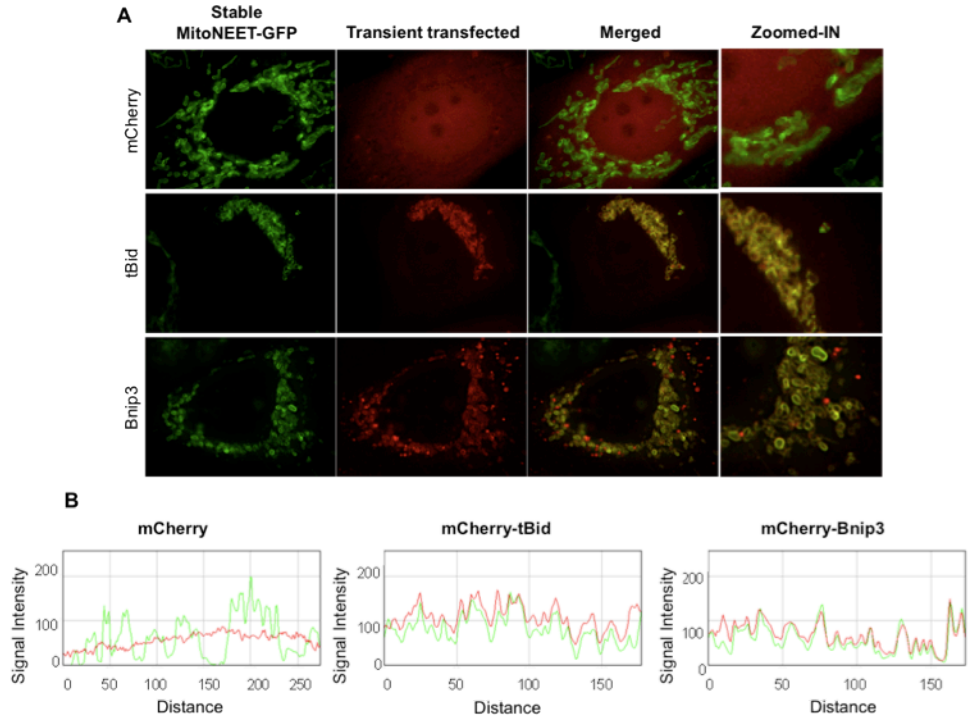

Figure IV- 4. tBid and Bnip3 colocalization with the mitochondrial outer membrane. (A) MCF-7 cells stably expressing mitoNEET-GFP were transiently transfected with mCherry alone, mCherry-tBid or mCherry-Bnip3. **(B)** RGB colocalization profile plots (ImageJ) for the respective images shown in (A).

Colocalization analysis was performed to determine the degree to which tBid and Bnip3 colocalized at the mitochondrial outer membrane. Therefore, mitoNEET-GFP stable cells were transfected with mCherry alone, mCherry-tBid or mCherry-Bnip3 (Figure IV- 4A). Colocalization was estimated by drawing a line in each merged (RGB) image and plotting the respective signal variation (Figure IV- 4B). This allowed for the calculation of the Pearson´s colocalization coefficient (ImageJ) that reports the distance between the mCherry (tBid or Bnip3) and GFP (mitochondrial outer membrane) signals. Both tBid and Bnip3 localized specifically to mitoNEET-GFP labeled mitochondrial outer membrane (Figure IV- 4). Specifically, mCherry-tBid exhibited high co-localization (Pearson's

coefficient=0.955±0.03) and mCherry-Bnip3 Pearson´s Coefficient was 0.770±0.05 (MAX colocalization=1). In contrast, mCherry alone did not colocalize with mitochondrial outer membrane (Pearson´s coefficient=0.004±0.02) (Figure IV- 4B).

IV-1.1.2 BH3-only proteins expression induces Bax activation.

Apoptosis caused by BH3-only proteins absolutely requires Bax and Bak (Figure IV- 5) (Wei, Lindsten et al. 2000; Wei 2001). Bax proteins can be found as monomers in the cytosol or loosely associated with the outer mitochondrial membrane when not activated. Bax translocates to and inserts into the mitochondrial outer membrane during the activation process (Hsu and Youle 1997; Wolter, Hsu et al. 1997; Billen, Kokoski et al. 2008). Following activation, Bax and Bak form homo-oligomers that can be visualized by microscopy via GFP-tagged Bax as they form clusters.

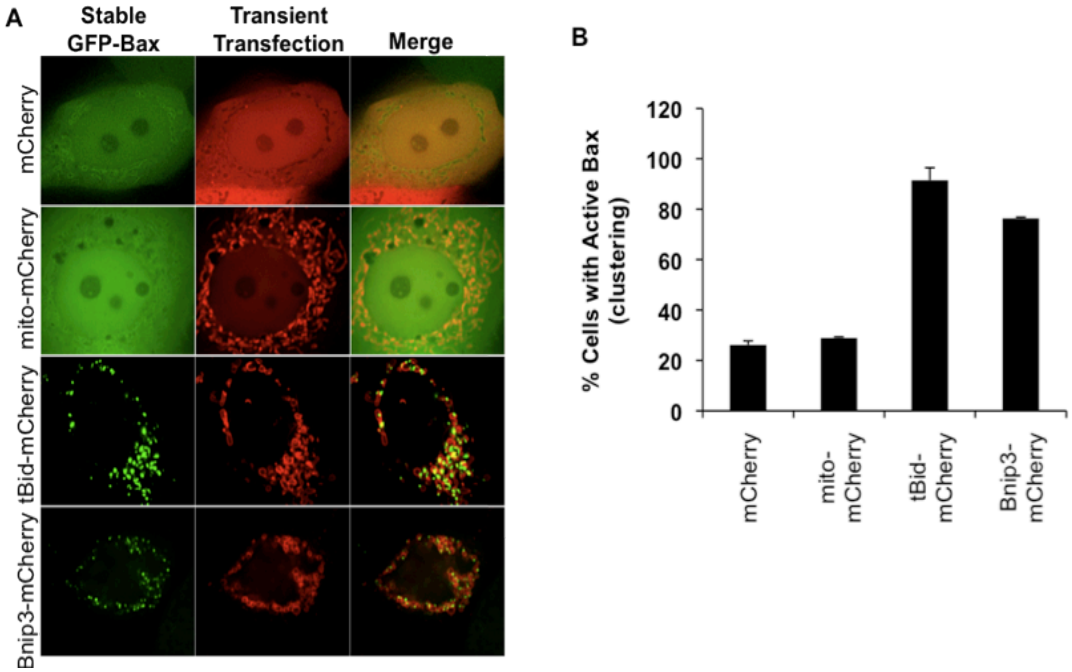

Figure IV- 5. BH3-only proteins-induced Bax activation. (A) MCF-7 cells stably expressing GFP-Bax were co-transfected with tBid/Bnip3-mCherry, mito-mCherry or mCherry alone and imaged 24 hours later. **(B)** Bax clustering was quantified for each BH3-only protein expression (tBid and Bnip3). (Approx. 100 cells; N=3).

In figure IV- 5A it can be observed how GFP-Bax signal under control conditions (mCherry and mito-mCherry) remains homogeneously distributed throughout the cytoplasm in contrast to a strongly punctuated signal in cells co-expressing tBid or Bnip3 (Figure IV- 5A). The intracellular GFP-Bax distribution was used to quantify Bax activation. Following 24 hours transfection with respective constructs (Figure IV- 5A), maximum Z-projection images were analyzed and cells were classified as exhibiting either diffuse cytosolic (inactive) or punctuate mitochondrial (active) GFP-Bax fluorescence (Figure IV- 5B). Our results show that tBid and Bnip3 greatly increase Bax clustering when compared to controls (Figure IV- 5B). Given that Bax activation constitutes a point of no return and therefore has lethal consequences, understanding how its activation is controlled is key to understanding how a cell makes the decision to undergo apoptosis.

IV-1.1.2. Ectopic expression of Bnip3 and tBid negatively affects cell viability.

Tumor necrosis factor α (TNFα) induced cell death is known to cleave Bid into tBid and activate the DR apoptotic cascade (Pei, Xing et al. 2007). Here we show both Bax and Bak activation under TNFα (43 ng/mL) treatment as previously described (Figure IV- 6A and B)(Perez and White 2000). Furthermore, it is known that activation of these effectors ´BH3-only´ proteins results in mitochondrial permeability and release of pro-apoptotic proteins from the intermembranar space of the mitochondria (e.g. AIF) (Wang 2001). In Figure IV- 6B it is possible to observe that cells which exhibit an accentuate Bax activation (intensive clustering) show less AIF-GFP signal, in contrast to cells where Bax clustering has just been initiated (Figure IV- 6B).

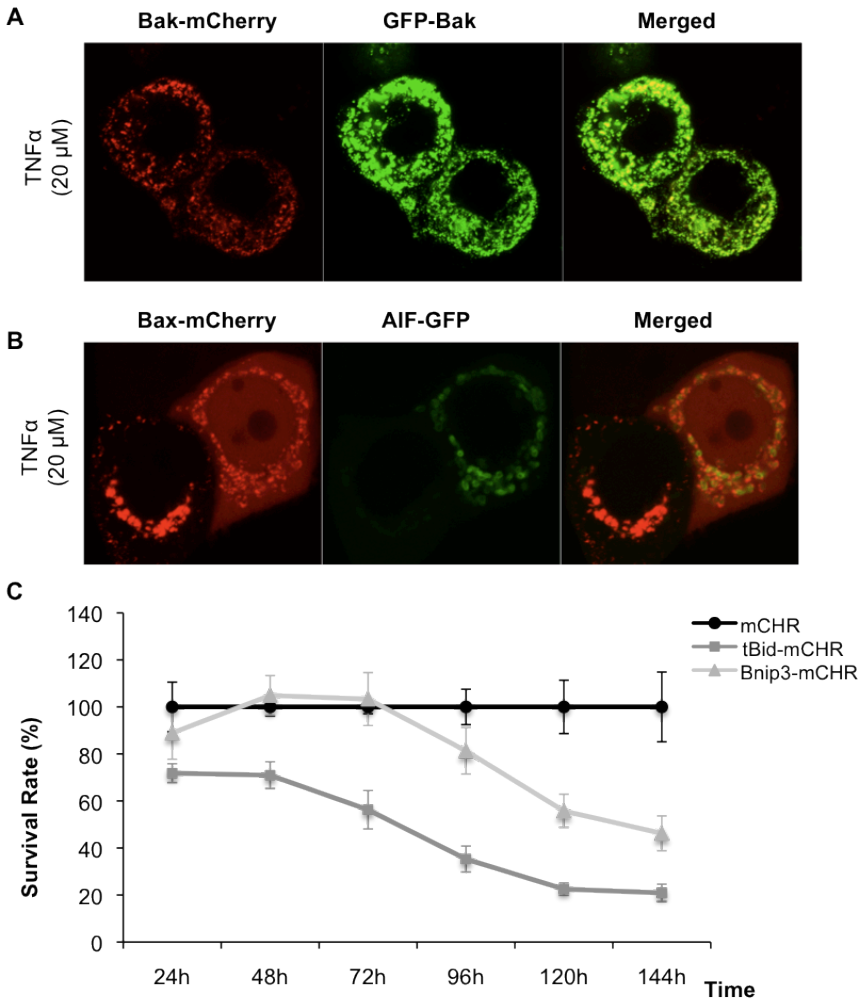

Figure IV- 6. Cell death induced by BH3-only proteins. (A) MCF-7 cells were co-transfected with GFP-Bax and mCherry-Bak and incubated at 37°C with TNFα for 24 hours. **(B)** MCF-7 cells were co-transfected with mCherry-Bax and AIF-GFP and incubated at 37°C with TNFα for 24 hours. **(C)** Percentage of cells alive over time after transfection with tBid-mCherry or Bnip3-mCherry. Survival rate was followed by flow cytometry and by gating to the mCherry signal.

The over-expression of either the active, truncated form of Bid (tBid), or Bnip3 is sufficient to trigger mitochondrial-mediated PCD (Kubli, Ycaza et al. 2007; Pei, Xing et al. 2007). To determine their impact on cell viability, tBid-mCherry and Bnip3-mCherry were transiently transfected into MCF-7 wt cells, and maintained in low serum (2% FBS) medium for slow growth conditions. As an index of cell viability we measured the percentage of mCherry-positive cells by flow cytometry every 24 hours, for up to 144 hours. Over the period of 144 hours, in mCherry-transfected control cells, mCherry expression remained constant. In both tBid-mCherry and Bnip3-mCherry transfected cells, a clear decrease in cell viability was observed. This was reflected by a decreasing mCherry signal starting at 72 hours that was constantly reduced until 144 hours after transfection (Figure IV- 6C).

IV-1.1.3. Mitochondrial fragmentation leads to cell death.

Broad variations in mitochondrial shape and morphology can be observed in various cells, but also within one cell, including small spheres or short rod-like shapes, long filamentous spaghetti-like mitochondria (Kuznetsov, Troppmair et al. 2006; Pelloux, Robillard et al. 2006). Significantly, mitochondrial dynamics, which controls morphology and organization of these organelles, can impact their functioning and metabolism regulation. Thus, mitochondrial shape might have crucial consequences for mitochondrial function (Chen, Chomyn et al. 2005; McBride, Neuspiel et al. 2006; Benard and Rossignol 2008).

Initially, we followed mitochondrial morphology by over-expressing Drp1, an established GTPase responsible for mitochondrial fission or its mutant Drp1-K38A (Pitts, Yoon et al. 1999; Smirnova, Griparic et al. 2001; Yoon, Pitts et al. 2001). Figure IV- 7A shows that Drp1 transfection resulted in intense cellular mitochondrial fragmentation while mitochondria remained fused under Drp1-K38A expression (Figure IV- 7A). The observed mitochondrial shapes and distributions were quite varied between difference cells and within one single cell as illustrated in Figure IV- 7A (Drp1-K38A, arrows for fragmented and elongated mitochodnria). Additonally, we measured the cell survival rate under Drp1 or Drp1-K38A expression (Figure IV- 7B). As expected, Drp1-induced fragmentation had an effect on cell death (Figure IV- 7B). Drp1-transfected cells revealed a slight decrease in cellular viability when compared with tBid and Bnip3, while inhibition of fragmentation (Drp1-K38A) did not affect cell viability (Figure IV- 7B).

Our initial results revealed mitochondrial variability in response to different genetic expression (Figure IV- 4, 6 and 7). At this point, we aimed at instituting an approach able to clearly classify mitochondrial morphology in a population-based manner and to account for intermediate states of individual mitochondria within single cells. Moreover, we were interested in investigating mitochondrial morphology variations under acute cell death stimuli (apoptotic drugs). The following sections describe, step by step, how we built the platform that enabled us to reach the announced aims.

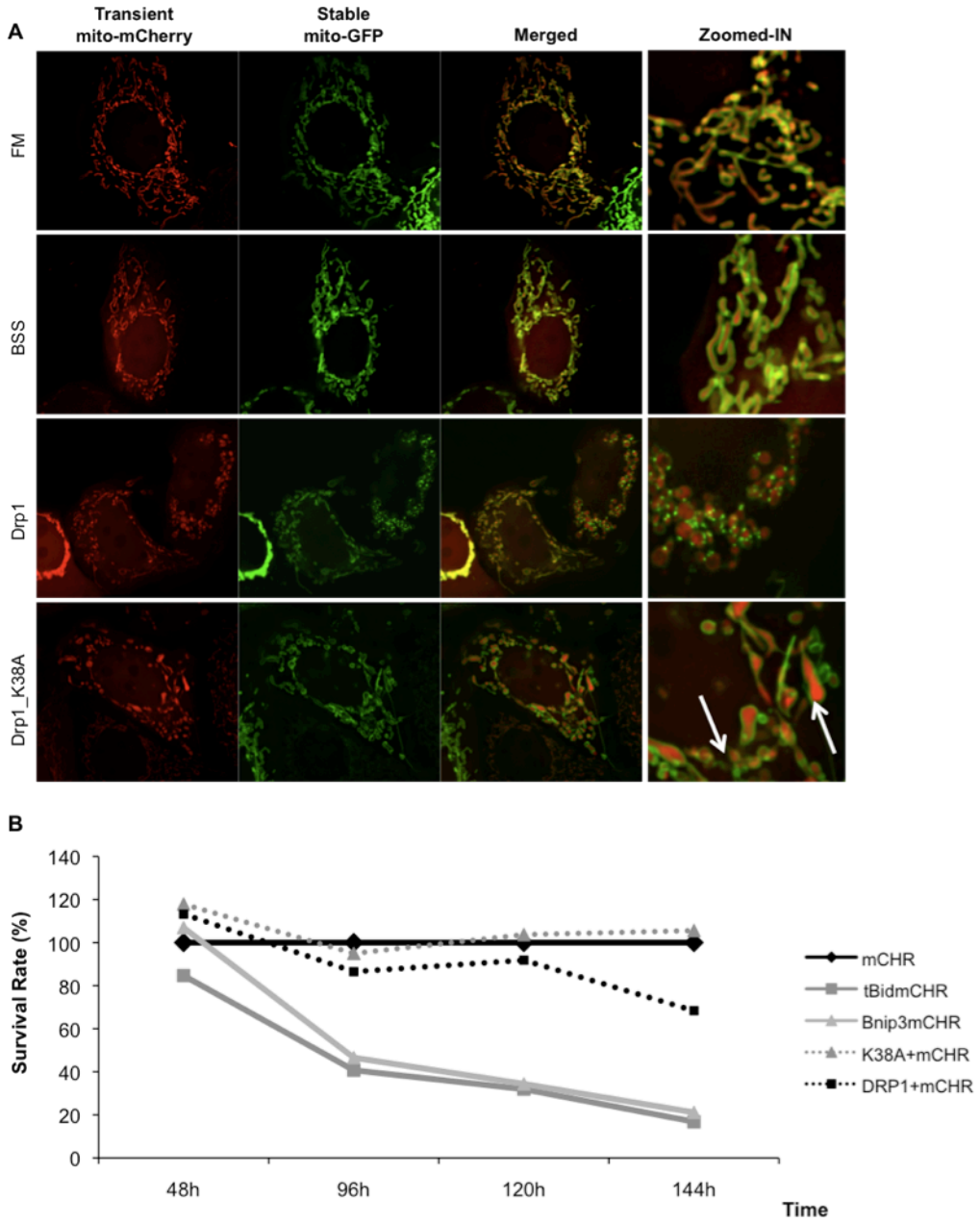

Figure IV- 7. Induced mitochondrial fragmentation. (A) Representative images of mitochondria phenotypes under Drp1 and Drp1-K38A expression. MCF-7 cells stably expressing mito-GFP were co-transfected with Drp1-pcDNA or Drp1-K38A-pcDNA and mCherry (mCHR) in a 1:2 ratio. Arrows in zoomed region point out one fused mitochondrion and one fragmented mitochondrion in the same cell. **(B)** Percentage of MCF-7 cells alive over time, after transfection with mCherry labeled tBid or Bnip3 as well as Drp1 and Drp1-K38A co-transfected with mCherry (1:2 ratio). Survival rate was followed by flow cytometry by gating to the mCherry signal. Results are shown normalized to control (mCherry, 100%).

IV-2. Mitochondrial morphology classification.

Changes in mitochondrial morphology have been primarily described in literature as a binary state between 'fragmented' and 'fused'. This classification is limited, as it cannot differentiate shifts in fission or fusion rates. In addition, many cell types exhibit fused (networked) mitochondria under normal conditions, making morphology classification a complex task. In reality, mitochondrial phenotypes are not limited to this classical binary state of fragmented/fused. Researchers have reported as well donut-shape, swollen or disk-shaped mitochondria (Benard and Rossignol 2008; Sauvanet, Duvezin-Caubet et al. 2010).

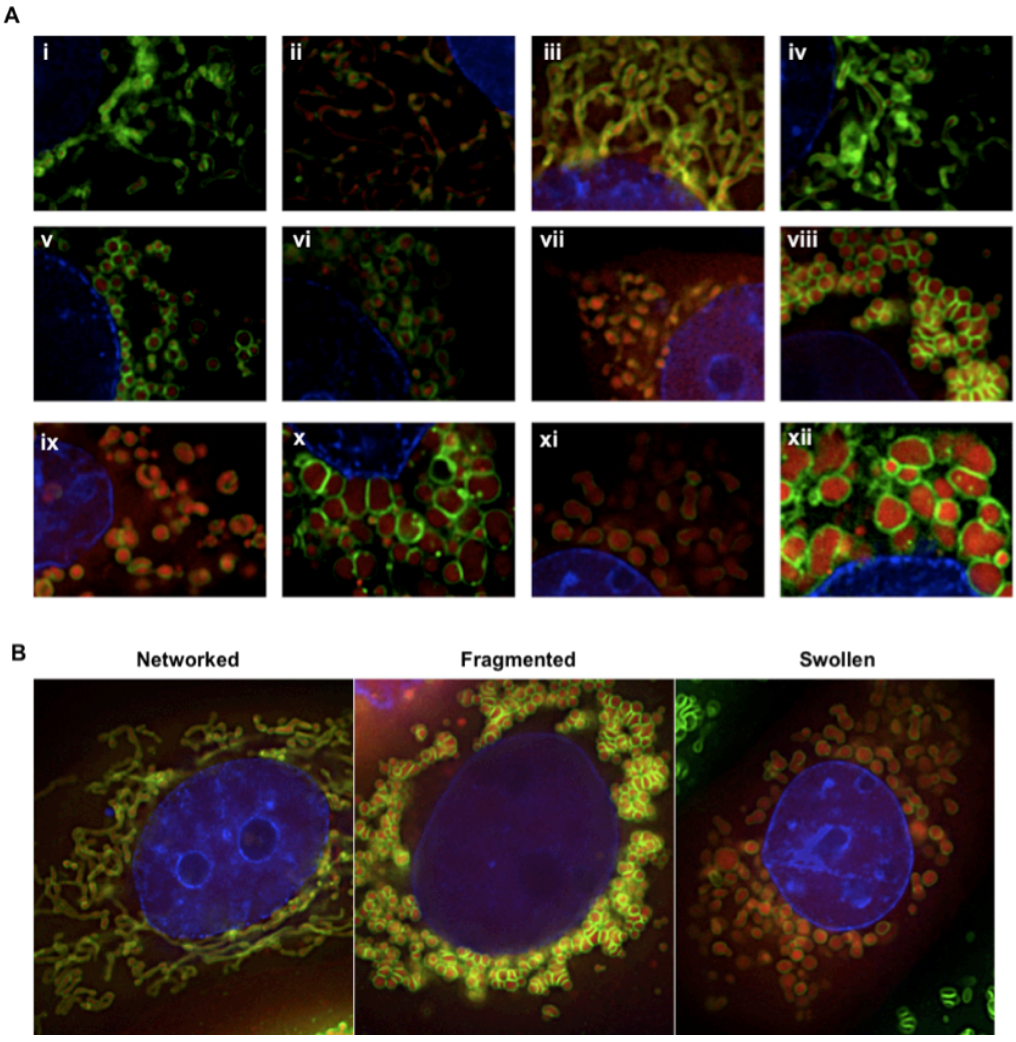

Figure IV- 8. Representative images of mitochondrial phenotypes. MCF-7 cells stably expressing mitoNEET-GFP (green) and transfected with mito-mCherry (red) were imaged. **(A)** Cropped ROIs were selected to exemplify **(i to iv)** networked-mitochondria. **(v to viii)** fragmented-mitochondria. **(ix to xii)** swollen-mitochondria. **(B)** Example of cells manually classified as `Networked´, `Fragmented´ or `Swollen´. Images correspond to the middle point slice from 3D stacks acquired with DeltaVision real time (DVRT) microscope and after deconvolution scope.

While inducing fragmented and fusion states by over-expression of Drp1 and its mutant (Figure IV-7), we observed a high variability of phenotypes. In Figure IV- 8 some examples collected in MCF-7 cells stably expressing mitoNEET-GFP and transiently transfected with mito-mCherry are depicted. Cells submitted to diverse acute apoptotic stimuli were blindly imaged, i.e. with no previous knowledge of applied treatments, in order to categorize all possible phenotypes. In Figure IV- 8 it is possible to observe that mitochondria exist in very different shapes and distributions. In some conditions, MCF-7 mitochondria appear elongated as part of a network that constantly moves dynamically throughout the cell and undergoes fusion/fission events (movie not shown). Some mitochondria can also appear as small-circular organelles (v, vi and viii) or small oval-shaped (vii) structures. Other are differentiated from the networked state, "fragmented", but still distinct from the small-rounded mitochondria (ix to xii). These are large-shaped mitochondria, with an increased volume (x and xii) or donut-shaped mitochondria (ix). The analysis of our preliminary results led us to define three most commonly observed mitochondrial morphologies: `Networked´, `Fragmented´ and `Swollen´ (Figure IV- 8B).

IV-2.1. Detection of mitochondrial phenotypic-states by high-resolution imaging.

Mitochondrial imaging has been used intensively to analyze important functional and morphological characteristics of mitochondria in living cells, as well as their intracellular distribution and arrangement (McConnell, Stewart et al. 1990; Dimmer, Fritz et al. 2002; Altmann and Westermann 2005; Meeusen, DeVay et al. 2006; Soubannier and McBride 2009). Currently, the field relies on semi-quantitative assays, which, even under optimal conditions, are labor-intensive, low-throughput, require complex imaging techniques and therefore are statistically weak. Image analysis consists of several steps, starting from image loading to the extraction of the results. The processes of loading an image as well as extracting results and exporting them to a database require a flexible input/output interface to handle data formats. Inherent image preprocessing predominantly deals with compensating acquisition artifacts. In this work, image acquisition was performed with a DeltaVision real time (DVRT) widefield fluorescence microscope (WFM) that allowed for a deconvolution step. Image analyses were carried out by taking advantage of the CellProfiler (CP) tool package software that performed rich-feature extraction of individual mitochondrial and cellular parameters (Carpenter, Jones et al. 2006; Lamprecht, Sabatini et al. 2007).

IV-2.1.1. The optimal protocol for mitochondrial imaging acquisition.

In order to improve upon the above-mentioned methods, we explored state of the art techniques to extract high-content information. This included the use of fluorescence proteins (e.g. mito-GFP; mitoNEET-GFP; mito-mCherry) and dye marker for labeling the cell membrane (CellMask™). The application of automated analysis techniques allows for a large amount of data to be extracted from images. The key to automated detection is image preprocessing and segmentation. Therefore we have adjusted our experimental protocol and CP modules in order to ensure an optimal detection and segmentation of individual mitochondrial and mother cells.

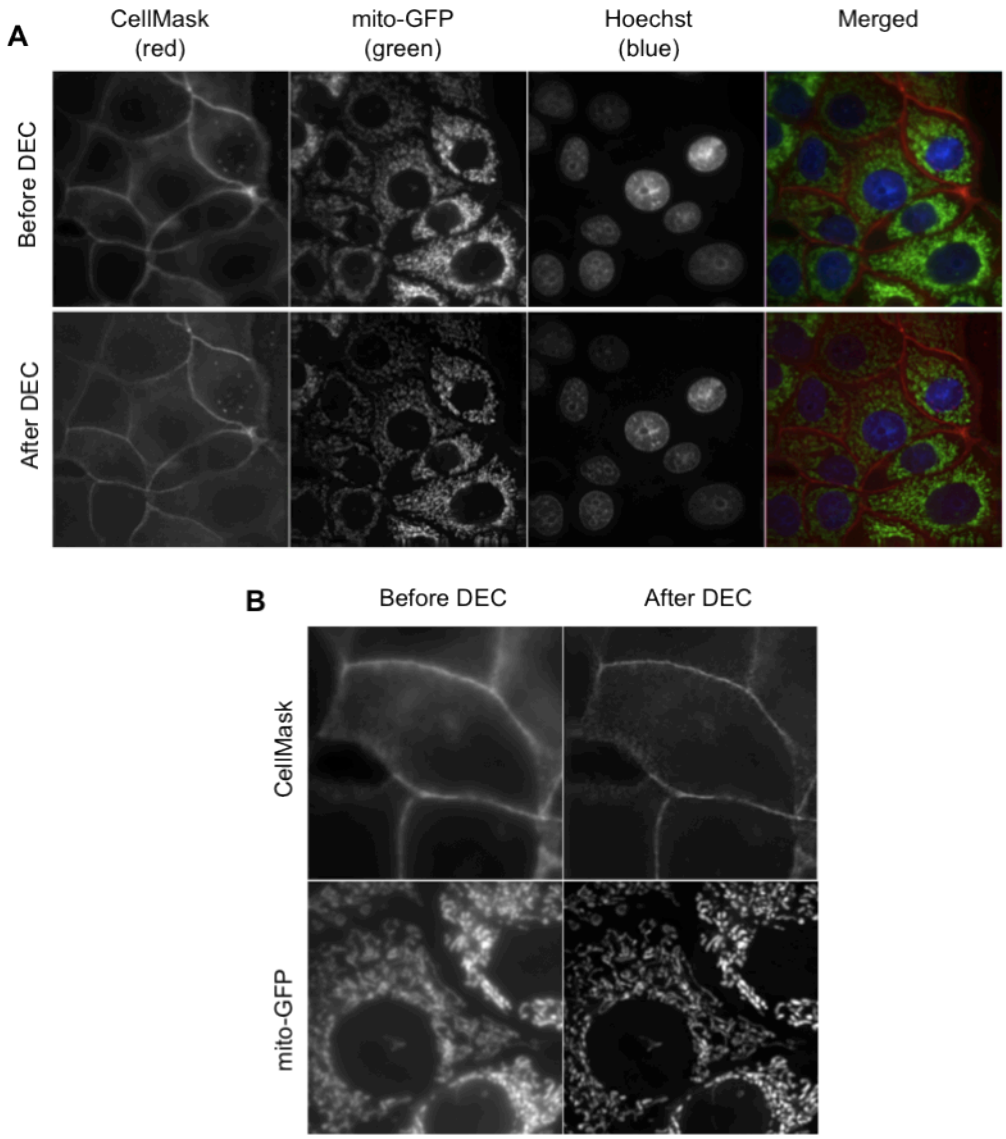

Figure IV- 9. Establishing the correct imaging and pre-processing settings. MCF-7 cells stably expressing mito-GFP were incubated (30 minutes, 37°C) with CellMask™ (5 ug/mL). Nuclei were detected using Hoechst (100 ng/mL). CellMask dyes the cell plasma membrane and was used to identify cell borders. **(A)** Representative image before and after deconvolution (DEC). **(B)** Zoomed-IN examples from (A) before and after deconvolution (DEC).

a) Pre-processing.

Microscopic images were processed as described in Materials and Methods section. The image was provided in its singled channels and contrast was automatically enhanced. One important step was to apply deconvolution algorithms to the acquired images that resulted in much sharper edges and therefore less noisy images (Figure IV- 9).

b) Object segmentation strategy.

To identify cells and mitochondria within cells it was necessary to perform image segmentation. Initial segmentation was based on the Hoechst-stained nucleus (see Materials and Methods for details). To identify cell boundaries, we initially used a cell membrane marker (CellMask Far-red dye) (Figure IV- 9). However, this step added complexity to method and some cells seemed to react to the dye alone, by showing an increase of fragmented mitochondria. Therefore, we have discarded this approach and instead identified cell border by extending the mitochondria signal, i.e, by using texture values and signal propagation (see Figure IV- 10).

c) Threshold application.

The process of segmenting individual mitochondria proved to be a difficult task, as fragmented mitochondria appeared either scattered throughout the cell or clusteres in the perinuclear region. This created an artifact since dense fragmented mitochondria were so close together that, upon segmentation, were mistaken as one elongated, networked mitochondria (Figure IV- 10; 0.1 thresholding in contrast with 0.3 thresholding). Finally, we chose a threshold value (0.28) that allowed for correct segmentation of these dense fragmented-mitochondria, although subtracting partial information from networked states. The next challenge was to verify the correct classification of the three main phenotypes: `Networked´, `Fragmented´ and `Swollen´.

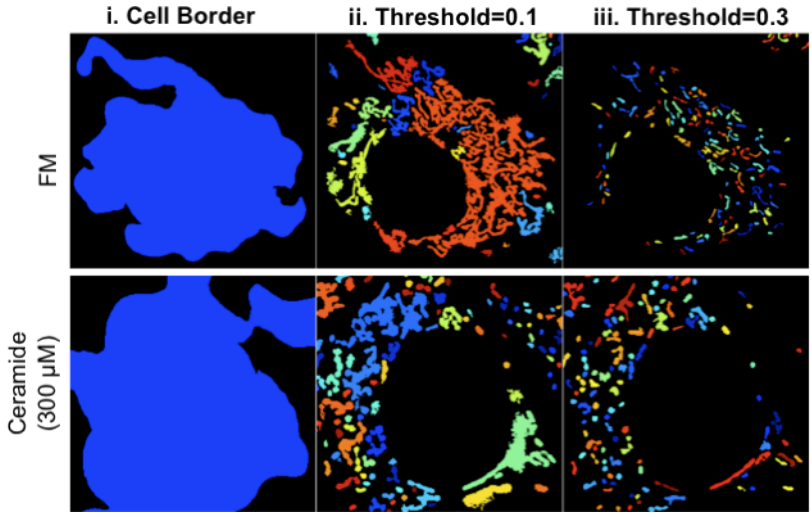

Figure IV- 10. Mitochondrial segmentation. Representative examples for MCF-7 cells stably expressing mito-GFP and incubated in full medium (FM) or apoptosis inducer, ceramide (300 µM). **(i)** Two examples of cell border definition and segmentation by CellProfiler (obtained from texture signal propagation). **(ii)** Mitochondrial segmentation based on mito-GFP signal using a threshold value of 0.1. **(iii)** Mitochondrial segmentation based on mito-GFP signal using a threshold value of 0.3. The different colors depict the automatically segmented mitochondrion.

IV-2.2. Final mitochondrial image analysis pipeline.

MCF-7 cells stably expressing mitochondrial targeted GFP (mito-GFP (Rizzuto, Dsandona et al. 1990)) were imaged by high-resolution WFM with CCD image capture. This allows for single-mitochondria resolution and is fast enough to capture the response kinetics and minimize light exposure, while preventing motion artifacts (Frigault, Lacoste et al. 2009).

Collected images were submitted to the workflow described in Figure IV- 11A. Importantly, images were first deconvolved using a constrained iterative algorithm (Figure IV- 9 and 11A-i) to increase the classification accuracy (93% accuracy for deconvolved vs. 65% accuracy for nondeconvolved; data not shown). Initial datasets were generated from putative conditions with enriched `Networked´, `Fragmented´ and `Swollen´ phenotypes (Figure IV- 11B). Networked-liked mitochondria are associated with a protective state, including reduced cytochrome *c* release and inhibition of Bax. The fragmented state is associated with mitochondrial outer membrane and inner membrane disruption, Bax activation, cytochrome *c* release, and ROS production (Parra, Eisner et al. 2008). The swollen state is associated with apoptotic events, including outer membrane rupture resulting from inner membrane matrix swelling as well as with a protective preconditioning response (Benard, Bellance et al. 2007; Benard and Rossignol 2008; Sauvanet, Duvezin-Caubet et al. 2010).

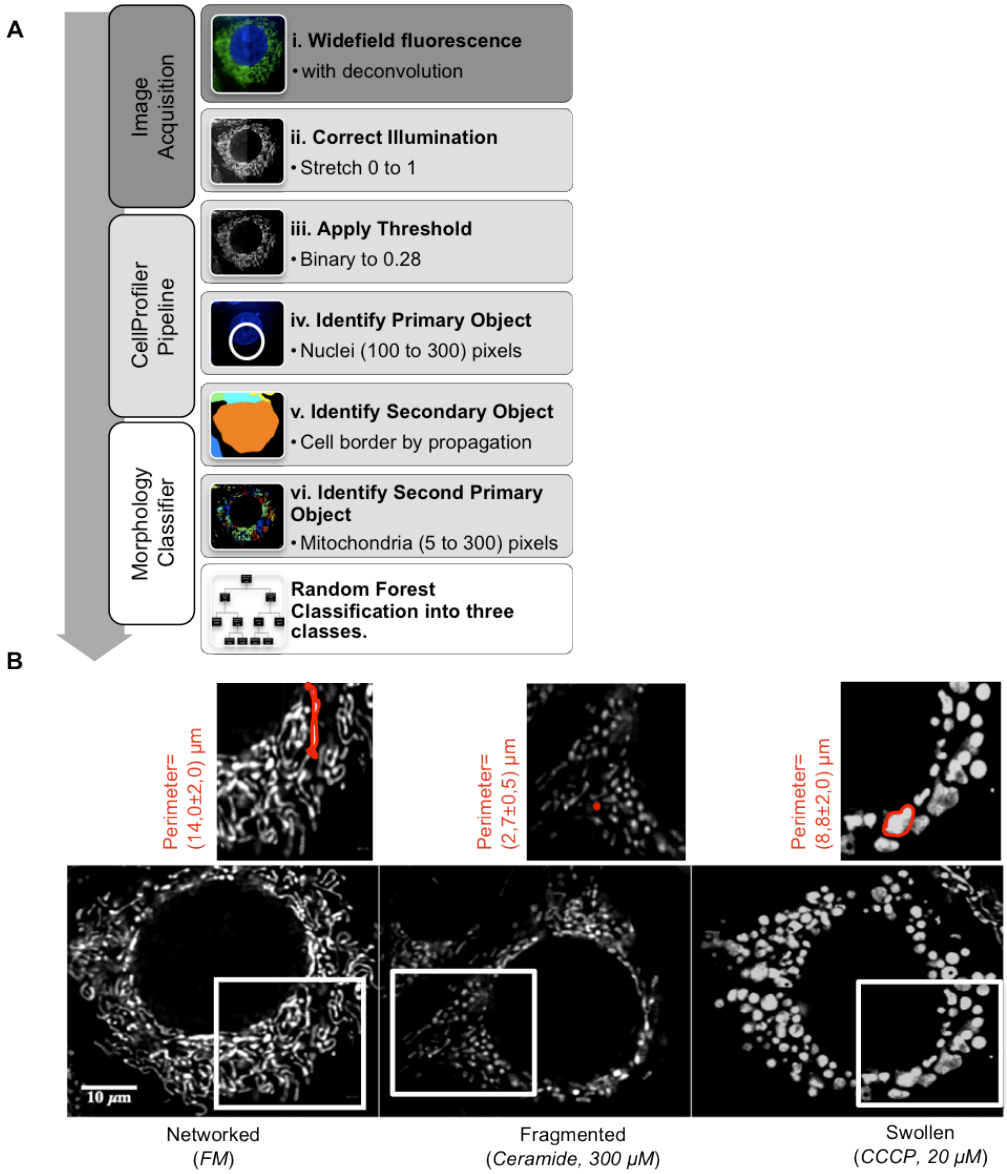

Figure IV- 11. Mitochondrial morphology classification. (A) Method pipeline - Principal modules: 1- Image acquisition; 2 - CellProfiler analysis; 3- Random Forest (RF) classification. MCF-7 cells stably expressing mito-GFP were submitted to different apoptotic drugs for 6 hours at 37°C. Microscopic images were randomly acquired with a DVRT microscope and deconvolved. **(i)** Example of a half non-deconvolved (left) and half deconvolved (right) cell. Images were loaded into the CellProfiler pipeline: **(ii)** Illumination correction. **(iii)** Threshold application. **(iv)** Primary object (cell) identification based on Hoechst-labeled nuclei. **(v)** Identification of the cell borders. **(vi)** Segmentation of individual mitochondria. Finally, 69 relative features were extracted and exported to build a Random Forest (RF) tree classifier. **(B)** Cell-based classification - MCF-7 cells stably expressing mito-GFP were incubated 6 hours under controlled conditions to induce networked (FM), fragmented (ceramide, 300 µM) and swollen (CCCP, 20 µM) mitochondria. Average perimeter values (example shown in red) were measured from 10 individual mitochondria from the zoomed region. Representative images correspond to the middle slice from 3D Z-stacks.

Networked states were obtained under full medium (FM) conditions. Fragmentation was induced by the pro-apoptotic lipid second messenger ceramide (Parra, Eisner et al. 2008) and swelling was achieved by using the mitochondrial uncoupler CCCP (carbonyl cyanide mchlorophenylhydrazone)

(Ganote and Armstrong 2003). Example images representing these three classes were initially characterized by manual extraction of mitochondrial perimeters (Figure IV- 11B). Perimeter size was greatest for networked mitochondria (14.0±2.0 μm), followed by swollen (8.8±2.0 μm) and fragmented (2.7±0.5 μm). Initial control perturbations revealed a high degree of perimeter variation within intracellular mitochondrial population and among cell populations. However, the manual analysis and extraction of single mitochondrion perimeter values was shown insufficient to characterize all mitochondria within one cell. In addition to this limitation, it was time-consuming and unfeasible for large-scale datasets.

Table IV- 1. Feature-categories extracted by the CellProfiler pipeline.

Shape Features	Signal Features	Texture Features	Number of Neighbors	Number of Mitochondria
Area Eccentricity Solidity Extent Euler Number Perimeter Major Axis Length Minor Axis Length Orientation	Integrated Intensity Mean Intensity Standard Intensity Min Intensity Max Intensity Integrated Intensity Edge Min Intensity Edge Max Intensity Edge Mass Displacement	Gabor X Gabor Y Angular Second Moment Contrast Correlation Variance Inverse Different Moment Sum Average Sum Entropy Entropy Difference variance Zernike Numbers	Number of Neighbors Percent Touching Angle between Neighbors	Number of Mitochondria per cell Mean Distance to the cell membrane

(All features are given as averaged values per cell; Min- Minimum; Max- Maximum.)

Therefore, our pipeline comprised automatic segmentation of individual nuclei, inference of cell boundaries based on mito-GFP signal, segmentation of mitochondria within assigned cells and feature extraction (Figure IV- 11A). Feature sets include mitochondrial size (e.g. area/volume), number and distribution within the cell, texture and shape features (Table IV- 1) for a total of 69 features per cell, which were automatically exported to a SQL database (Table III- 2 to 4). These extracted features were used for machine learning and therefore constitute the basis of the mitochondrial morphology classifier.

IV-2.3. Machine learning based classification of mitochondrial morphology.

Machine learning is an area of artificial intelligence that deals with finding an optimal algorithm to solve a complex problem. In this study, our specific problem was to analyze a set of images. Supervised learning was achieved by presenting the machine learning method with training data. Therefore, we first estimated the number of cells necessary to obtain more than 80% of classification accuracy (Figure IV- 12).

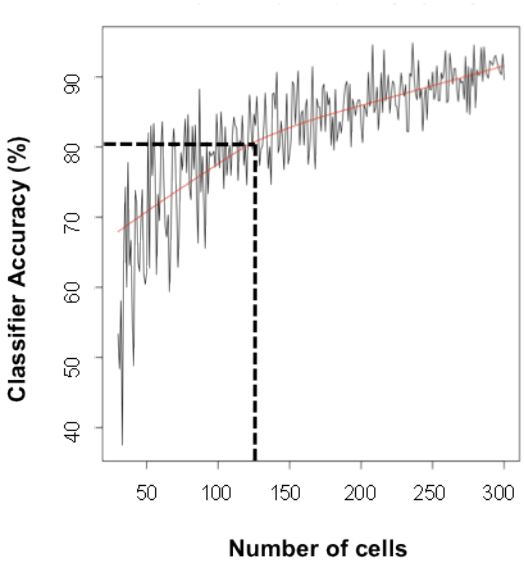

Figure IV- 12. Classifier accuracy simulation. Bootstrap of 70 original cropped MCF-7 cells stably expressing mito-GFP. Dotted line shows that approximately 125 cells are necessary to obtain 80 % of classifier accuracy.

IV-2.3.1. Morphology classifier performs with 92% accuracy in single cells.

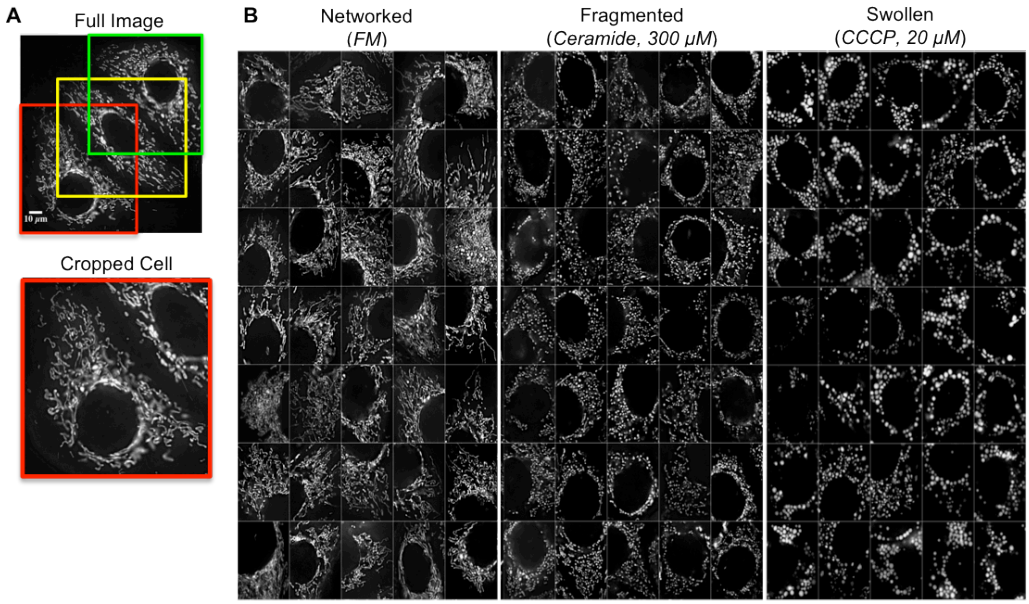

Figure IV- 13. Single-cell analysis. (A) Training sets were built from manually cropped single cells. An example of a "full image" with regions of interest (ROIs) for individual cells and a corresponding "cropped cell" are depicted. **(B)** Phenotypic variability- representative examples of mitochondrial phenotypes selected for training each class. MCF-7 cells stably expressing mito-GFP were incubated 6 hours at 37°C with the 3 control conditions: full medium (FM), ceramide (300 µM) and CCCP (20 µM).

Next, we developed a supervised learning approach using an image set of cells, which were individually cropped and manually classified as `Networked´, `Fragmented´ or `Swollen´ (Figure IV-13). These image sets were obtained from the above-described control conditions (FM, ceramide and CCCP) and submitted to the CP pipeline (see Methods for detailed description). The extracted features (Table III- 2 to 4) were used to build the Random Forest (RF) classifier. Two training sets of cropped and manually classified cells were used to build and validate the RF classifier (see Figure IV- 13 and 14). In order to compare our manual classification with the RF classification, we have assigned one class per cell. This is necessary due to the impossibility to distinguish intermediate classes within one single cell by eye. Our classifier is able to discriminate sub-populations of classes within one cell and offers a percentage of belonging to each class per cell ((%Networked/%Fragmented/%Swollen =N/F/S)/cell). Therefore, the class with the highest percentage (major score) was considered for comparison and validation purposes. Training sets were cross validated and resulted in 92% overall accuracy (Figure IV- 14).

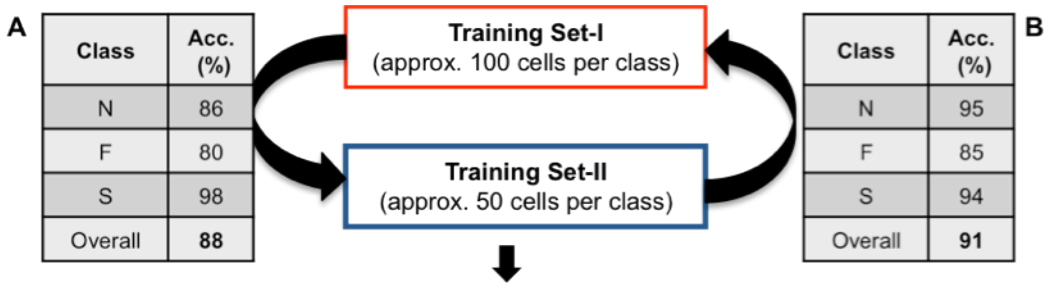

C

10x10 Fold Cross-Validation	Networked	Fragmented	Swollen	Accuracy (%)
Networked	136	12	0	92
Fragmented	7	140	1	95
Swollen	0	15	129	90
Overall				**92**

Figure IV- 14. Random forest classifier. (A) The classification algorithm was first trained with training set I (approx. 100 cropped cells per class) and tested in training set II (approx. 50 cropped cells per class). **(B)** Classifier was trained with training set II and validated on training set I. **(C)** Both datasets (set I and set II) were combined and used to train the final model. Each tree in the ensemble was calculated using a subset of cells stratified according to class and experimental origin. A 10x10 fold cross validation gives an overall accuracy (Acc.) of 92%.

IV-2.3.1.1. Identification of key features for mitochondrial classification.

RF method (Breiman 2001) is an established classification algorithm that shows a very robust and competitive performance on diverse data sets. The algorithm is an extension of the bagging principle (Breiman 1996), a method for improving results of machine learning classification, and consists of a

collection of classification trees. Decision trees are a well-established technique for classification. A classification result is obtained by traversing a tree, with a decision being made at each branch point, until an end point is reached. Decisions are based on attribute values. The end points of a decision tree are class types (Figure IV- 15).

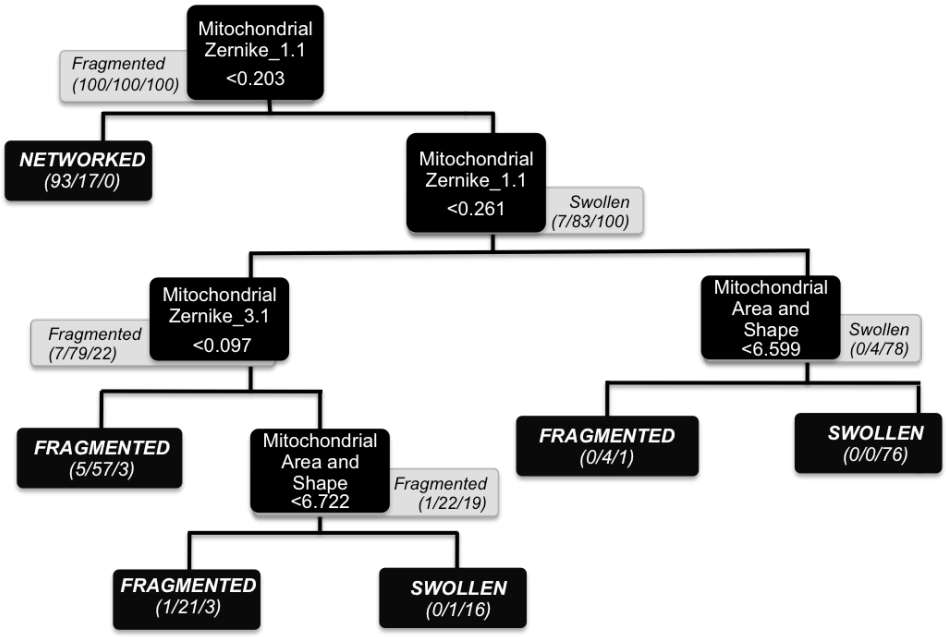

Figure IV- 15. Representative decision tree. Tree consists of fork nodes, each labeled with an attribute and an intermediate class decision, and leaf nodes representing the final morphology classes: (Networked/Fragmented/Swollen)=(N/F/S). Split selection for the tree building process was weighted by the respective feature importance for the classifier accuracy.

While complex ensemble models offer a high accuracy, human interpretation of the model is not feasible. In order to construct an easy to interpret single tree representation of our complex RF classifier, we made use of the Mean Decrease in Accuracy (MDA) score (Figure IV- 15 and 16). This score is a given measure of how important a feature was in the RF model. Thus, scalings were applied when considering splits for the representative tree (Figure IV- 15), so that the improvement on the splitting of a variable is weighted by its cost (1/MDA) when deciding which split to choose (Figure IV- 16).

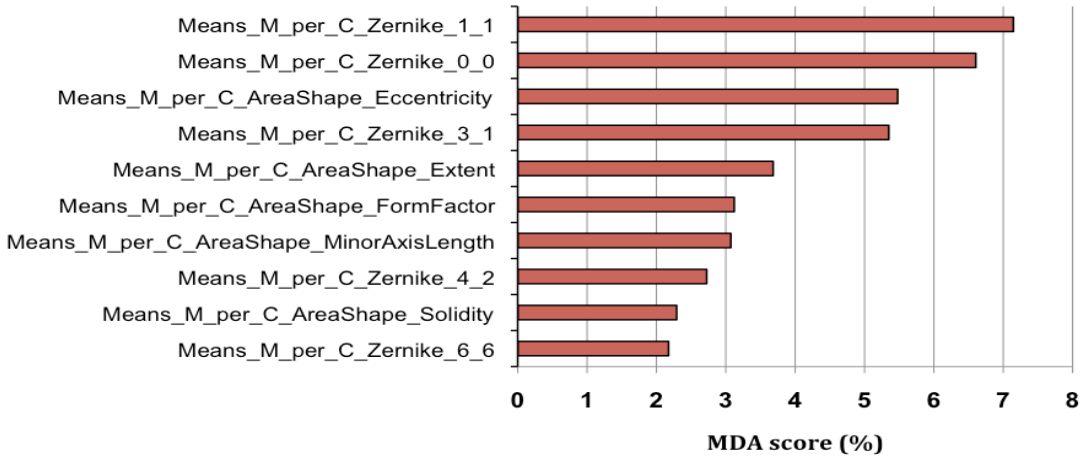

Figure IV- 16. Mean decrease in accuracy (MDA). Estimation of the degree of importance of each feature in the final classification. Chart shows the 15 most important features that affect the classifier accuracy from 0 to 7.25%. (M- mitochondria; C- cell).

Our results show that the "Zernike" features and the mitochondrial "Area and Shape" features were the most relevant for our classification (Figure IV- 15 and 16). Zernike numbers reflect an object "roundness" and are closely related to mitochondrial shape. Additionally, our decision tress shows that `Networked´ is the most differentiated mitochondrial class, followed by `Fragmented´ and `Swollen´, where the mitochondrial "Area and Shape" is determinant for deciding between these two classes (Figure IV- 15). The representative tree was not used for classification purposes; all classification results used for further analysis were obtained directly from the RF model build upon the training sets (Figure IV- 13). Subsequently, the prediction of our classifier (1) was not substantially biased for new cells, which did not undergo manual classification (Figure IV- 14), and (2) describes mitochondrial intracellular heterogeneity by assigning a degree of belonging (RF score) to each class for each cell (%(N/F/S)/cell). This is based on the percentage of trees in the ensemble voting for a specific class, and is the basis for all further analysis steps.

IV-2.3.2. The RF classifier can be used in multiple cells images.

The feature extraction pipeline was created and optimized for the morphological classes using cropped singled cells, manually classified as ´Networked´, `Fragmented´, or `Swollen´ phenotypes (Figure IV-11B and 13). Nevertheless, the ultimate challenge in machine learning is that a "learned" algorithm works correctly on (previously unseen) test data. Only the comparison against such test data provides an objective measure of the quality of the "learned" algorithm, and ultimately of the machine learning method. Thus, this pipeline was applied to full images that had not undergone manual cropping.

A

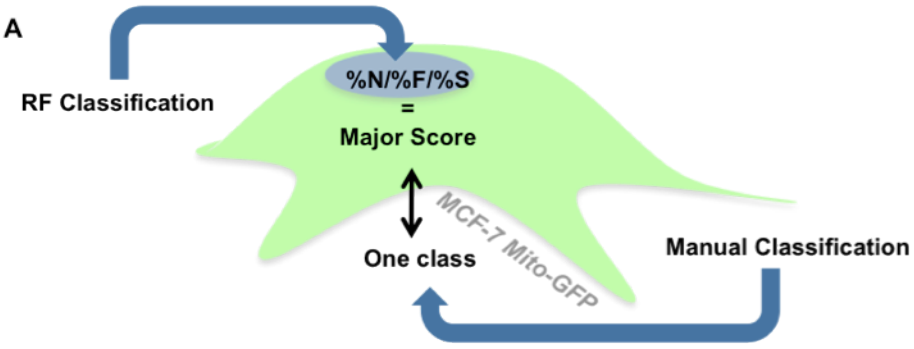

B

Full Images Set	*Networked*	*Fragmented*	*Swollen*	SUM
Manually classified	54	55	50	159
RF classification	58	47	54	159
Class Accuracy (%)	93	85	92	
Mean Accuracy (%)	90%			

Figure IV- 17. Automatic classification of raw images. (A) Scheme representing the random forest (RF) classification of one cell-mitochondria population into a percentage of `Networked´, `Fragmented´ and `Swollen´. From the three classes, the one with the highest percentage (major score) is taken for comparison purposes with manual classification. **(B)** Manual versus classifier classification- individual cells within their original image were manually classified and the same set of cells were submitted to our RF classifier.

To determine the classifier accuracy on raw images, a new dataset consisting of randomly chosen images from distinct conditions was assembled. From this set, 159 individual cells with a clear definable phenotype were manually classified and manual classification of single cells was assessed against RF classification of the same cells within their original raw images (Figure IV- 17). Once again, for comparison with manual classification, we took in consideration only the major score (highest percentage) within each cell (Figure IV- 17A). The results show that our method presents comparable results when classifying individual cells within full images to manual classification (90% accuracy; Figure IV- 17B).

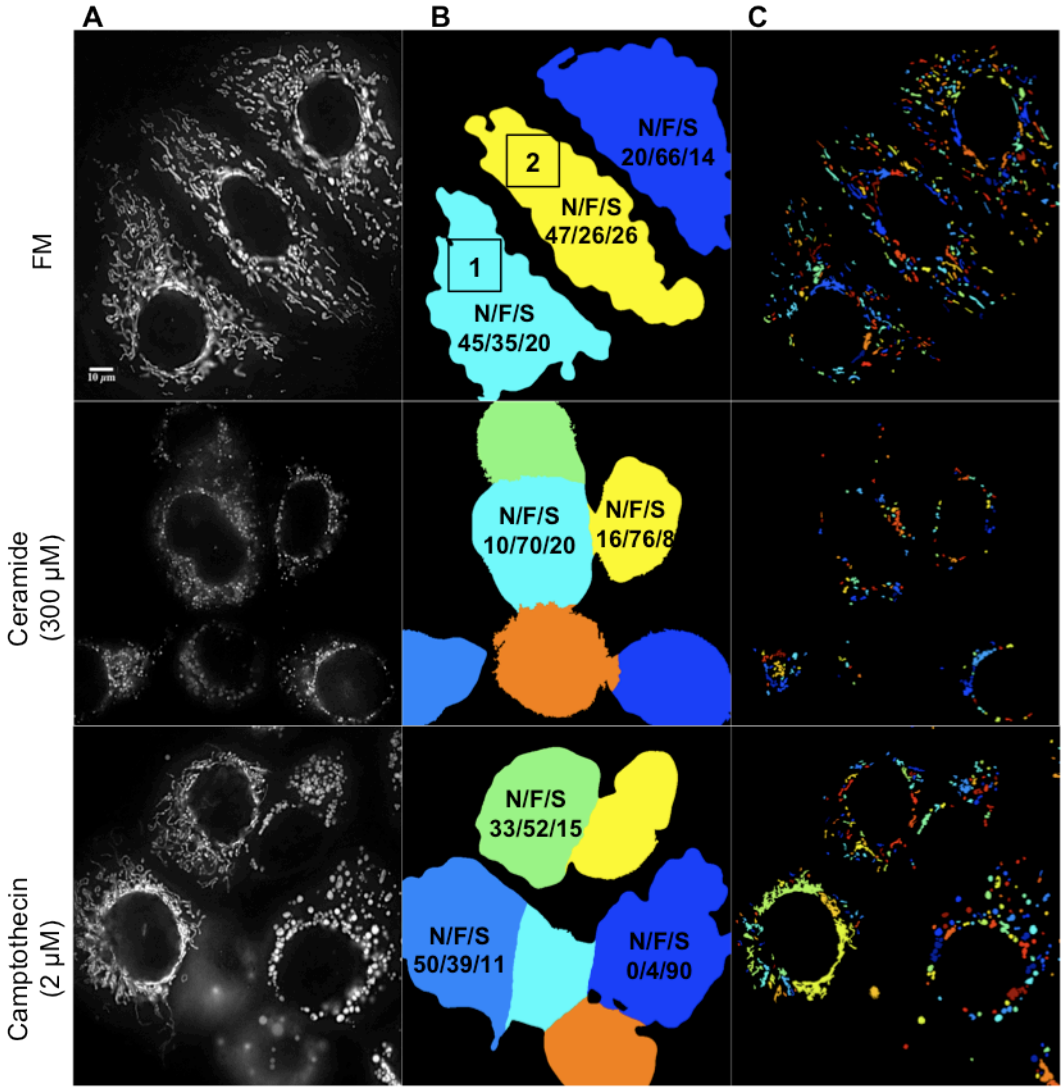

Figure IV- 18. Population-wide analysis of mitochondrial morphology. CellProfiler pipeline applied to raw images. MCF-7 cells stably expressing mito-GFP after 6 hours incubation (37°C) in control condition (FM) and drug conditions (ceramide, 300 µM, camptothecin, 2 µM). **(i)** Representative examples of images as obtained by the DVRT microscope after deconvolution. **(ii)** Cell border identification and segmentation with final classification for each considered cell (color code corresponds to single cell segmentation). **(iii)** Mitochondrial segmentation per cell (color code corresponds to single mitochondrion segmentation). Percentage values of Networked/Fragmented/Swollen (N/F/S) mitochondria are attributed to each cell. These values (N/F/S) can next be averaged per condition to obtain whole cell population shifts on mitochondrial morphology under the tested condition.

In Figure IV- 18 we show representative examples of segmented images (cell and mitochondria) by the CP and respective cell-based RF classification. The classifier attributes a degree of belonging to each of the three main classes: `Networked´, `Fragmented´ and `Swollen´ (N/F/S) for each cell and these three values are always taken into consideration, averaged per condition. Initial conditions revealed a high degree of intracellular and population-based heterogeneity. Interestingly, cells treated with FM showed high intracellular variability, as exemplified in Figure IV- 18: *cell 1* shows close

percentages of all classes and *cell 2* has as much fragmented as swollen mitochondria. Additionally, some conditions revealed high intercellular heterogeneity as illustrated for camptothecin where each cell presents a clearly different major class (Figure IV- 18). In contrast, ceramide-treated cells presented a very consistent classification, with fragmented mitochondrial scoring the highest within individual cells (Figure IV- 18).

In summary, the generated pipeline was accurate when applied to images containing multiple cells (Figure IV- 17 and 18) and was able to quantify the mitochondrial morphology response as a function of perturbation-induced shifts of networked, fragmented, and swollen sub-populations. Moreover, we were able to identify "intermediate" classified cells and thereby provide a quantitative index of intracellular heterogeneity (Figure IV- 18).

IV-2.4. Population analysis of mitochondrial morphology dynamics in response to diverse apoptotic stimuli.

We next quantified redistributions of morphology sub-populations in response to various pro-apoptotic stimuli. Cells were treated with compounds known to impact mitochondrial bioenergetics and induce mitochondrial apoptosis. It is important to note that our experimental model, MCF-7 breast cancer cells, lack caspase 3 (Jänicke, Sprengart et al. 1998), and therefore undergo a slower progression of cell death. Additionally, as apoptosis progresses, cell shrinkage and blebbing occur (Kerr, Wyllie et al. 1972), making analysis of mitochondrial distribution more complex and prone to artifacts. Therefore, we chose an early timepoint to investigate mitochondrial morphology (6 hours).

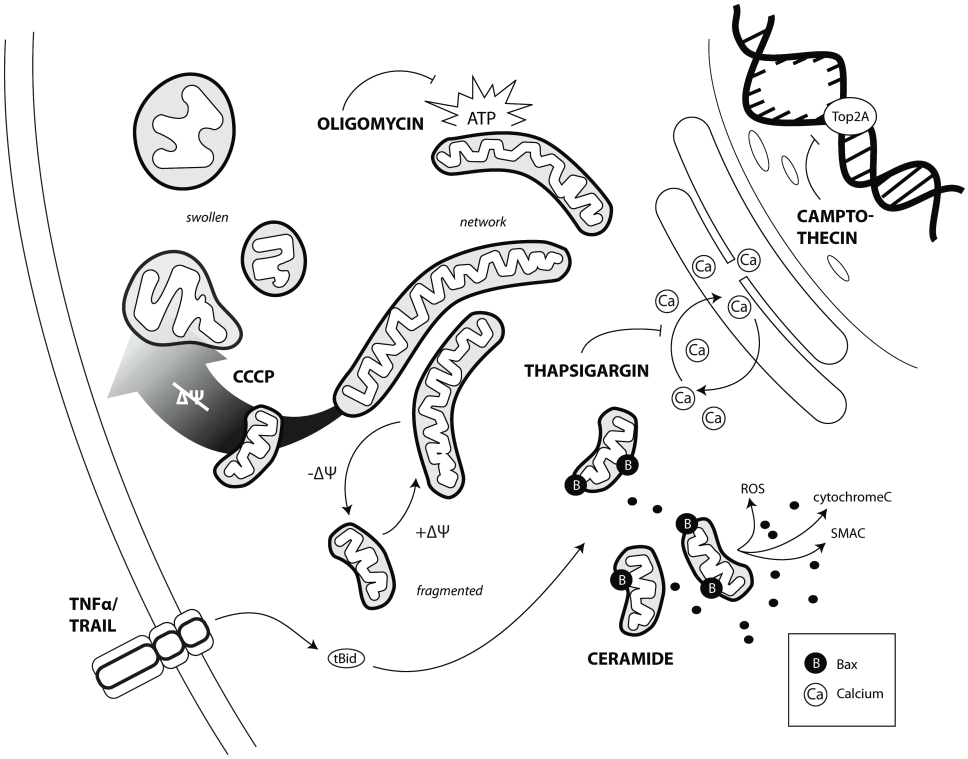

Figure IV- 19. Pro-apoptotic conditions. Cartoon scheme representing the tested apoptotic drugs and its targets. MCF-7 cells stably expressing mito-GFP were incubated for 6 hours at 37 °C with 7 different apoptotic drugs causing a variety of cellular stress: calcium (Ca) overload (thapsigargin, 1 μM); DNA synthesis inhibition (camptothecin, 2 μM); ATP synthesis inhibition (oligomycin, 10 μM); death receptor (DR) pathway activation (TNFα, 43 ng/mL and TRAIL, 20 ng/mL); mitochondrial fragmentation (ceramide, 300 μM); as well as a mitochondrial uncoupler (CCCP, 20 μM). The scheme summarizes the subcellular impact of our drug selection and depicts the three possible morphologic states of mitochondria: `Networked´, `Fragmented´ and `Swollen`. For example, DR activation cleaves Bid into tBid, which leads to Bax clustering at the mitochondria. Mitochondria are shown in a fragmented state during cytosolic release of pro-apoptotic signaling factors and related to a swollen stated upon loss of $\Delta\Psi_m$ (gradient arrow).

Drugs were selected which initiate mitochondrial apoptosis in a spatially heterogeneous manner (Figure IV- 19). DR ligands TNFα (43 ng/mL) and TRAIL (20 ng/mL) activate the mitochondrial death pathway via caspase 8-mediated cleavage of Bid (Li, Zhu et al. 1998). The ER Ca^{2+} pump inhibitor thapsigargin (1 μM) induces ER stress, cytosolic Ca^{2+}, and subsequent activation of BH3-only proteins (Puthalakath, O'Reilly et al. 2007). Camptothecin (2 μM), a DNA topoisomerase I inhibitor, induces mitochondrial apoptosis (Shimizu and Pommier 1997). Bioenergetic perturbations were induced with oligomycin (10 μM), which inhibits oxidative phosphorylation at the mitochondrial ATP synthase (Penefsky 1984).

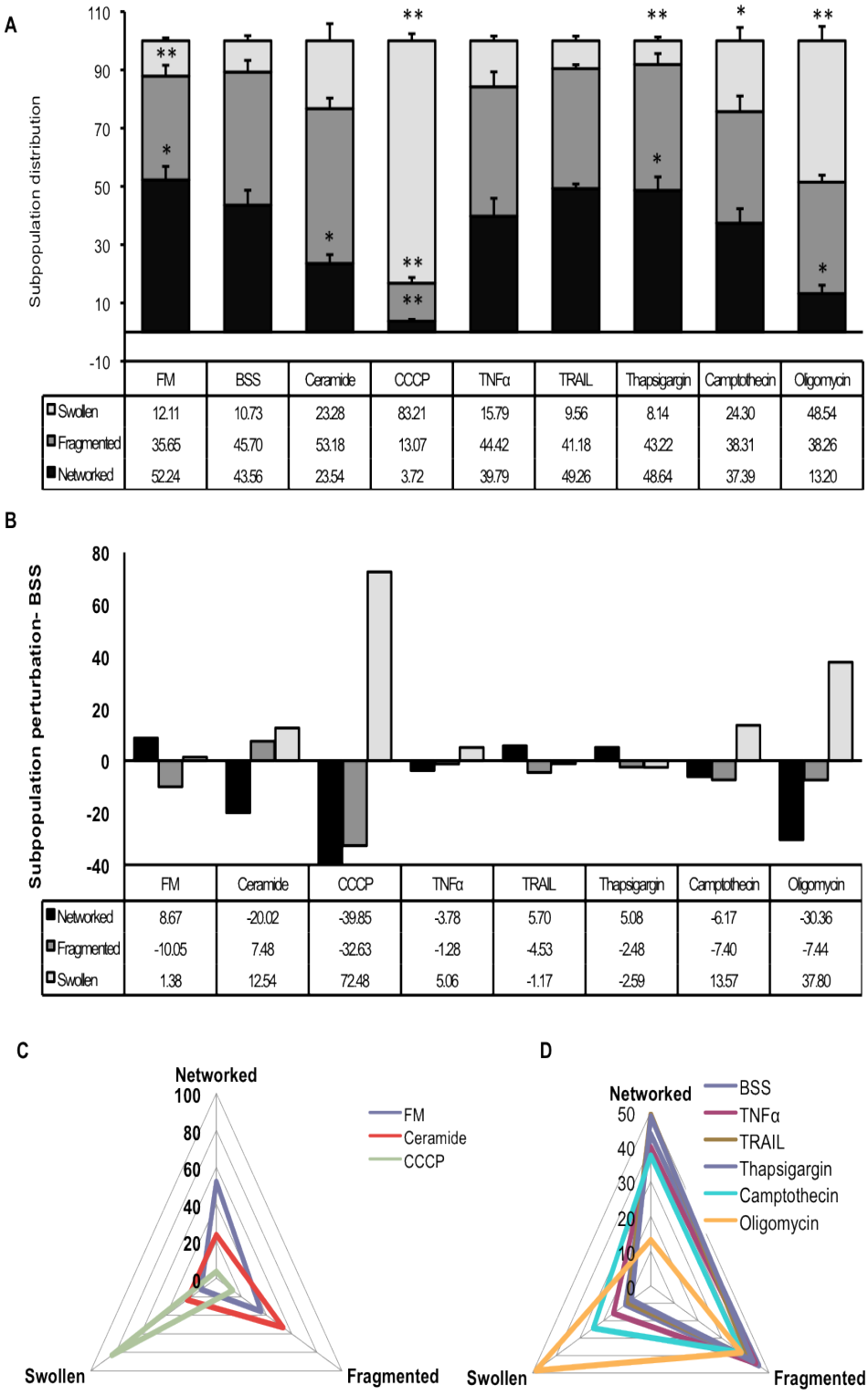

Figure IV- 20. Mitochondrial morphologic classes quantification in response to apoptotic stimuli. (A) Classes distribution during apoptosis- Column chart shows the Random Classifier (RF) classification into `Networked´ (black), `Fragmented´ (gray) and `Swollen´ (white) for the different conditions. Values are given as mean percentage ± s.e.m. (N=3, approx. 300 cells per condition). **(B)** Normalization with control- Results plotted in A are normalized to BSS (0%). **(C)** Radar plots corresponding to control conditions. **(D)** Radar plots corresponding to other tested conditions. (C and D correspond to the same values as A and therefore are plotted as percentages).

As explained above, images were acquired following 6 hours of respective treatment at 37°C and approximately 100 cells per condition were classified in at least 3 individual experiments. Plotted results reflect the drug impact on mitochondrial sub-populations, as (N/F/S) percentage distributions are all taken into account and averaged throughout the whole cell population for each N (Figure IV-20). In parallel to the apoptotic conditions, cells were incubated with two control conditions: FM and BSS (basic salt solution). Under FM conditions, mitochondria were mostly networked ((N/F/S)±s.e.m. = (52,24±4,62/35,65±3,70/12,11±0,98)%). Cells incubated in BSS showed changes ((N/F/S)±s.e.m. = (43,56±5,11/45,70±4,00/10,73±1,74)%), with increased fragmentation and decreased networked mitochondria (Figure IV- 20A). As expected, CCCP revealed a 72% increase in the population of swollen mitochondria compared to the control (BSS) (Figure IV- 20B and C). Interestingly, ceramide incubation resulted only in a small increase of fragmented mitochondria ((N/F/S)±s.e.m. = (23,54±3,03/53,18±3,59/23,28±5,86)%) when compared with BSS (Figure IV- 20B and C). Ceramide has been previously reported to cause increased mitochondrial fragmentation (Parra, Eisner et al. 2008), which was confirmed by our single-cell analysis (Figure IV- 11, 13 and 18). In contrast, our population-based results revealed a wider picture. When comparing population with single cells analyses, we observed that ceramide-treated cells showed the greatest percentage of fragmented mitochondria (Figure IV- 20B). However, networked and swollen mitochondrial population showed an increase of 22% (Figure IV- 20B and C). This difference suggests that ceramide-induced fragmentation in single cells analysis is limited and further supports the use of automated mitochondrial morphology classifiers in a population-based manner.

TNFα and TRAIL ligands showed subtle but distinct changes in mitochondrial morphology distribution compared to BSS (Figure IV- 20B). While the population of swollen mitochondria increased for TNFα, networked mitochondria remained unchanged in response to TRAIL (Figure IV-20B). Oligomycin considerably increased the number of swollen mitochondria ((N/F/S)±s.e.m. = (13,20±2,87/38,26±2,39/48,53±4,91)%) (Figure IV- 20B and D). Thapsigargin treated cells exhibited a high percentage of networked mitochondria with fragmentation and swollen populations smaller than the control ((N/F/S)±s.e.m. = (48,64±4,62/43,22±3,74/8,14±1,26)%) (Figure IV- 20B and C). Finally, camptothecin revealed a similar percentage of both networked and fragmented mitochondria ((N/F/S)±s.e.m. = (37,39±4,96/38,31±5,33/24,30±4,55)%) with a 13% increase of swollen mitochondria when compared to BSS (Figure IV- 20B and C). Figures IV- 20C and D show radar plot sub-representations of the results (A and B) where it is possible to identify the conditions that showed the most outliner behaviors when compared to each other.

In summary, FM incubation maintained the most networked-mitochondria, while CCCP revealed the highest percentage of swollen mitochondrial population, which was followed by oligomycin, camptothecin and TNFα respectively. In these analysis, thapsigargin and TRAIL showed the least impact on mitochondrial morphology when compared to BSS (Figure IV- 20C and D).

Table IV- 2. Intercellular variances of mitochondrial class sub-populations under the different drug treatments.

SD (%)	Networked	Fragmented	Swollen	Mean SD (%)
FM	31.26	22.73	14.34	22.78
BSS	28.16	23.40	11.52	21.03
Ceramide	18.39	18.28	18.71	18.46
CCCP	7.60	16.27	21.07	14.98
TNFα	29.48	24.42	18.67	24.19
TRAIL	29.31	24.67	11.09	21.69
Thapsigargin	27.21	23.75	10.67	20.54
Camptothecin	31.06	21.15	27.49	26.57
Oligomycin	12.25	19.06	25.35	18.89

(SD- Standard Deviation calculated based on total mitochondrial population per condition)

The results discussed above were obtained by averaging all partial percentages (%N/%F/%S) per condition and reflect the mean classification of mitochondrial population per experimental "N". In order to assess intercellular heterogeneity after the individual drug treatments, we further calculated the respective variances (Table IV- 2). Intercellular variances (standard deviation, SD) reflect the changes in mitochondrial morphologies throughout the whole mitochondrial population, useful to identify subpopulations shifts. Camptothecin showed the highest intercellular heterogeneity after treatment (SD=25%), while CCCP revealed the least population heterogeneity (SD= 15%) (Table IV- 2). Interestingly, FM revealed a high intercellular variance for networked class, which enhances the intrinsic mitochondrial heterogeneity in standard (no stress-inducing) conditions.

The number and morphology of mitochondria within a cell are a function of fusion and fission events (Bereiter-Hahn and Vöth 1994). Mitochondria display a complex architecture that varies from highly interconnected networks (Rizzuto, Pinton et al. 1998), to precisely structured individual units (Kuznetsov, Usson et al. 2004). Our results show that mitochondrial morphology can vary in a population manner and that subtle but significant differences can be observed (Figure IV- 20).

It is generally acknowledged that there is a correlation between several human pathologies and mitochondrial dysfunction (mitochondrial diseases). However, the dysfunction in these diseases can be related to aberrant mitochondrial "dynamics" (e.g. mitochondrial shape, mobility, and distribution) or to aberrant energy metabolism. In order to explore changes on mitochondrial morphology in the context of apoptosis, we determined the impact of the drugs employed above on mitochondrial energetic state, MPT sensitivity, ROS production, cytochrome *c* release and Bax activation.

IV-3. Drug impact on mitochondrial function and PCD activation.

MOMP is not only regulated by interactions between pro- and anti-apoptotic Bcl-2 members, but also by a family of GTPases, which control mitochondrial morphology (for review see, (Karbowski and Youle 2003)). During the early stages of apoptotic cell death, network fragmentation and cristae remodeling are widely reported (Frank, Gaume et al. 2001; Frieden, James et al. 2004; Karbowski, Arnoult et al. 2004; Lee, others et al. 2004; Szabadkai, Simoni et al. 2004). However, the relationship between morphology and apoptotic signaling remains unresolved, and appears paradoxical. For example, pro-apoptotic Bax can promote mitochondrial fusion (Karbowski, Norris et al. 2006) and fragmentation may be preceded by increased fusion (termed hyperfusion (Tondera, Grandemange et al. 2009)). Furthermore, a pre-fragmented state confers protection by limiting mitochondrion-to-mitochondrion apoptotic signaling (Szabadkai, Simoni et al. 2004). We were interested in investigating early cell death events directly related to mitochondrial function and injury. Thus, we monitored $\Delta\Psi_m$, Bax activation and cytochrome *c* release under matching conditions.

IV-3.1. $\Delta\Psi_m$ as a measure of cell sensitivity to apoptotic stimuli.

The use of dyes is more challenging compared to GFP-based sensors, due to photo-toxicity and loading concerns (Bouchier-Hayes, Muñoz-Pinedo et al. 2008).

Tetramethylrhodamine methyl ester (TMRM), a fluorescent lipophilic cation that electrophoretically accumulates in mitochondria (Métivier, Dallaporta et al. 1998), can be photoactivated to generate ROS levels within the mitochondrial matrix, sufficient to trigger mitochondrial potential transition (MPT) (Bradham, Qian et al. 1998). In turn, dichlorodihydrofluorescein diacetate (H_2DCF- DA) is one of the most commonly used indicator of ROS production (e.g. H_2O_2) (Presley, Fuller et al. 2003). Because of the heterogeneous sensitivity of mitochondria to MPT activation, we measured multiple parameters of mitochondrial energetic response to stress. As such, single cell (and sub-cellular) MPT events were quantified and averaged over the population.

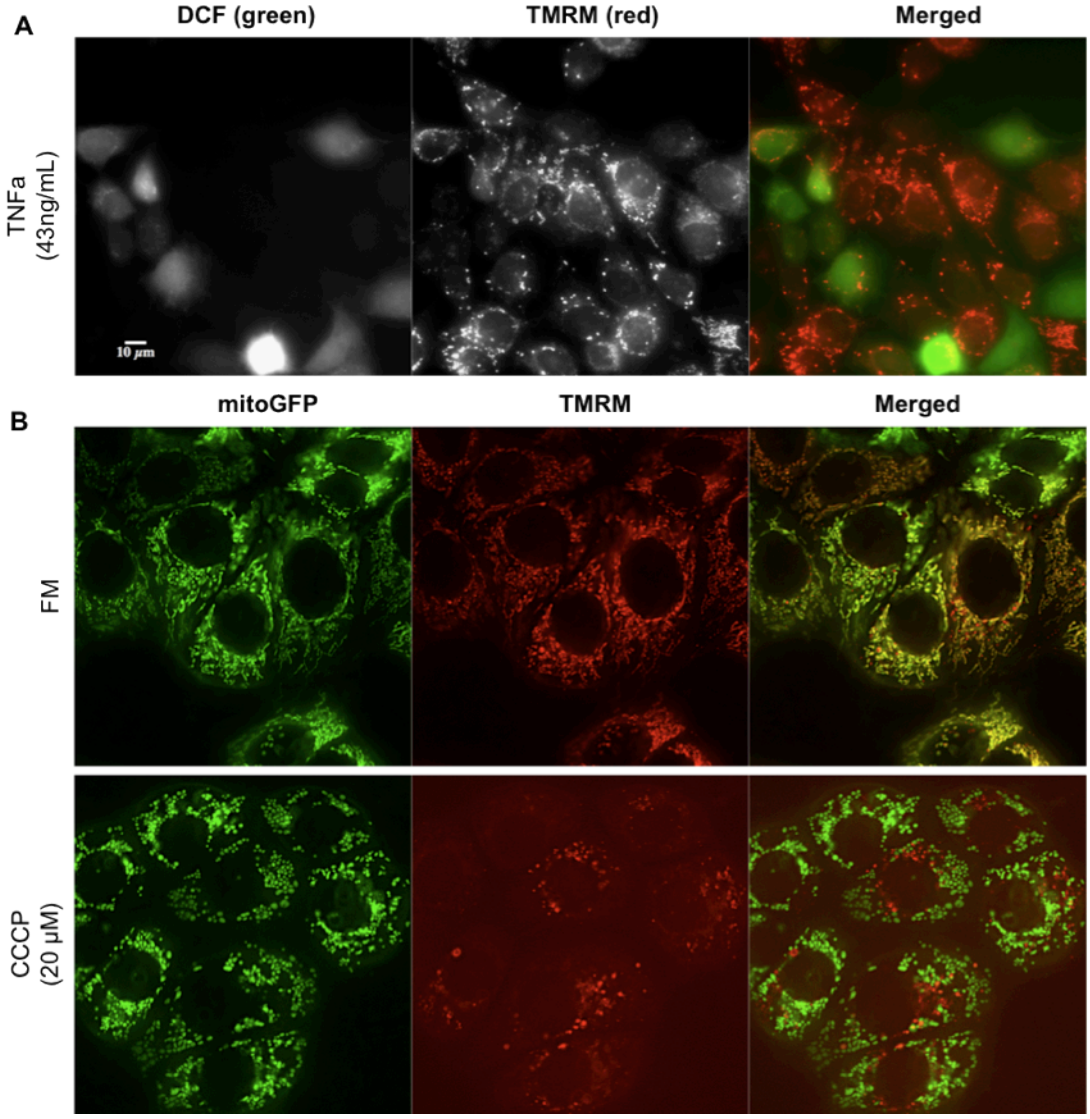

Figure IV- 21. Imaging of ROS production and $\Delta\Psi_m$. (A) Representative region of MCF-7 wt cells treated with TNFα (43 ng/mL, 6 hours) were stained for ROS production (H_2DCF- DA green, 10 μM) and for mitochondrial membrane potential ($\Delta\Psi_m$) (TMRM-red, 25 nM). **(B)** MCF-7 cells stably expressing mito-GFP were treated for 6 hours with CCCP (20 μM) or with full medium (FM) and stained with tetramethyl rhodamine methyl-ester (TMRM, 25 nM).

Figure IV- 21A shows an example of cells simultaneously stained with TMRM (25 nM, red) and H_2DCF- DA (10 μM, green). Here it can be observed that cells in which TMRM signal is low (loss of $\Delta\Psi_m$) show accumulation of H_2DCF- DA signal (ROS production). Upon 6 hours incubation with TNFα, elevated ROS production is detected in cells with low or no TMRM signal (Figure IV- 21A). Likewise, CCCP-treated cells showed reduced or no TMRM signal after 6 hours. Noticeably, these mitochondria lost their elongated shape when compared with control (FM) (Figure IV- 21B).

IV-3.1.1. Population analysis of $\Delta\Psi_m$ in response to diverse apoptotic stimuli.

When using rhodamine derivatives, depolarization is assessed from the changes in mitochondrial fluorescence. We found that 25 minutes incubation with 25 nM TMRM at 37°C resulted in a matrix loading so that photo-oxidatively activated species caused local fluctuations in mitochondrial membrane potential ($\Delta\Psi_m$). These were apparent as localized *decreases* in mitochondrial fluorescence (Figure IV- 22B). Therefore, continuous fluorescence imaging was performed for 5 minutes to induce ROS-dependent triggering of the MPT (Figure IV- 22, 23A and see Figure III- 2) as it has been previously reported (Brady, Elmore et al. 2004).

Initially, mitochondria appeared as homogeneously polarized and then entered a phase of stochastic flickering, i.e. transient redistribution of TMRM (Figure IV- 22). Eventually, $\Delta\Psi_m$ collapsed within mitochondrial populations (Figure IV- 22B). In Figure IV- 22A, representative examples are shown for single mitochondria after control (FM) or drug treatment (TNFα). By following the TMRM signal intensity over time in mitochondrial areas (mean signal intensity plotted in red) or cytosolic regions (mean signal intensity plotted in blue) it is possible to observe a gradual decrease in mitochondrial-TMRM and an increase in the cytosolic-TMRM signal (Figure IV- 22A). The time to $\Delta\Psi_m$ loss reports the threshold for MPT induction, and can be used as a gauge for mitochondrial sensitivity to specific stresses (Neuspiel 2005).

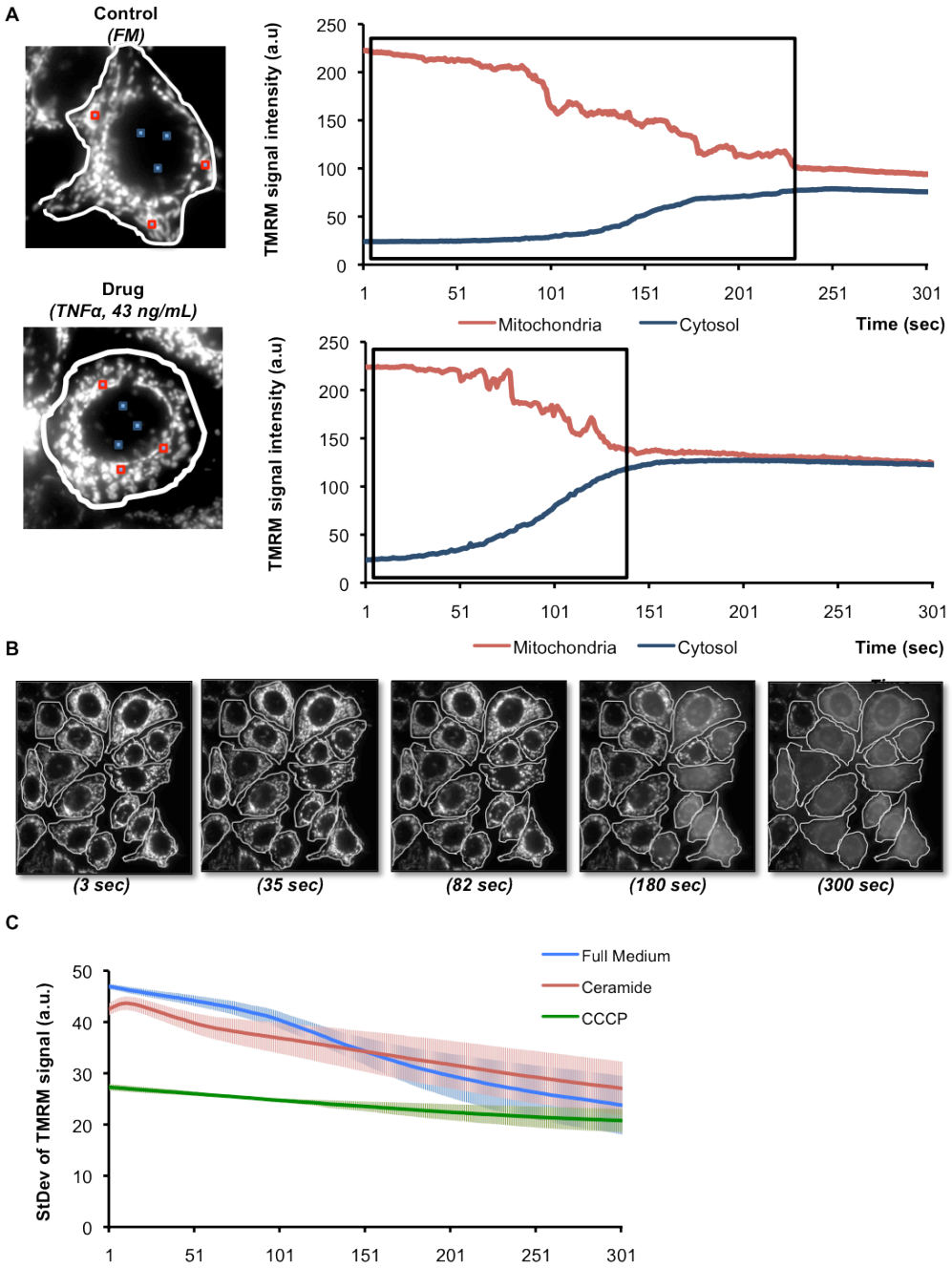

Figure IV- 22. Mitochondrial membrane depolarization. MCF-7 wt cells were incubated with tetramethyl rhodamine methyl-ester (TMRM, 25 nM) for 25 minutes at 37°C after 6 hours treatment. **(A)** Sequential images of TMRM fluorescence were acquired every second using exposure times of 20 milliseconds, during a total of 5 minutes. Plotted curves show the TMRM signal over 5 minutes time for one representative cell incubated in FM (control) and one cell incubated in TNFα (drug, 43 ng/mL). The curve plots reveal how the signal varies over time in a mitochondrial region (red) and in the cytosol/nucleus region (blue). Values correspond to the mean value from the 3 regions depicted in the image over time. **(B)** Standard deviation (StDev) of TMRM signal - Distribution of the TMRM signal throughout the whole cell was followed over time by the StDev value that corresponds to the standard deviation of the average gray values within the ROI selection (each individual cell, in white). A single focal plane for 3, 35, 82, 180 and 300 seconds in cells under FM is depicted. **(C)** $\Delta\Psi_m$ loss over time- StDev values per cell are averaged per condition. Here are exemplified the depolarization events for three conditions: FM, Ceramide (300 μM) and CCCP (20 μM). Images were acquired by DVRT microscope with a 40x objective and the middle Z-stack was followed. (Mean values ± s.e.m. per condition are shown; experiments N=4, approx. 400 cells per condition).

To quantify the kinetics of TMRM release, we measured the standard deviation (StDev) of the TMRM signal, which corresponds to the change in TMRM signal over time within one cell (Figure IV- 22B and C). The use of the StDev has been previously applied to monitor cytochrome *c* redistribution during apoptosis (Waterhouse, Goldstein et al. 2001) and to follow the level of distribution of potentiometric dyes in mitochondria (Toescu and Verkhratsky 2000). Additionally, it has been proposed as an optimal approach to distinguish $\Delta\Psi_m$ from the cell membrane potential ($\Delta\Psi_p$) (Duchen, Surin et al. 2003)..

Approximately 100 cells per condition were analyzed in 4 individual experiments and the mean StDev value was plotted (Figure IV- 22C). Figure IV- 22C shows the StDev of TMRM signal over time for FM, ceramide and CCCP, our control conditions for mitochondrial morphology classification. While $\Delta\Psi_m$ loss occurs slowly under FM incubation, ceramide initially causes mitochondrial depolarization in an accentuated fashion, but the TMRM signal is kept stable over time. CCCP, as previously reported and observed here (Figure IV- 21B), shows $\Delta\Psi_m$ loss at the onset of the experiment (Figure IV- 22C).

IV-3.1.2. Photo-toxicity assay induces MPT.

In order to verify that MPT was induced, we first monitored ROS production under our assay conditions and confirmed that after 5 minutes of continuous imaging, ROS was produced under BSS (Figure IV- 23A). Secondly, we tested mitochondrial permeability transition pore (MPTP) inhibition with cyclosporin A (CsA) and bongkrekic acid (BA). CsA and BA are two commonly used MPTP inhibitors, which act at different sites. Namely, CsA binds to the cyclophilin D within the matrix and BA inhibits the inner membrane protein ANT (ATP/ADP translocator) (Figure I- 4) (Zorov, Filburn et al. 2000). Inhibition of $\Delta\Psi_m$ collapse by both compounds independently would implicate the participation of the MPTP. Therefore, MCF-7 cells were treated with either CsA (5 µM, 30 minutes) or with BA (50 µM, 1 hour) previously to 6 hours incubation in BSS. Results show that CsA caused a delay in $\Delta\Psi_m$ decrease and BA blocked $\Delta\Psi_m$ collapse when compared to BSS alone, confirming that MPT is induced (Figure IV- 23B and C).

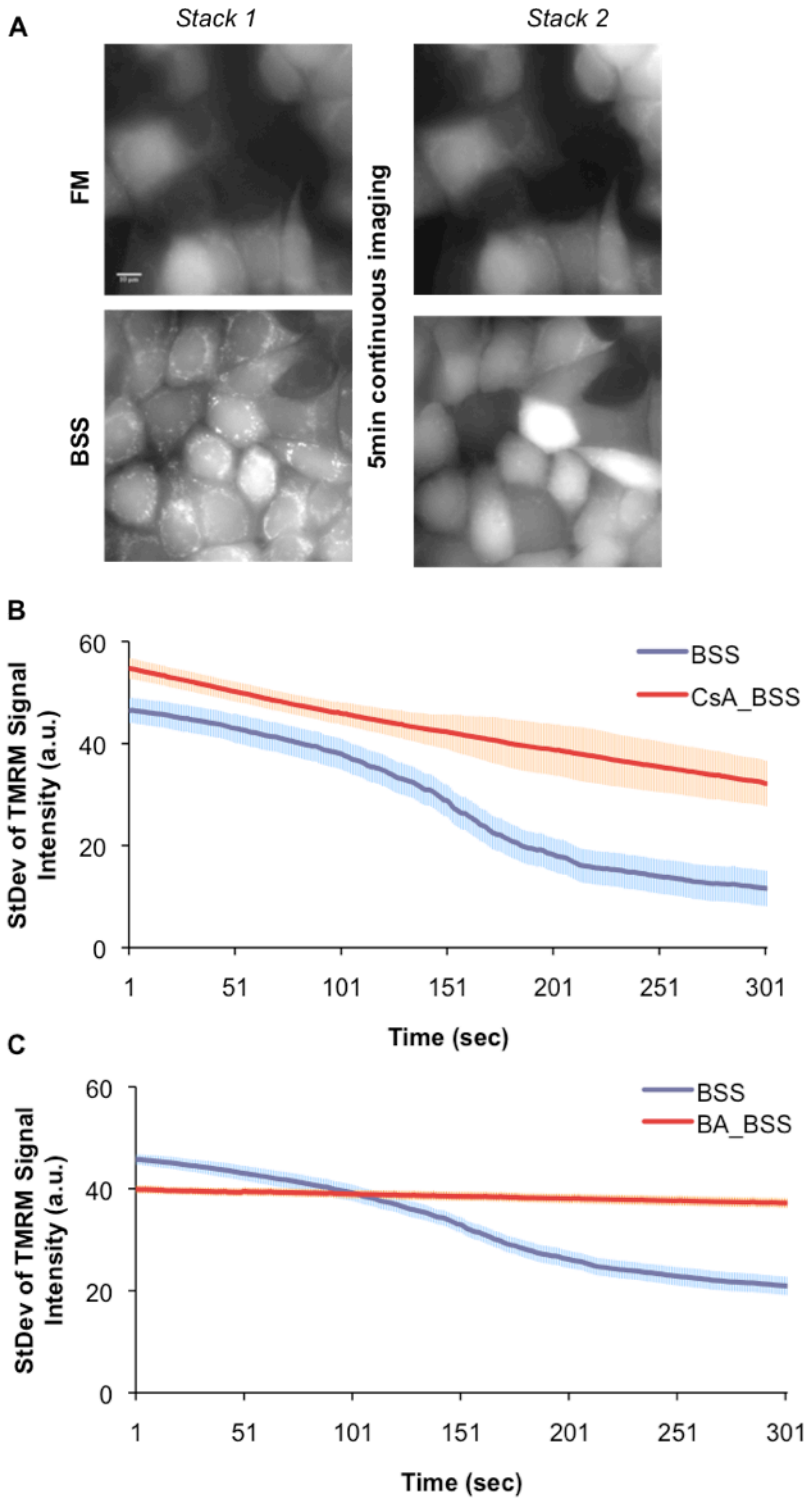

Figure IV- 23. Photo-induction of MOMP. (A) ROS production by laser-induced phototoxicity. - H_2DCF- DA (45 minutes at 37°C) reveals intracellular ROS generation. Stack 1 corresponds to initial ROS production under full medium (FM) or basic salt solution (BSS). Stack 2 is acquired after causing membrane potential damage by a 5 minutes time lapse movie with the red channel for TMRM. **(B)** MPTP inhibition- Cyclosporin A (CsA)- MCF-7 wt cells were treated with CsA (5 µM, 30 minutes) prior to 6 hours incubation in BSS, followed by TMRM addition as described above. **(C)** Bongkrekic acid (BA)- MCF-7 wt cells were treated with BA (50 µM, 1 hour) prior to 6 hours incubation in BSS, followed by TMRM staining as described. (Mean values ± s.e.m. per condition are shown; experiments N=2, approx. 100 cells per condition were followed).

IV-3.1.3. Depolarization responses can be grouped in three main clusters.

Signal dissipation curves for all conditions (Figure IV- 24A) were represented as heatmaps (Figure IV- 24B) to allow an easy comparison between the drugs. As expected, under FM (negative control), TMRM signal dissipation occurred at the latest timepoint (approx. 232 seconds). Euclidean clustering of our results (dendogram in Figure IV- 24B) suggested three main groups: 1) conditions which did not impact initial mitochondrial polarization state, 2) drugs which sensitized mitochondria to depolarization, and 3) drugs which depolarized mitochondria.

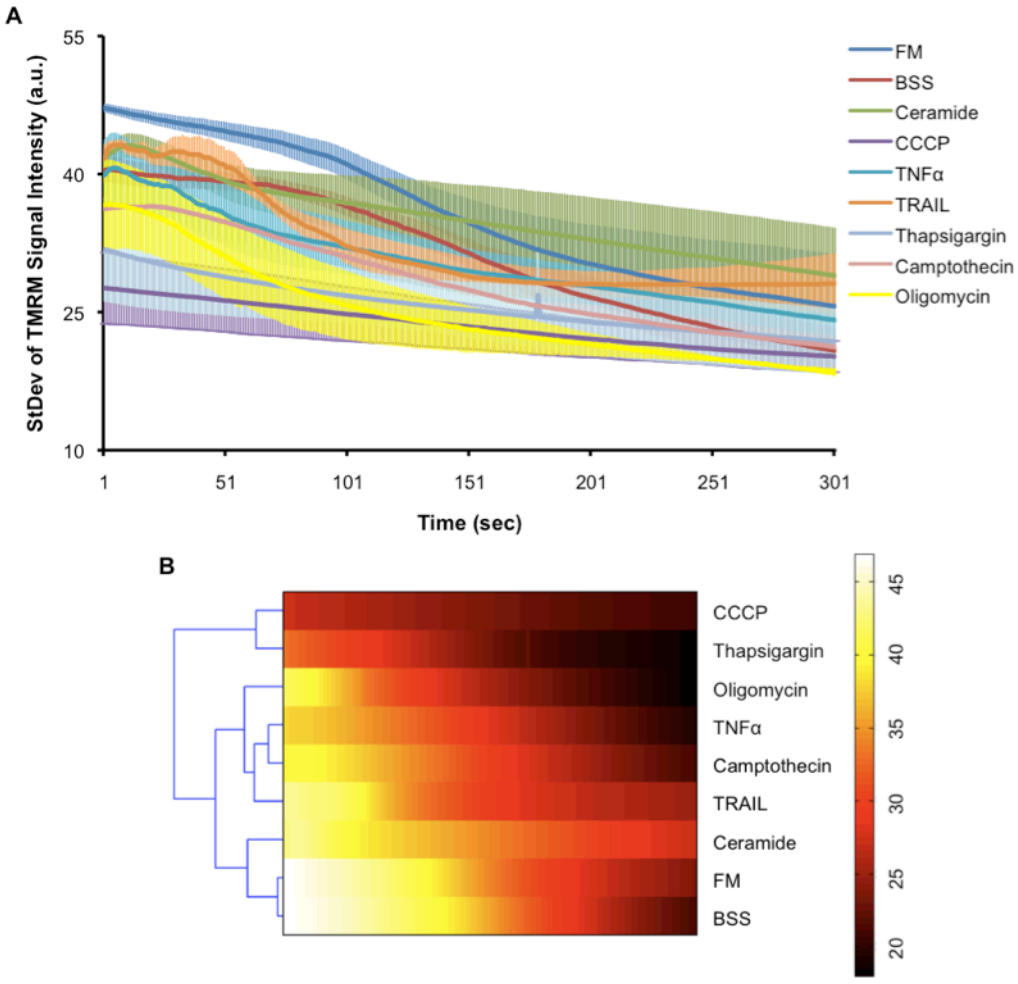

Figure IV- 24. Quantification of $\Delta\Psi_m$ sensitivity in response to apoptotic stimuli. MCF-7 wt cells were incubated with TMRM (25 nM) for 25 minutes at 37 °C after 6 hour treatment with the apoptotic drugs. Sequential images of TMRM fluorescence were then acquired every second using exposure times of 20 milliseconds, during a total of 5 minutes. TMRM signal over time is reported as the StDev value, which corresponds to the standard deviation of the average gray values within each individual cell. **(A)** Depolarization profiles. TMRM signal StDev over 5 minutes (301 seconds) for the all tested conditions: FM, BSS, ceramide (300 µM) CCCP (20 µM), TNFα (43 ng/mL), TRAIL (20 ng/mL), thapsigargin (1 µM), camptothecin (2 µM) and oligomycin (10 µM). Values are presented as mean ± s.e.m. (N=4, approx. 400 cells/condition). **(B)** Data plotted in (A) was depicted as a heatmap. Euclidean clustering (dendogram in blue) revealed cluster 1, 2 and 3.

The latter was apparent for CCCP (20 μM) and thapsigargin (1 μM), in which $\Delta\Psi_m$ was collapsed at the onset of the experiment (Figure IV- 24). In the intermediate group, TRAIL (20 ng/mL), camptothecin (2 μM), oligomycin (10 μM) and TNFα (43 ng/mL) similarly sensitized mitochondria to depolarization events. As expected, under control FM and BSS conditions, $\Delta\Psi_m$ loss occurred at later timepoints, compared to drug treatments. Surprisingly, ceramide (300 μM) clustered together with control conditions. Although the initial StDev of the TMRM signal was low, ceramide revealed a very mild impact on mitochondrial membrane depolarization over time (Figure IV- 24).

IV-3.1.3.1. $\Delta\Psi_m$- Subset extraction.

The dynamic $\Delta\Psi_m$ response was further characterized by extracting three subset features: the half time of StDev-signal decay ($t_{1/2}$_decay); the spread of the StDEv-signal (Y_spread) and the maximum initial StDev-value (MAX) (Figure IV- 25). By extracting this subset, we were able to quantify essential differences in our dataset. For example, our results show that mitochondria incubated with the control conditions (FM and BSS) were more resistant to initial depolarization ($t_{1/2}$_decay) while revealing the highest variation (Y_spread) (Figure IV- 25). In addition, the extracted subset was later incorporated into the fuzzy logic (FL) modeling pipeline in order to infer direct relationships between depolarization events and mitochondrial morphology.

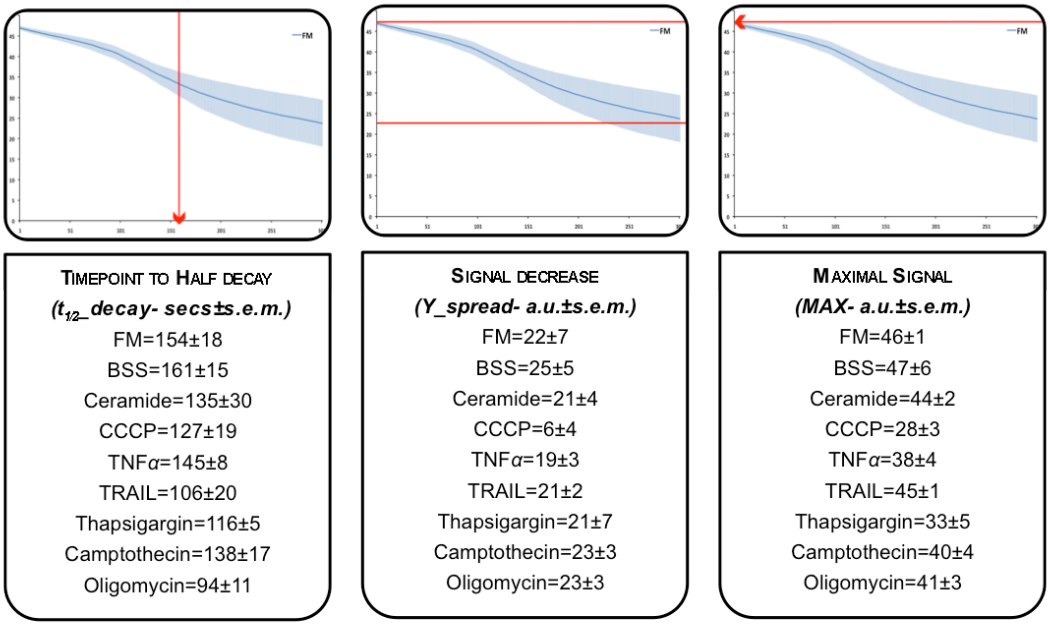

Figure IV- 25. TMRM-derived dataset. Three parameters were extracted per each StDev curve: 1. $t_{1/2}$_decay- time that takes for the signal to reach half of its initial value; 2. Y_spread- Total decrease of the signal over time; 3. MAX- The initial maximum value. These parameters were extracted by using of a MATLAB function (see METHODS for details). Boxes show a representative curve example for the StDev curve of FM over time (301 seconds). (Mean values ± s.e.m. per drug are shown; experiments N=4, approx. 400 cells per condition were followed).

IV-3.2. Apoptotic compounds result in different levels of Bax activation.

In response to apoptotic stimuli, Bax, a multi-domain pro-apoptotic member of the Bcl-2 family, translocates from the cytosol to the mitochondria where it induces MOMP (Wolter, Hsu et al. 1997). In fact, Bax and Bak double-knockout cells fail to undergo MOMP in response to different death stimuli, including staurosporine, ultraviolet (UV) radiation, growth-factor deprivation, DNA damage and endoplasmic reticulum (ER) stress (Wei 2001). Upon activation at the mitochondria, Bax forms high molecular weight aggregates at mitochondrial fission sites, considered the key event for cytochrome *c* release (Wolter, Hsu et al. 1997). Apoptosis caused by BH3-only proteins absolutely requires Bax and Bak (Kuwana, Bouchier-Hayes et al. 2005; Lindsten and Thompson 2006) (Wei 2001) (Wei, Lindsten et al. 2000). We have previously confirmed Bax activation (clustering) in cells expressing tBid and Bnip3 (Figure IV- 5). Next, we were interested in quantifying Bax activation under the same apoptotic conditions used to assess mitochondrial morphology and MPT induction.

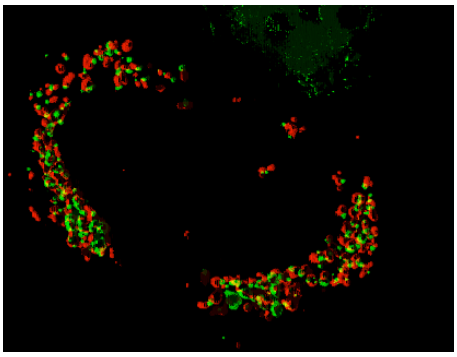

Figure IV- 26. Drp1-induced fragmentation and Bax activation. 3D-resolved image to illustrate Bax clustering under Drp1 expression. MCF-7 cells stably expressing GFP-Bax were co-transfected with mito-mCherry and Drp1_pcDNA. 24 hours after transfection, cells show Drp1-induced fragmentation and GFP-Bax clusters (green) surrounding mitochondria (red).

Bax has been shown to promote both mitochondrial fusion (Conradt 2006) and to participate in fragmentation events (Desagher and Martinou 2000). Drp1, which promotes fission, can enhance Bax activation and cytochrome *c* release (Figure IV- 26) (Eskes, Antonsson et al. 1998). Additionally, the pro-fusion protein, Mfn2, was shown to block Bax activity (Karbowski, Arnoult et al. 2004). We therefore measured Bax activity in response to drug treatments.

We established MCF-7 cells stably expressing GFP-Bax and incubated for 6 hours with the described compounds (Figure IV- 5 and IV- 27A). Under control conditions (Figure IV- 27A, FM and SBB), GFP-Bax was homogeneously distributed within the cytosol, with low basal activation (5% shown in

Figure IV- 27B). In response to apoptotic stimuli, GFP-Bax became punctuated and clustered at the mitochondria (e.g., Figure IV- 27A, e.g. Camptothecin). The intracellular GFP-Bax distribution was used to quantify Bax activation. Following 6 hours incubation with the respective drugs, maximum Z-projection images were analyzed and cells were classified as exhibiting either diffuse cytosolic (inactive) or punctuate mitochondrial (active) GFP-Bax fluorescence (Figure IV- 27B).

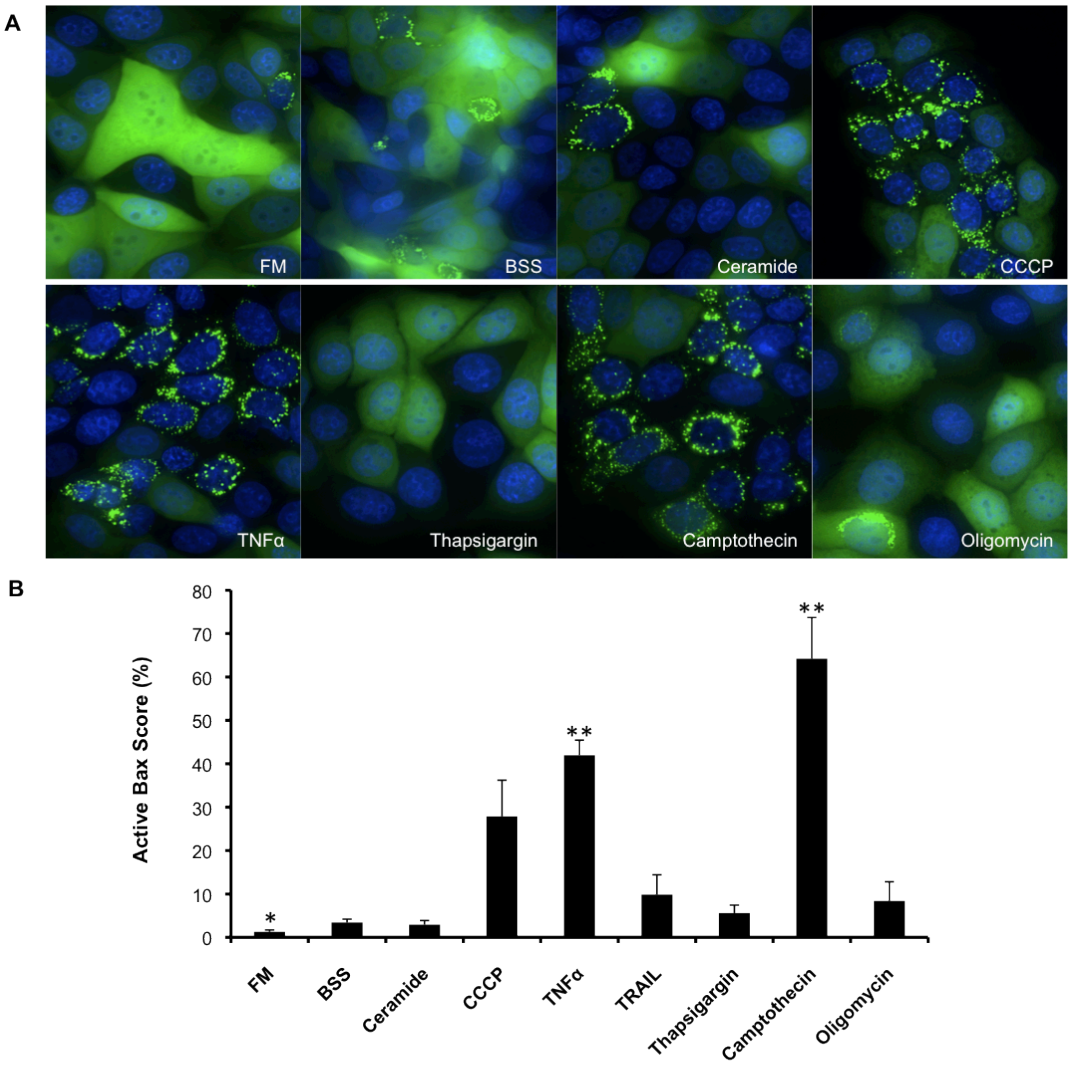

Figure IV- 27. Bax clustering under apoptotic stress. (A) Representative microscope region for each pro-apoptotic condition is shown. **(B)** Bax levels- Cells with GFP-Bax clusters were scored as "positive" for Bax activation and plotted as shown. Values are presented as mean percentage ± s.e.m. (N=5, approx. 500 cells/condition; *, $P \leq 0.05$, * *, $P \leq 0.01$, t-test). Images correspond to Z-maximal projection of individual 0.22 μm stacks and were acquired with a DVRT scope and a 40x objective.

Our results reveal that in cells treated with CCCP (20 μM), TNFα (43 ng/mL), or camptothecin (2 μM), 30% to 80% of the cells showed GFP-Bax clustering (Figure IV- 27B). Low levels of GFP-Bax clustering were observed in response to ceramide (300 μM), thapsigargin (1 μM) and oligomycin (10

μM) (Figure IV- 27B). Notably, the two DR ligands, TNFα (43 ng/mL) and TRAIL (20 ng/mL), showed marked differences in Bax activation (Figure IV- 24B). While both TNFα and TRAIL treatments resulted in a relatively small population of fragmented mitochondria (Figure IV- 20), TNFα increased the number of swollen mitochondria, while TRAIL maintained a high population of networked mitochondria (Figure IV- 20B). Moreover, although both treatments increased Bax activation, the response was about 4-fold higher with TNFα than with TRAIL (Figure IV- 27). These results showed a heterogeneous Bax response to the several treatments, including drugs with similar targets like both DR ligands.

IV-3.2.1. Cytochrome *c* release is directly correlated with Bax activation.

Several independent studies have shown that cytochrome *c* release precedes mitochondrial morphologic changes by a few minutes (Dinsdale, Zhuang et al. 1999; Gao, Pu et al. 2001; Arnoult, Rismanchi et al. 2005). We were therefore interested in monitoring cytochrome *c* under control and drug conditions. MCF-7 cells stably expressing GFP-Bax were subjected to the indicated conditions for 6 hours and immunostainned for cytochrome *c* and COXIV (protein within the mitochondrial inner membrane). High-resolution imaging shows cells where mitochondrial cytochrome *c* is retained within the mitochondria (intermembrane space) (Figure IV- 28, FM and BSS). In opposition to control conditions, drug treatment resulted in cytochrome *c* release, showed by a diffused cytoplasmatic signal (yellow) that does not colocalize with mitochondrial signal (red) (Figure IV- 28, apoptotic drugs). Our results showed that, without exception, expression of active GFP-Bax (clusters) resulted in cytochrome *c* release (Figure IV- 28). This result is in accordance with previous reports of Bax acting as an indicator of the cell's commitment to apoptosis, (Wolter, Hsu et al. 1997; Jürgensmeier, Xie et al. 1998; Shimizu and Tsujimoto 1999; Wang 2001; Adachi, Higuchi et al. 2004). Therefore, cytochrome *c* release analysis was not included in our modeling approach as the results are overlapping and thus redundant with the quantification of Bax activity. Ultimately, our aim was to integrate all these heterogeneous datasets (´Bax´, ´$\Delta\Psi_m$`, ´Morphology´) and infer possible hierarchical relationships among them.

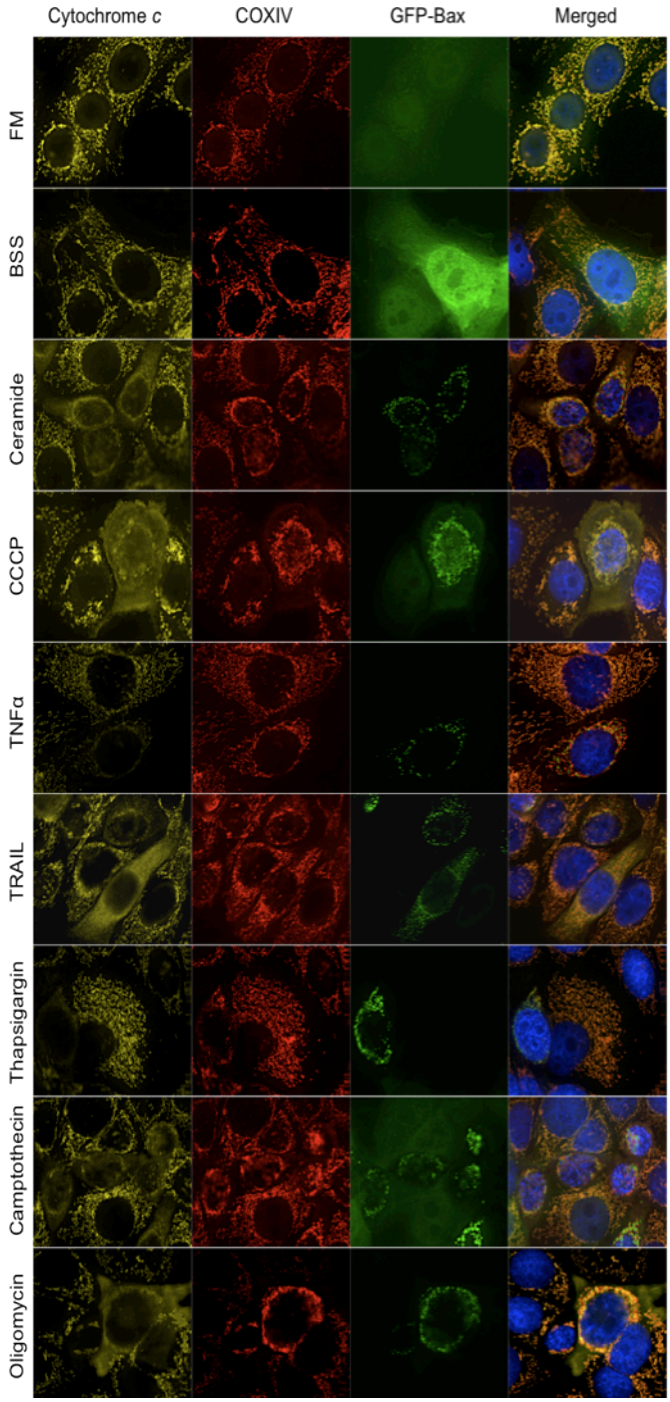

Figure IV- 28. Drug-induced cytochrome *c* release. Representative MCF-7 cells stably expressing GFP-Bax and immunostained for cytochrome *c* and COXIV (mitochondria) following 6 hours subjection to control (FM, BSS) or drug conditions. Nuclei were detected using Hoechst (100 ng/mL). Images were acquired with a DVRT microscope and a 63x objective (approx. 60 cells per condition were imaged).

IV-4. FL modeling of mitochondrial morphology and cell death datasets.

In this study, multivariate, heterogeneous datasets were produced concerning mitochondrial morphology and apoptotic steps. Our goal was to detect and quantify changes in mitochondrial morphology resulting from MCF-7 cells cultured in pro-apoptotic drugs and to determine whether these changes contribute to cell apoptosis/death. Upon exposure to the respective treatments, morphological and functional parameters were determined for each cell and used for quantitative comparisons of the mitochondrial network transition among treatments (Figure IV- 29).

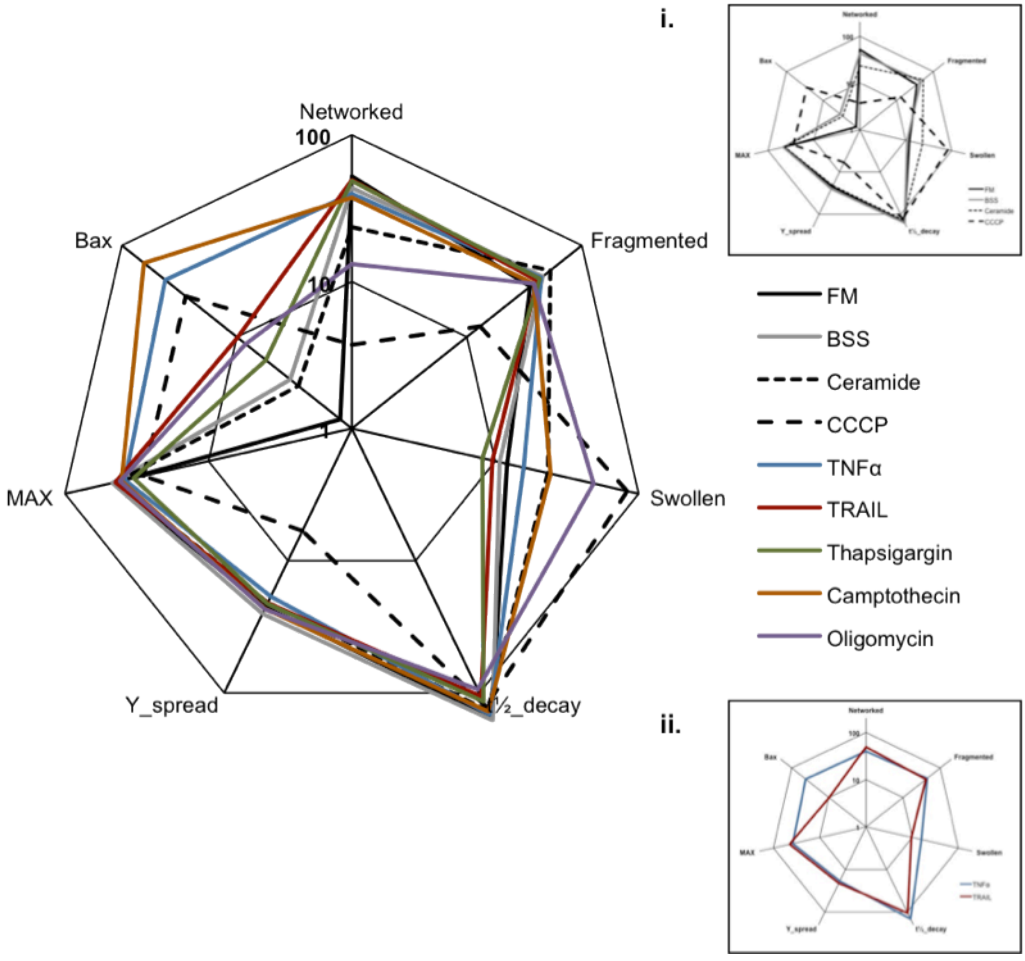

Figure IV- 29. Ensemble of parameters extracted from imaging datasets. Data concerning mitochondrial morphology classification, Bax activation scores and $\Delta\Psi_m$ derived dataset were acquired for matched apoptotic condition after 6 hour incubation at 37°C. Here we show the ensemble datasets plotted together as a radar plot. It is possible to observe how each of the acquired parameters (mitochondrial morphology classes, $\Delta\Psi_m$ subset and Bax activation) varies among all tested conditions. i) Zoomed version for the main control conditions: FM, BSS, ceramide and CCCP. ii) Zoomed version for death receptor (DR) ligands. It is possible to observe that TNFα and TRAIL caused distinct mitochondrial responses, with TNFα treatment resulting in an increased swollen mitochondria and greater Bax activation.

A first look into the global results was performed by compilation of the individual datasets into a radar plot (Figure IV- 29). Interestingly, there was no evident direct (linear) correlation between mitochondrial morphology and the early apoptotic features (Bax activation and $\Delta\Psi_m$ loss). In fact, our results were quite divergent as drugs inducing a particular morphologic class resulted in different Bax activation or depolarization rates (Figure IV- 29).

For example, under CCCP incubation, Bax activation can be associated with swollen mitochondria and with very low $\Delta\Psi_m$. However, this is not true for all swollen-related drugs. Namely, oligomycin results in 49% `Swollen´ class and only 9% cells show active Bax (Figure IV- 20 and 24). In addition, concerning the $\Delta\Psi_m$ response, thapsigargin clustered together with CCCP (Figure IV- 24B), although presenting a dissimilar mitochondrial morphologic distribution (Figure IV- 20). Likewise, conditions that induced mitochondrial fragmentation (e.g. ceramide, TNFα; Figure IV- 20) led to extremely different degrees of Bax activation (ceramide=2.92%; TNFα=41.95%; Figure IV- 27). This suggests that, in some cases, Bax activation is downstream of mitochondrial fragmentation. Finally, the conditions that less affected mitochondrial networked-state (FM, BSS, TRAIL and thapsigargin) lead to similar (low) levels of Bax activation, with exception of TRAIL that resulted in 10% increase of Bax activation (Figure IV- 27).

In summary, the results plotted in Figure IV- 29 suggest more complex, non-linear interactions between mitochondrial morphology and early apoptotic events. Therefore, we performed computational modeling to suggest cause-and-effect relationships between morphological and functional features of mitochondria in response to cell death activation.

IV-4.1. FL modeling confirms non-linear interactions between parameters.

Primary and secondary metrics contain biologically relevant information, yet are not possible to incorporate using mechanistic modeling frameworks such as ordinary differential equations (ODE), due to lack of knowledge of the underlying interactions at the molecular level. FL is a rule-based approximate artificial reasoning method suitable for investigating signal transduction pathways (Bosl 2007). FL-based approaches allow for the integration of prior knowledge and experimental data enabling high interpretability (Aldridge, Burke et al. 2006; Aldridge, Saez-Rodriguez et al. 2009).

The primary analysis of our results showed no linear relationship between the different datasets (Figure IV- 29). Thus, FL modeling was used to investigate non-linear relationships within datasets through an exhaustive search approach, and learning algorithms were used to fit the model to our data

Our FL approach allowed us to combine the divergent datasets and to uncover non-linear relations between the relevant players.

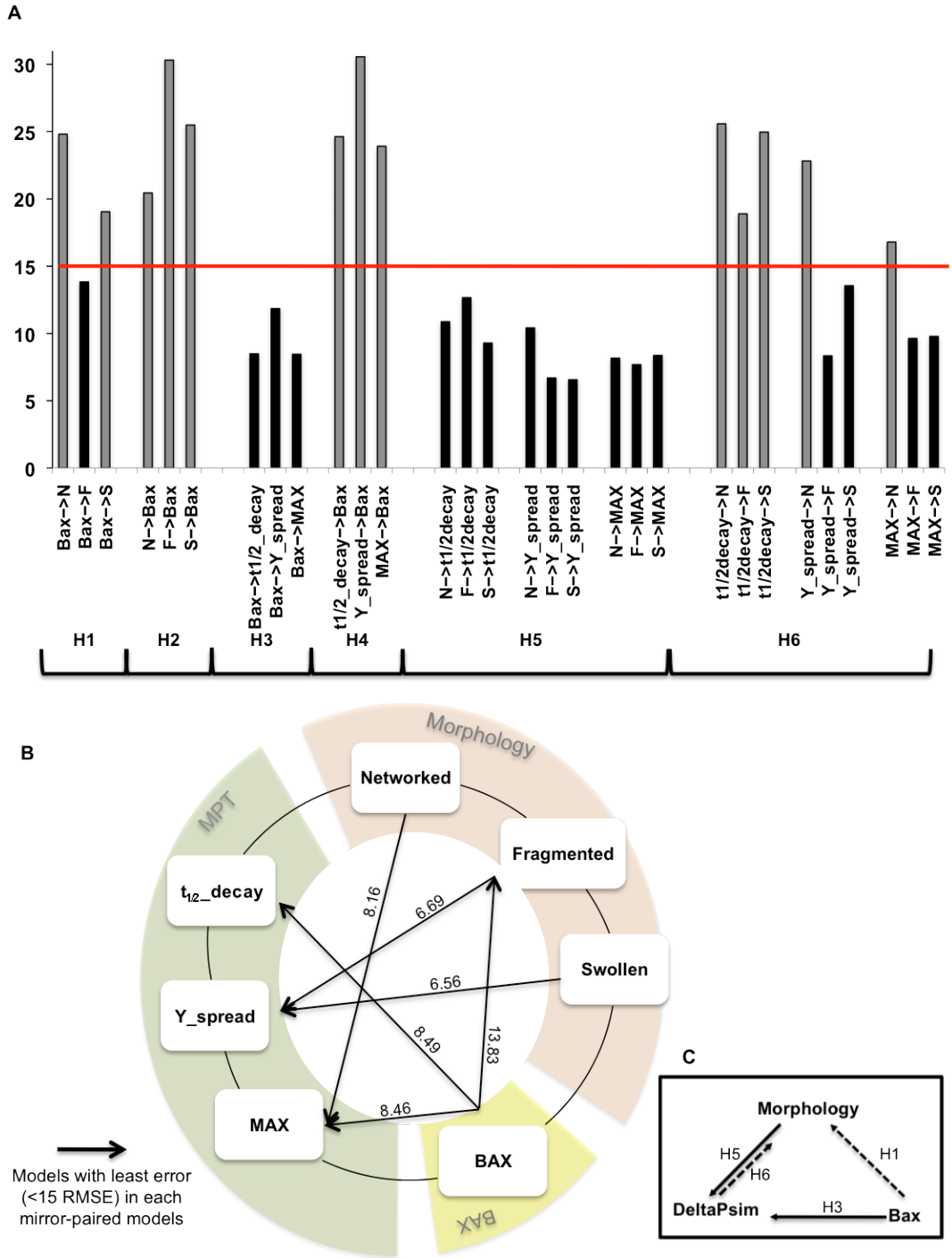

Figure IV- 30. Fuzzy logic predictions. After assembly, all Single Input-Single Output (SISO) models were trained with the data for the corresponding interaction. Model accuracy was measured upon calculation of root mean squared error (RMSE). **(A)** Root mean square error (RMSE) of all 30 models. Here are plotted the RMSE for all possible hypothesis (H): H1. "mitochondrial morphology classes (N/F/S) cause Bax"; H2. "Bax is

responsible for morphology classes"; H3. "Bax causes each of mitochondrial membrane potential ($\Delta\Psi_m$) subset"; H4. "$\Delta\Psi_m$ subset induces Bax"; H5. "Mitochondrial morphology induces $\Delta\Psi_m$ subset"; H6. "Each of the $\Delta\Psi_m$ subset is responsible for the morphologic classes". First selection was made by discarding all models with a RMSE>15 (threshold in red). Secondly, the least errors between "mirror-models" were chosen (black bars). For clarity, H1-model is the "mirror-model" of the H2-model as H3-model is the opposite of H4-model and as H5-model is for H6-model. **(B)** Detailed causality predictions between datasets- Scheme representing the final 6 most relevant predictions out of the 30 models. To assign these directional arrows, associated RMSE errors of the individual "mirror-models" were compared, e.g. H1-RMSE against H2-RMSE. Arrow direction was chosen based on the smaller error between "mirror-models" per dataset: `Morphology´, `Bax´ and `$\Delta\Psi_m$´. The numeric values associated with the arrows correspond to the actual RMSE value resultant for the directional model prediction. **(C)** Simplified scheme summarizing main interactions and causality suggested by our modeling results. Arrow line strength corresponds to the degree of relation, i.e., the stronger (filled) arrow represents the smaller RMSE obtained for the specific model.

Initially, we performed an exhaustive search for all possible interactions by constructing 30 single input-single output (SISO) FL models (see Figure III- 3 and IV- 30A). Each interaction represents a biologically possible cause-and-consequence relationship. In order to assemble a SISO FL model, we used two membership functions (MFs) to represent the single input in our fuzzy system, and combined them linearly upon aggregation of two rules per model (Figure III- 3). This stepwise linear combination allowed for the simulation of non-linearity. A parameter distribution mimicking the structure of a neural network (NN) enabled the use of learning algorithms (Ubeyli 2009). Importantly, this eliminated the bias inherent to manually implementing the model. As a parameter reduction strategy, input parameters for the MFs were fixed, and thereby excluded from the model training. Hence, only output MF-parameters were required to be learned. The SISO model was then fit to the data. An advantage of this method is the possibility to easily extend the approach to a multiple input-single output model (see Materials and Methods for details).

To determine directionality of all interactions (relationships between morphological and functional responses), we analyzed each model in a pair-wise manner (Figure IV- 30A). In detail, the two analogous models encoding the two potential senses are termed "mirror-models", e.g. the models which consider Bax influence on mitochondrial morphology classes were compared against the models in which mitochondrial morphology classes influence Bax activity. Model predictions were compared against the experimental data and a root mean squared error (RMSE) was calculated to reflect model deviation and likelihood. From each pair of "mirror-models", the one with a RMSE higher than 15 was excluded (red line threshold in Figure IV- 30). Thereby, we obtained a set of models with a defined directionality of input-output (Figure IV- 30B). From the remaining models those with the least error within each "mirror-model" were selected and are represented in Figure IV-30B (black arrows for the smaller RMSE). The main conclusions are summarized in Figure IV- 30C, where Bax is suggested to be upstream of mitochondrial depolarization and mitochondrial fragmentation. In turn, fragmented and swollen mitochondria strongly influence and are influenced by

$\Delta\Psi_m$ dynamics (Figure IV- 30B). Nevertheless, mitochondrial morphology implication in $\Delta\Psi_m$ showed a smaller error (RMSE approx=6.60a.u.), suggesting a stronger interaction in this direction.

Table IV- 3. Summary of model predictions. Here are stated the final most relevant modeling predictions and the literature references that validate them.

Causality	Least error parameter (RMSE)	Reported interactions
Bax→Mitochondrial Morphology	***Fragmented*** (13.83)	Active Bax redistributes to the mitochondria and stimulates Drp1-mediated fission during apoptosis, leading to fragmentation (Desagher and Martinou 2000; Frank, Gaume et al. 2001; Karbowski, Lee et al. 2002; Bossy-Wetzelz, Barsoum et al. 2003; Karbowski and Youle 2003; Arnoult 2007; Cho, Nakamura et al. 2010).
Bax→$\Delta\Psi_m$	***Max*** (8.46) $t_{1/2}$_decay (8.49)	Bax undergoes conformational changes and oligomerization resulting in loss of $\mathbf{\Delta\Psi_m}$ and subsequent MOMP (Wolter, Hsu et al. 1997; Pastorino, Chen et al. 1998; Pastorino, Tafani et al. 1999; Nechushtan, Smith et al. 2001; Wang 2001; Waterhouse, Goldstein et al. 2001; Kuwana, Mackey et al. 2002; Wasiak, Zunino et al. 2007; Kim, Tu et al. 2009).
Mitochondrial Morphology→ $\Delta\Psi_m$ (Y_spread)	***Fragmented*** (6.69) ***Swollen*** (6.56)	Inhibition of fragmentation has been shown to delay MOMP (Frank, Gaume et al. 2001; Youle 2005; Arnoult 2007). Disruption of the mitochondrial outer membrane and consequent loss of $\Delta\Psi_m$ can result from intensive swelling (Vander Heiden, Chandel et al. 1997; Petit, Goubern et al. 1998; Minamikawa, Williams et al. 1999; Scarlett, Sheard et al. 2000).

(RMSE- Root mean squared error; $\Delta\Psi m$ - mitochondrial membrane potential; MOMP- Mitochondrial outer membrane permeability)

First, Bax is actively involved in causing mitochondrial fragmentation, consistent with reports that its interaction with mitochondrial fission protein Drp1 regulates fragmented states (Table IV- 3). Secondly, our model proposes a strong connection between $\Delta\Psi_m$ and non-networked states of mitochondrial morphology, fragmentation in particular (Figure IV- 30C). Indeed, previous studies have shown that by inhibiting mitochondrial fragmentation a delay in MPT can be observed (Table IV- 3) (Chen, Chomyn et al. 2005). Finally, our model correctly predicted that Bax activation is

upstream of MPT, consistent with the previously experimentally demonstrated (Wasiak, Zunino et al. 2007). Here, the authors showed that Drp1-mediated mitochondrial fragmentation can be downstream of Bax activation, but occurs prior to $\Delta\Psi_m$ loss in HeLa cells (Table IV- 3).

Overall, our FL modeling results are in accordance with literature reports (Table IV- 3) and thus validate our approach as a suitable tool to look into mitochondrial apoptotic events. Next, we were interested in collecting additional datasets and incorporate them into our global pipeline.

IV-4.2. Addition of new apoptotic datasets.

In this work we were able to establish and validate a platform that allowed for automated segmentation and feature extraction of mitochondrial images, accurate classification of mitochondrial morphological states and a modeling approach to combine these with early cell death parameters reporting mitochondrial injury. The following aim is to acquire and add relevant datasets that might shed some light into mitochondrial morphology role in cell death. Hence, we monitored ROS production and total cell death under matched conditions.

IV-4.2.1. ROS production and total cell death.

To assess ROS production we made use of H2DCF- DA dye (10 μM). Following 6 hours incubation with respective drugs, H2DCF- DA was added and incubated for 30 minutes in 37°C prior to plate reader analysis. In Figure IV- 31A, H2DCF- DA signal readouts for each condition are plotted. Our results show that, at 6 hours incubation, ROS production is increased for TNFα and Thapsigargin when compared to BSS (Figure IV- 31A). BSS alone is responsible for ROS production, as it has been previously described for cells under starvation conditions (Scherz-Shouval and Elazar 2007; Scherz-Shouval, Shvets et al. 2007; Chen, McMillan-Ward et al. 2008; Chen, Azad et al. 2009). This suggests that for the tested drugs, it is premature to monitor ROS levels at 6 hours. After 24 hours treatment, all conditions caused an increase of absolute ROS levels (data not shown). However, BSS showed the highest levels of ROS production (24 hours; Figure IV- 3A). This might be explained by the fact that cells remain viable under starvation conditions (Scherz-Shouval and Elazar 2007), whereas ROS production in drug-treated cells that dye and detach can not be accounted for. Similarly, ROS increase under FM (24 hours) can be due to the continuous growth of cells in the presence of serum, which induces cellular stress (over confluency).

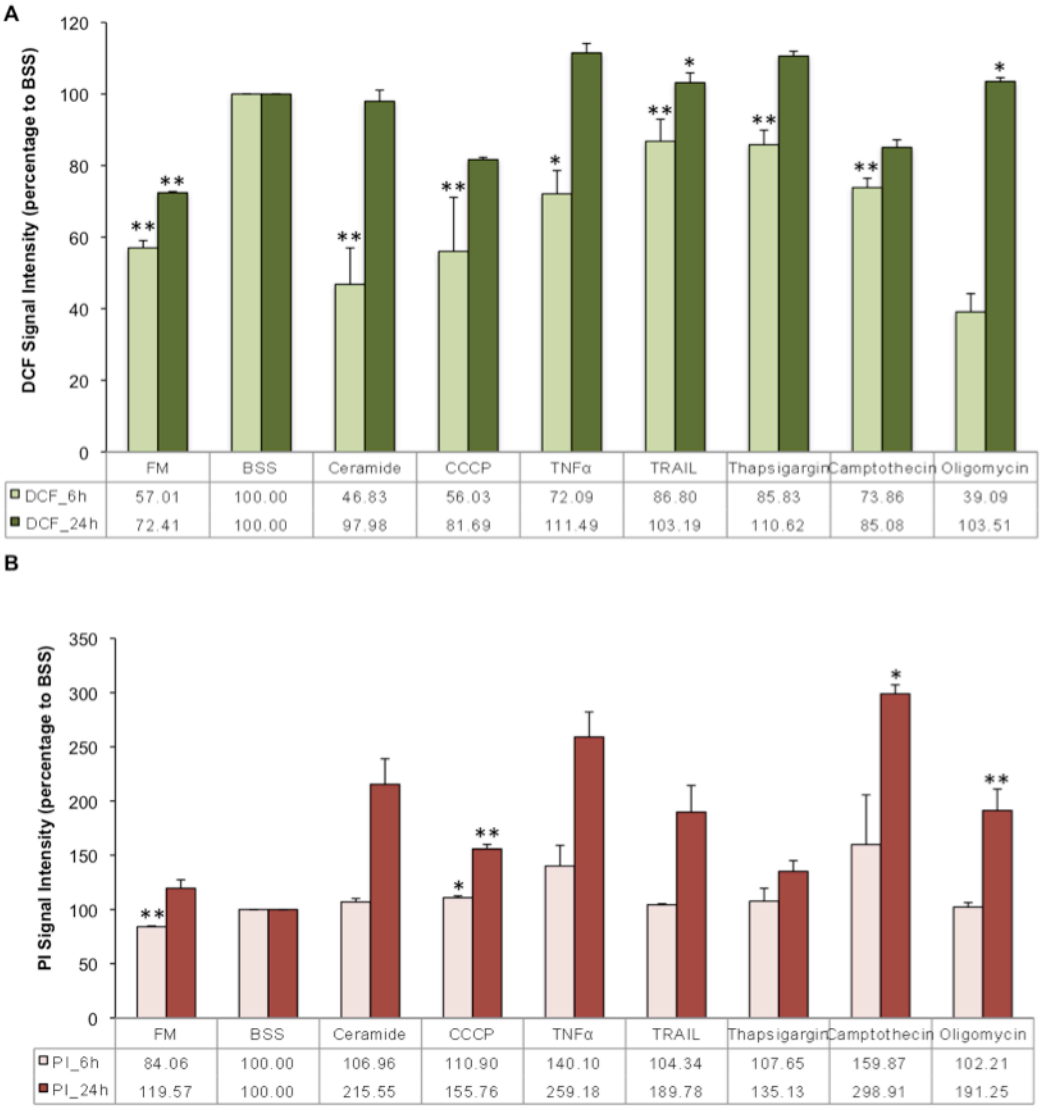

Figure IV- 31. Cell death datasets. (A) ROS production. MCF-7 wt cells were incubated with respective drugs for 6 hours and 24 hours. ROS signal was detected by plate reader measurements of H_2DCF- DA dye signal. **(B)** Cell death was quantified for each condition after 6 hours and 24 hours incubation with respective drugs at 37°C. Dead cells were stained with propidium iodide (PI, 1.0 ug/ml) and signal intensity obtained by plate reader measurements. Results (A and B) are shown normalized to control in percentage ± s.e.m (BSS, 100%). (N=4).

Additionally, we quantified cell death following 6 hours treatments and observed that cell death was minimal under most conditions (Figure IV- 31B). At this timepoint (6 hours), only camptothecin caused significant cell death, which was in accordance to the high levels of Bax activation (Figure IV- 27B and 31B). For most conditions, cell death was only evident at the later timepoint (24 hours; Figure IV- 31B). These results suggest that a 6 hour-timepoint is too early to evaluate events

downstream of mitochondrial-PCD, although remaining a relevant timepoint to analyze early mitochondrial dysfunctional responses.

Next, the newly acquired datasets were integrated into our FL modeling approach in order to infer relationships between mitochondrial morphology and cell death parameters. In this work, FL was used in combination with NN algorithms for parameter training (Ubeyli 2009). Our pipeline first creates all possible rules, which account for any possible scenario, and then learns to which degree these rules happen in the given experimental dataset by means of the specified algorithm. This, in combination with the input-associated two standard membership functions, enables the easy addition of new datasets and direct comparison with the previous predictions (see Methods for detailed description).

We have therefore included ROS production and cell death as new parameters. Models were established to account for all possible hypothesis (`H´) concerning cause (input) and consequence (output) (Figure IV- 32):

a) 6 hours- H1: all individually measured parameters cause cell death; H2: all individually measured parameters cause ROS; H3: ROS causes each parameter (Figure IV- 32A).

b) 24 hours- H1: Cell death and ROS production are the consequences of all individual parameters measured at 6 hours (H1 and H2; Figure IV- 32B).

FL models predictions were automatically compared to the data and the resulting RMSE plotted in Figure IV- 32. Once again, a threshold of RMSE<15a.u. was chosen for initial model exclusion and from those, the most relevant (smaller RMSE value) interactions were schematized in Figure IV- 33.

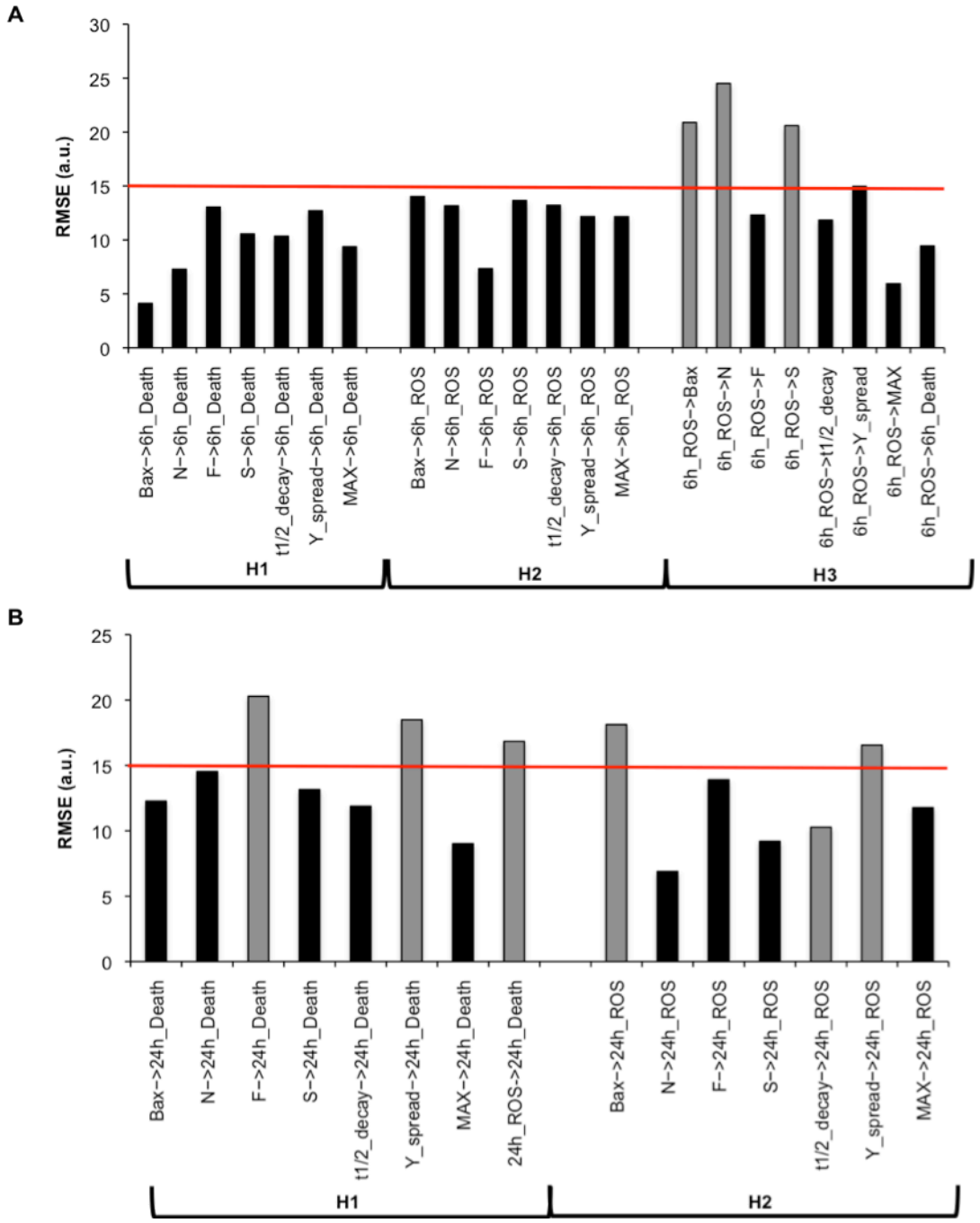

Figure IV- 32. Modeling of the new cell death datasets. Root mean square error (RMSE) of all logical models. After assembly, all Single Input-Single Output (SISO) models were trained with the data for the corresponding interaction. Model accuracy was measured upon calculation of RMSE. **(A)** Here are plotted the RMSE for all general hypotheses (H) at 6 hours: H1. "all parameters are related to cell death"; H2. "all parameters are related to ROS production"; H3. "ROS production is related to all parameters". **(B)** Shows the RMSE for all possible hypothesis (H) at 24 hours: H1. All parameters are related to late apoptotic cell death"; H2. "all parameters are related to ROS levels". First selection was made by discarding all models with a RMSE>15 (threshold in red). Secondly, the least errors between "mirror-models" were chosen (black bars).

IV-4.2.1.1. Mitochondrial fragmentation has a central role at 6 hours after apoptosis induction.

Final RMSE results show that, at 6 hours, Bax activation is strongly related to cell death levels (Bax causing cell death-RMSE=4.12a.u.) (Figure IV- 32A and 33A). In particular, CCCP, TNFα and camptothecin show the highest Bax activation within all tested drugs, as well as relatively high cell death rates at 6 hours (Figure IV- 27B and 31B). The morphology-based models suggest `Networked´ class as the mitochondrial class most closely related to cell death (Figure IV- 32A). However, this result corresponds to a negative correlation, i.e. the more steady-state networked mitochondria, the less cell death occurs. This is true for FM and ceramide (Figure IV- 20B and 31B).

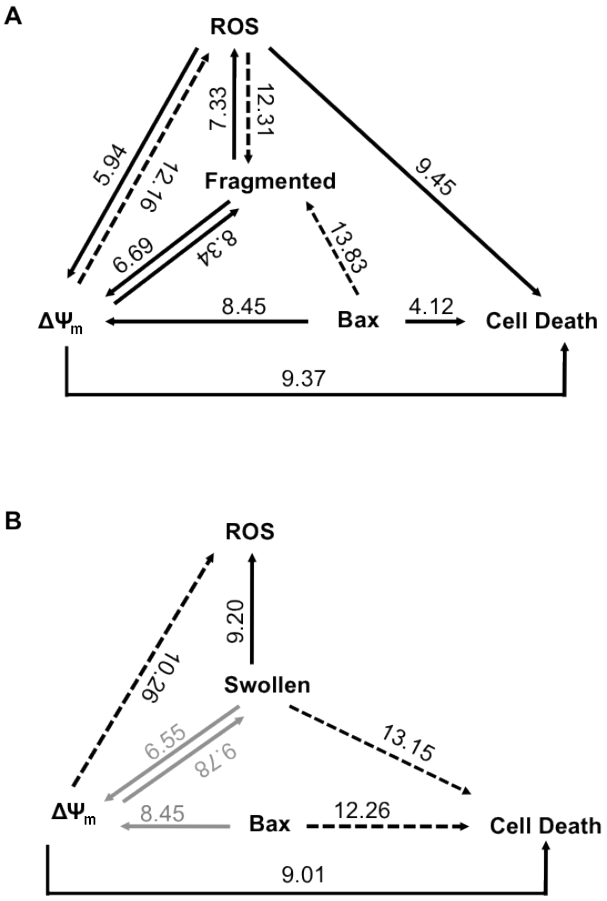

Figure IV- 33. Ensemble of fuzzy logic modeling results. (A) Main interactions and causality suggested by our modeling results for 6 hours datasets. **(B)** Main interactions and causality suggested by our modeling results for 24 hours datasets. Arrow in grey corresponds to a prediction based on 6 hours datasets. (A)(B) Arrow line strength corresponds to the degree of relation, i.e., the stronger (filled) arrow represents the smaller RMSE (numeric values are shown) obtained for the specific model.

As expected, mitochondrial depolarization events were also implicated in cell death and ROS production (Figure IV- 33A) (Bradham, Qian et al. 1998; Lee, Bender et al. 2002; Gottlieb, Armour et al. 2003; Hamacher-Brady, Stein et al. 2010). Namely, for TNFα, camptothecin and CCCP, high MAX-$\Delta\Psi_m$ initial values were inversely correlated with cell death, whereas a low MAX-$\Delta\Psi_m$ was strongly related to high ROS detection (Figure IV- 32A).

Interestingly, fragmented-mitochondria were found to have a central position in our analysis. First, as previously described (Table IV- 3), mitochondrial fragmentation was predicted to be regulated by Bax (Figure IV- 30). Secondly, fragmentation was associated with low levels of $\Delta\Psi_m$ (MAX initial value) (Figure IV- 30A and Table IV- 3). Finally, when analyzed against ROS at 6 hours, it revealed a very strong interaction with ROS production in both directions (H2 and H3 from Figure IV- 32A).

The paradox between mitochondrial morphology and ROS production has been extensively investigated in the past years ((Gottlieb 2003; Scott and Logan 2007); for review see (Alirol and Martinou 2006)). Yu and colleagues found that mitochondrial fragmentation mediated by the fission process is a necessary component for high glucose-induced respiration increase in hyperglycemic conditions (Yu, Robotham et al. 2006). In fact, inhibition of mitochondrial fission prevented periodic fluctuation of ROS production during high glucose exposure (Yu, Robotham et al. 2006). Our modeling results are therefore in accordance with reports of a strong correlation between fragmented state and ROS production (Figure IV- 33A). This is visible for ceramide BSS and TNFα treatments, which induced mitochondrial fragmentation and a parallel increase in ROS levels (Figure IV- 20 and 33A). Curiously, mitochondrial fragmented state did not show the highest correlation with total cell death (Figure IV- 32A, RMSE=13.04a.u.), suggesting that fragmentation is not directly associated with the later apoptotic outcome. Instead, from the two non-networked states, swollen-mitochondria showed the stronger connection to cell death, independently of Bax activation (Figure IV- 32A).

IV-4.2.1.2. Swollen mitochondria are strongly related to late apoptotic stages.

While networked states are associated with a protective state, swollen phenotypes have been previously linked to low $\Delta\Psi_m$ levels (Table IV- 3). Interestingly, swollen-mitochondria become the center of interactions at 24 hours, by causing ROS and consequently cell death (Figure IV- 33B). Therefore, our modeling results confirm previous reports of swollen-associated states with ROS increase (Peng and Jou 2004) and go one step further in suggesting a more direct connection with apoptotic cell death (Figure IV- 33B). In particular, swollen-mitochondria are closer related to ROS than ROS is to cell death (RMSE in Figure IV- 32B), suggesting that swelling is upstream of mitochondrial ROS production (Figure IV- 34). However, the lack of a strong correlation between ROS production and cell death might be solely due to the low ROS detection at 24 hours when

normalized against BSS (Figure IV- 31A). Furthermore, at 24 hours, Bax-deadly causality is less evident (Figure IV- 32B and 33A). This is shown by a weak relation to cell death (RMSE=12.26a.u. in Figure IV- 33B) and no direct association with ROS levels (RMSE=18.13a.u.). This result strongly suggests that at later timepoints, Bax activity is less relevant for the final outcome although remaining the main cell death effector at 6 hours (RMSE=4.12a.u.; Figure IV- 33B and 34). Future work will include active-Bax quantification at 24 hours for a more accurate and direct comparison.

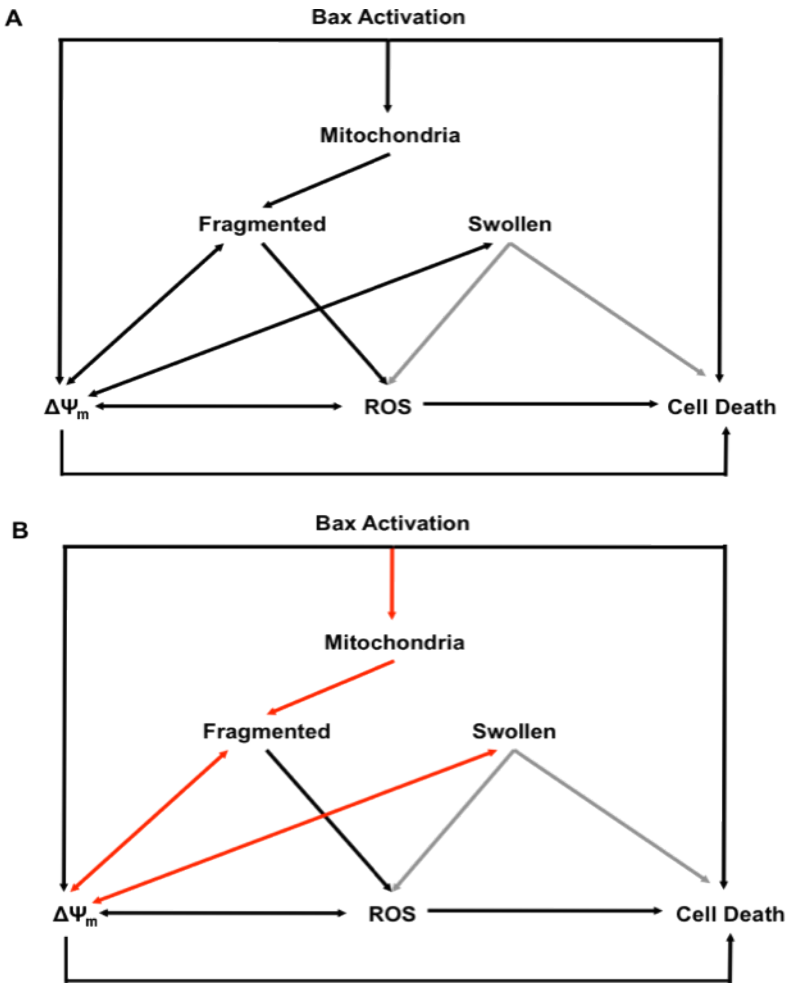

Figure IV- 34. Proposed hierarchy of events. (A) Here are shown the final most likely interactions as predicted by our FL models (lower RMSE values). The scheme represents the proposed hierarchy of events under the tested apoptotic conditions for 6 and 24 hours (black arrows) or true only after 24 hours (grey arrows). **(B)** In red is illustrated a possible sequence of events to explain swollen states association with Bax levels, leading to cell death at a later timepoint (24 hours).

IV-4.3. Modeling summary: proposed hierarchy of apoptotic events.

The final FL modeling predictions are summarized in Figure IV- 34 and are ordered by the number of downstream connections, i.e., which parameter is proposed to cause or be the consequence of more parameters. Our results confirm previous reports of Bax activation as the point-of-no-return in cell death events (Wolter, Hsu et al. 1997). As expected, early Bax activation (6 hours) is shown to affect $\Delta\Psi_m$, ROS and cell death (Figure IV- 32A). Bax clustering is concomitant with Bax translocation to the mitochondria and fragmentation induction. At 6 hours, both fragmented and swollen states strongly relate to $\Delta\Psi_m$ events, specifically, to the degree of mitochondrial membrane depolarization (Y_spread, Figure IV- 30B). Additionally, fragmented mitochondria are closely related to ROS production at 6 hours, but not at 24 hours, while swollen states are only associated with ROS at the latter stage (Figure IV- 34, grey arrow from `Swollen´ to ROS). This result suggests mitochondrial fragmentation as an early apoptotic event, while swollen-mitochondria are closely related with late apoptotic phenotypes. Surprisingly, our modeling predictions do not associate Bax activity with swollen states in contrast to our experimental results (CCCP, TNFα and camptothecin) (Figure IV- 29 and 34). Furthermore, Bax is not regulated by any of the swelling-associated interactions ($\Delta\Psi_m$ and ROS production) (Figure IV- 34A, Bax arrows are unidirectional). This raises the possibility that, under these particular stimuli, the link between Bax activity and swollen mitochondria is in fact an initial fragmented state (Figure IV- 34B). Specifically, the models suggest that Bax levels regulate fragmentation, which in turn causes $\Delta\Psi_m$ loss that will lead to mitochondrial swelling. Swelling is then associated with ROS production and cell death (Figure IV- 34B). Future work includes the incorporation of time-resolved analysis (instead of a single timepoint) and combined acquisition of datasets in one cell.

In summary, our modeling results are in accordance with previously reported observations and support the postulation that mitochondrial morphology transition is an early and specific indicator of subsequent cell death in MCF-7 cells. In addition, it suggests a new hierarchy of events where mitochondrial morphology shifts might be determinant to cell fate decisions.

V- DISCUSSION AND OUTLOOK

Mitochondria play a central role in cellular functions and are active players in disease. Namely, mitochondria are directly implicated in the pathophysiological mechanism of oxidative stress, ischemia reperfusion injury, inherited diseases, toxicological injury, and side effects of pharmacological treatments (for review see (Scatena, Bottoni et al. 2007)). Even though mitochondrial function and regulation have been extensively studied, the interplay between the different roles of mitochondria is still poorly understood. For a long time, mitochondrial dynamics were seen merely as an indicator or a consequence of several cell dysfunctions. Today, there is growing evidence that the machinery behind mitochondrial morphology and distribution can actively participate in disease and apoptotic scenarios. Remarkably, in various disease models, the artificial manipulation of fusion or fission events can partially rescue a disease phenotype (Cho, Nakamura et al. 2010; Kane and Youle 2010; Ong and Hausenloy 2010).

Here we investigated mitochondrial morphologic changes in MCF-7 cells subjected to several apoptotic stimuli. Our aim was to classify and quantify mitochondrial-network shifts after different drug treatments and relate it to the mitochondrial death pathway.

Our results revealed that multivariate stimuli led to subtle but distinct mitochondrial population-based modifications. Remarkably, these results showed no linear correlation with the measured apoptotic features. Instead, mitochondrial morphology function in cell death seems to be more complex than expected and specific to a particular insult.

In order to uncover possible non-linear relationships between the different players, we established a modeling approach based on our experimental datasets. These included quantification of mitochondrial morphology classes, Bax activation, induction of $\Delta\Psi_m$ loss, ROS production and cell death levels under matched conditions. Our rule-based model predictions are in accordance with published reports and suggest a new hierarchy of events where the balance between fragmented and swollen mitochondria might influence cell-death decisions. Finally, our global approach hereby tested and validated for MCF-7 cells, can be extended to incorporate new datasets and applied to further study mitochondrial morphology in health and injury.

V-1. Mitochondrial morphologic analysis requires sophisticated methods.

High-resolution imaging is uniquely suited for addressing complex events within single cells. As signaling events do not function in a synchronized binary manner, it was necessary to measure changes at the population level. Therefore, we have developed a quantitative and straightforward mitochondrial morphology classification platform that can be applied to investigate mechanistic and regulatory aspects of mitochondria dynamics. Our approach comprehends three main blocks:

1. High-content and high-resolution image acquisition that includes a deconvolution step (Figure IV- 3, 8 and 9);

2. A protocol for automated mitochondrial segmentation and rich feature extraction (Figure IV- 10; see Methods section);

3. The use of a Random Forest (RF) algorithm to classify mitochondria into `Networked´, `Fragmented´ or `Swollen´ (N/F/S) (Figure IV- 11).

In detail, our RF classifier attributed a degree of belonging to each class per cell and these values were averaged per condition. Following training and validation (>90% accuracy; Figure IV- 14) our classifier was not only able to reflect intercellular variability, but could also assess intracellular heterogeneity (Figure IV- 18 and 20; Table IV- 2).

Previously, researchers have focused only on two morphologic phenotypes: fragmented versus tubular and classifications were mostly applied on yeast models. Here we report three main classes: ´Networked´, ´Fragmented´ and ´Swollen´ that have we have observed during apoptotic responses. Network-like mitochondria are linked to a non-stressed state, including reduced cytochrome *c* release and inhibition of pro-apoptotic Bax. The fragmented state is associated with mitochondrial outer membrane disruption, Bax activation, cytochrome *c* release, and ROS production (for review see (Arnoult 2007)). The swollen state is associated with bioenergetic collapse, outer membrane rupture resulting from inner membrane matrix swelling (Minamikawa, Williams et al. 1999). The differences in mitochondrial size and their dynamic distribution, call for a suitable identification and classification of mitochondrial morphology.

V-1.1. Conclusions.

Simple visual inspection and manual classification have obvious disadvantages when compared to automated image analysis and a non-biased classifier algorithm. Specifically, our approach is less tedious, more objective and quantitative. Although the experimental set up can be time-consuming, the analysis of large datasets is much faster.

V-2. Bioenergetic and apoptotic events result in diverse mitochondrial morphology.

The heterogeneous response of mitochondria to stress allowed for identification of three distinct mitochondrial morphologies and classification of phenotypic responses based on redistributions of sub-populations. It was critical to include the "swollen" phenotype (Scorrano, Ashiya et al. 2002) in our analysis, as it greatly enhanced functional information content, serving as an indicator for bioenergetic dysfunction. Bioenergetic collapse was induced with CCCP, which is presumed to cause mitochondrial swelling by osmotic disruption and water influx (Ganote and Armstrong 2003). Similarly, inhibition of F1F0-ATPase with oligomycin enhanced the swollen sub-population (Figure IV- 20). Indeed, swollen sub-populations revealed the greater variation in response to our drug collection, indicating that, in a classically used classification limited to two phenotypes (networked and fragmented), these swollen mitochondria would be misclassified as fragmented. It is notable that both thapsigargin and CCCP induced a potent physiological impact (Figure IV- 24), which was not equally reflected by their resultant morphological changes. In contrast to CCCP, thapsigargin treated cells-mitochondria showed some fragmentation but remained greatly networked (Figure IV- 20B). Interestingly, cells incubated with ceramide showed highly fragmented mitochondria when analyzed in a single-cell basis (Figure IV- 11, 13 and 18) as previously described (Parra, Eisner et al. 2008). However, population-based analysis revealed co-existence of swollen and networked population (approx. 22%; Figure IV- 20B). This fact enhances the need for a single-mitochondrion classification that is able to distinguish intermediate mitochondrial states within a single cell, otherwise misclassified by the human eye. Additionally, it further supports the establishment of a population-based analysis instead of single-cell observations. Interestingly, fragmentation was not the most prominent phenotype, even under conditions where Bax activation was considerably high (e.g. TNFα, camptothecin, CCCP). Apoptotic drugs had the strongest impact on the swollen phenotype, suggesting its association with apoptosis (Bax activation, ROS production and cell death quantification) rather

than the fragmented state. This observation was later supported by our modeling predictions (Figure IV- 34).

V-2.1. Conclusions.

By applying our image analysis and mitochondrial classification pipeline, we were able to examine mitochondrial morphology changes under diverse apoptotic stimuli. Our results show that even under control conditions (FM, BSS), intercellular and intracellular variance are significant (Figure IV- 18 and 20; Table IV- 2) and thereby it becomes ultimately relevant to consider whole cell populations in order to better evaluate cell-to-cell heterogeneity. Instead, the manual classification of a few individual cells is prone to subjectivity and can be true for a sub-population of cells without accounting for total cell-to-cell variability (e.g. single cell analysis of ceramide). Importantly, our results demonstrate that different stress inducers, with different intracellular targets can induce distinct mitochondrial responses. Additionally, this study shows that one class alone (fragmented) is not sufficient as an indicator of mitochondrial perturbation. Our approach allows, for the first time, to quantify intermediate states of mitochondria and to classify early mitochondrial morphology events for a diversity of apoptotic drugs in an unbiased, systematic and statistically relevant manner.

V-3. Bax activation does not *necessarily* correlate with fragmentation.

To directly address the apoptotic mitochondrial state we measured Bax activation, an apoptotic point-of-no-return step that occurs as a single event in mitochondrial PCD (Wolter, Hsu et al. 1997). GFP-Bax reports a binary cellular response, allowing for precise manual classification of the population response to different apoptotic stimuli. Therefore, cells with active (clustered) GFP-Bax molecules were scored as positive-Bax and cells where GFP-Bax signal was homogeneously distributed in the cell were taken as negative for Bax activation. It should be noted that GFP-Bax over-expression in stable cell lines likely sensitized cells to apoptotic stimuli, so that endogenous Bax activity at the 6 hours timepoint is likely not matched. However, such an approach offers insight into the rate at which Bax is impacted by the different conditions.

Three of the tested drugs induced significant Bax activation: CCCP, TNFα, and camptothecin (Figure IV- 27 and 29). Likewise, these were the conditions that resulted in detectable cell death at 6 hours treatment (Figure IV- 31B). Notably, there was no apparent relation between distribution of mitochondrial morphologies and levels of Bax activation (Figure IV- 29). CCCP-induced Bax activation (28%), suggests that Bax clustering is downstream of compromised mitochondrial

bioenergetics. However, it has been shown that CCCP alone is not sufficient to trigger Bax in wt MCF-7 cells (Smaili, Hsu et al. 2001), suggesting that our over-expressed GFP-Bax-MCF-7 cell line is more sensitive to bioenergetic stress. Nonetheless, oligomycin, which similarly enhanced swollen and mitochondrial sub-populations, had little impact on GFP-Bax levels (8%) (Figure IV- 29). Furthermore, activation of different DR by TNFα and TRAIL showed subtle but distinct effects. Whereas TNFα increased the incidence of swelling, TRAIL-networked mitochondria were not greatly affected. Similarly, TNFα and TRAIL acted differently on GFP-Bax activation (TNFα, 42% and TRAIL, 10%) (Figure IV- 27).

The observed lack of correlation between Bax activation and mitochondrial morphology might be due to the dual roles of swelling. On one hand, mitochondrial swelling has been associated with mitochondrial membrane permeability and cytochrome *c* release (Sauvanet, Duvezin-Caubet et al. 2010). On the other hand, swollen mitochondria have been and cytoprotection (Chang and Reynolds 2006).

V-3.1. Conclusions.

Apoptosis caused by BH3-only proteins absolutely requires Bax and Bak (Kuwana, Bouchier-Hayes et al. 2005; Lindsten and Thompson 2006) (Wei 2001) (Wei, Lindsten et al. 2000). Our results showed that, at 6 hours incubation, only a few conditions induced GFP-Bax activation and it was not directly correlated with their mitochondrial morphology class distribution. These results suggest that under certain conditions, mitochondrial network-shifts can occur prior or independently of Bax activation.

V-4. Photo-activation of mitochondrial membrane potential collapse reveals heterogeneous drug action.

The use of dyes is more challenging compared to GFP-based sensors, due to photo-toxicity and loading concerns (Bouchier-Hayes, Muñoz-Pinedo et al. 2008). We exploited the photo-toxicity effect and used it to locally induce ROS within the mitochondrial matrix. Because of the heterogeneous sensitivity of mitochondria to MPT activation, we measured multiple parameters of mitochondrial energetic response to stress. As such, single cell (and sub-cellular) MPT events were quantified and averaged over cell population. High cytosolic Ca^{2+} accumulation induces mitochondrial uncoupling and opening of the MPTP to trigger matrix swelling (O'Rourke 2007). Therefore it was not surprising that CCCP (mitochondrial uncoupler) and thapsigargin (responsible for Ca^{2+} overload) resulted in a fast mitochondrial membrane depolarization and therefore clustered together (Figure IV- 24). However, these two drugs differentially impacted mitochondrial morphology and Bax activation

(Figure IV- 29), suggesting that MOMP can occur independent of or primary to Bax activation and mitochondrial swelling as previously reported (human cardiac mitochondria (Hüser, Rechenmacher et al. 1998); rat hepatocytes (Petronilli, Miotto et al. 1999)).

In accordance with MPT association with swollen states, conditions inducing the most swollen-populations (TNFα, camptothecin and oligomycin) triggered MPT to a similarly extent (Figure IV-24). Given that the $\Delta\Psi_m$ drives mitochondrial fusion (Mattenberger, James et al. 2003; Song, Chen et al. 2007), we expected a negative correlation between initial $\Delta\Psi_m$ (MAX), time to depolarization ($t_{1/2}$_decay) and mitochondrial-networked state. However, this was true only for control conditions (FM and BSS). For instance, ceramide had little impact on $\Delta\Psi_m$ (Figure IV- 24 B), although it reduced networked mitochondria (Figure IV- 29). Similarly, we also expected negative correlations between Bax activation and networked state, yet camptothecin induced the highest Bax activation (64%) while maintaining networked-mitochondria (N±s.e.m.= (37,39±4,96)%) (Figure IV- 29).

V-4.1. Conclusions.

Based on our results, we can conclude that $\Delta\Psi_m$ sensitivity was quite distinct for the tested drugs and had no direct correlation with the respective mitochondrial morphology.

On the other hand, drugs that clustered together by causing a considerable impact on MOMP (e.g. TNFα, camptothecin and TRAIL) presented relatively high levels of Bax activation. This is in accordance with previous studies where Bax has been shown to induce $\Delta\Psi_m$ through its clustering action (Wolter, Hsu et al. 1997). Likewise, cell treated under conditions that caused only a minimal impact on $\Delta\Psi_m$ loss, showed non-active cytoplasmatic Bax (Figure IV- 29). These results confirm previous studies of Bax-associated depolarization events, but show no linear connection with the observed phenotypic response of mitochondrial morphology. In conclusion, the simple acquisition and manual analysis of mitochondrial-apoptotic events is no longer sufficient and a fitting modeling approach was proved to be necessary.

V-5. Rule-based modeling of collective dataset suggests a new hierarchy of mitochondrial apoptotic events.

Fuzzy logic (FL) modeling was used to investigate non-linear relationships within datasets through an exhaustive search approach, and learning algorithms were used to fit the model to our data.

Karbowski *et al* have shown that there is a temporal relation between Bax activation and fragmentation (Karbowski, Arnoult et al. 2004), but their results could not infer a causality relation

between these two events in apoptosis. In the same way, the order of events between MPT and Bax raises many questions and has shown to be ambiguous in certain cases (for review (Henry-Mowatt, Dive et al. 2004)). In order to unravel hidden relations and propose an order of events in mitochondrial PCD, we built singular FL models based on individual hypothesis, e.g. "Is Bax activation responsible for mitochondrial fragmentation?" or "Does fragmentation lead to Bax activation?". These models cover all possible and biological meaningful hypothesis and the plotted results reflect the hypothesis-based models with higher likelihood (smaller RMSE) (Figure IV- 30, 32 and 33).

Our predicative model suggests that first, Bax is actively involved in causing mitochondrial fragmentation, consistent with reports that its interaction with mitochondrial fission protein Drp1 regulates fragmented states (Table IV- 3). Secondly, our models suggest that mitochondrial morphologic states are tightly linked to MPT dynamics (Figure IV- 30 and 34). Specifically, our modeling results propose strong connections between $\Delta\Psi_m$ and non-networked phenotypes of mitochondrial morphology, fragmentation in particular (Figure IV- 32 and 33A) (Chen, Chomyn et al. 2005). Finally, FL results predicted that Bax activation is upstream of MPT, as previously demonstrated experimentally (Wasiak, Zunino et al. 2007). Here the authors showed that Drp1-mediated mitochondrial fragmentation can be downstream of Bax activation, but occurs prior to $\Delta\Psi_m$ loss in HeLa cells (Table IV- 3). Strikingly, the prediction scenario for 24 hours suggests that swollen-mitochondria are more closely related to later apoptotic stages than fragmented-mitochondria (Figure IV- 33). This result supports our experimental observations of a central role for swollen mitochondrial phenotypes in cell death. Specifically, it proposes a tight connection between fragmented and swollen mitochondria where fragmentation is likely to occur at early apoptotic stages and then lead to swelling, membrane permeability and cell death.

V-5.1. Conclusions.

Our rule-based exhaustive search method is able to integrate heterogeneous datasets and infer non-linear relationships among them. Furthermore, the established FL platform allows for an easy addition of new datasets (e.g. cell death) and can therefore be extended to include new phenotypic classes of mitochondrial morphology and other related measurements. Importantly, FL-derived predictions based upon these measurements are in accordance with published data, thereby suggesting the utility of our approach in future work aimed at determining the role of mitochondrial network maintenance in the regulation of apoptotic cell death.

V-6. General conclusions and perspectives.

The recent findings that a mitochondrial division inhibitor (Mdivi-1) attenuates the effect of a Parkinson disease promoter gene, that otherwise would cause mitochondrial fragmentation and neuron degeneration (Cui, Tang et al. 2010), supports the possibility that conditions favoring mitochondrial connectivity may be beneficial for cell survival. This can be true in normal growth conditions, but also when cells are challenged with apoptotic stimuli and thereby make mitochondrial morphology an important target for novel therapeutic approaches.

Overall, our results demonstrate that the integrated response of the mitochondrion to diverse stimuli is rarely, if ever, linear. Cell-to-cell heterogeneity represents a rich source of biological information, but remains relatively unexploited due to challenges in its detection and quantification. To that end, we utilized high-content biosensors and rich feature extraction to quantify subcellular mitochondrial phenotypes, identify single cell dynamics and phenotype distributions in sub-populations of cells. Our transferable platform can now be extended and further applied on mitochondrial-related studies according to researchers interests.

V-6.1. Next steps and possible applications.

V-6.1.1. Time-resolved analysis of mitochondrial morphology in apoptosis.

In order to further investigate mitochondrial morphology and relate mitochondrial states with cell death events, we are interested in extending our approach in a time-resolved manner. Thus, the next step will be to follow mitochondrial morphology from earlier to later stages instead of a single timepoint (6 hours). We have observed that networked and fragmented mitochondria can coexist in the same cell, as well as fragmented and swollen (Figure IV- 18). Nevertheless, networked mitochondria were not detected together with swollen mitochondria within one cell as reflected by the RF classifier (representative decision tree; Figure IV- 15). In the same manner, the FL modeling results suggest that, in some cases, mitochondrial fragmentation precedes or closely induces swelling by reducing $\Delta\Psi_m$ levels (Figure IV- 34B). To further validate this hypothesis, a time course of changes from networked mitochondria into fragmented or swollen will be monitored simultaneously with Bax activation or depolarization events. We propose that the approach we have established in our lab is the best tool to answer these questions.

V-6.1.2. Mitochondrial morphology classification in different cell lines.

In this work we tested and validated our approach in human MCF-7 cells that undergo cell death in a relatively slow progression (Jänicke, Sprengart et al. 1998). This allowed us to investigate early mitochondrial morphology states before cell bebbling and detachment (Kerr, Wyllie et al. 1972). However, future work will focus on adapting our analysis pipeline to other cell types (e.g. primary cells) and relevant human pathologies where mitochondrial homeostasis plays a central role (Zeviani and Di Donato 2004; Ong and Hausenloy 2010).

Mitochondrial population in MCF-7 cells was seen as a filamentous (networked) structure of organelles that went trough constant fission and fusion events. In order to apply the image analysis and classifier modules to a new cell line, adjustments will take place to account for structurally distinct mitochondria (Collins, Berridge et al. 2002; Kuznetsov, Usson et al. 2004; Kuznetsov, Troppmair et al. 2006). Initially, it becomes necessary to adjust our CP pipeline to recognize new phenotypes (e.g. hyperfused (Tondera, Grandemange et al. 2009)) and to enable identification (segmentation) of individual mitochondria, which vary in shape and distribution. This step implies the collection of new training and validation sets to be tested by the RF classifier.

Nevertheless, our FL modeling approach can be directly applied to datasets originated in different cell lines due to the use of NN algorithms for parameter training (see Methods for detailed description). Our method of systematically distinguishing individual mitochondrial classes has the potential to redefine previous reports concerning mitochondria in MCF-7 breast cancer cells and other models (e.g. non-cancer cell line). Ultimately, this approach can be used to unravel disease-relevant differences in mitochondrial behavior.

V-6.1.3. High-throughput analysis.

We have established control conditions (FM, ceramide and CCCP) for the three main classes observed under the selected apoptotic conditions: `Networked´, `Fragmented´ and `Swollen´. Our compound selection covered various apoptotic triggers, with distinct targets that resulted in subtle, but significant differences. Although our image-analysis is semi-automated, the image acquisition process requires manual performance and is therefore time-consuming.

To overcome this limitation, we aim to establish automated-microscopy acquisition. We have started by adjusting the experimental protocol for 384 well plates and 40x objective in an automated microscope with deconvolution (Olympus IX81). We are now optimizing the image analysis process so that it can properly segment mitochondria in images with a lower resolution. As such, this approach would be useful for identifying compounds/RNAi and therefore target precise events (e.g. morphology

molecular proteins). Furthermore, our FL results would greatly improve with a larger compound library. We would be interested in comparing mitochondrial morphology changes under particular drugs (e.g. antagonistic) in order to infer specific mitochondrial mechanisms. All together, the tools established in this work will allow for a population-based, unbiased classification of a high-throughput, high-content dataset of mitochondrial-related events.

Literature References

Abou-Sleiman, P. M., M. M. K. Muqit, et al. (2006). "Expanding insights of mitochondrial dysfunction in Parkinson's disease." Nat Rev Neurosci **7**(3): 207-219.

Adachi, M., H. Higuchi, et al. (2004). "Bax interacts with the voltage-dependent anion channel and mediates ethanol-induced apoptosis in rat hepatocytes." American journal of physiology Gastrointestinal and liver physiology **287**(15044178): G695-705.

Aldridge, B. B., J. M. Burke, et al. (2006). "Physicochemical modelling of cell signalling pathways." Nature cell biology **8**(17060902): 1195-1203.

Aldridge, B. B., J. Saez-Rodriguez, et al. (2009). "Fuzzy logic analysis of kinase pathway crosstalk in TNF/EGF/insulin-induced signaling." PLoS Comput Biol **5**(4): e1000340.

Alexander, C., M. Votruba, et al. (2000). "OPA1, encoding a dynamin-related GTPase, is mutated in autosomal dominant optic atrophy linked to chromosome 3q28." Nature Genetics **26**(11017080): 211-215.

Alirol, E., D. James, et al. (2006). "The Mitochondrial Fission Protein hFis1 Requires the Endoplasmic Reticulum Gateway to Induce Apoptosis." Molecular biology of the cell **17**(November 2006): 4593–4605.

Alirol, E. and J. C. Martinou (2006). "Mitochondria and cancer: is there a morphological connection?" Oncogene **25**(16892084): 4706-4716.

Almind, K., M. Manieri, et al. (2007). "Ectopic brown adipose tissue in muscle provides a mechanism for differences in risk of metabolic syndrome in mice." Proceedings of the National Academy of Sciences of the United States of America **104**(7): 2366-2371.

Altmann, K. and B. Westermann (2005). "Role of essential genes in mitochondrial morphogenesis in Saccharomyces cerevisiae." Molecular biology of the cell **16**(16135527): 5410-5417.

Amchenkova, A. A., L. E. Bakeeva, et al. (1998). "Coupling Membranes As Energy-transmitting Cables I. Filamentous Mitochondria in Fibroblasts and Mitochondrial Clusters in Cardiomyocytes." The Journal of Cell Biology **107**: 1-15.

Arnoult, D. (2007). "Mitochondrial fragmentation in apoptosis." Trends in cell biology **17**(17116393): 6-12.

Arnoult, D., N. Rismanchi, et al. (2005). "Bax/Bak-dependent release of DDP/TIMM8a promotes Drp1-mediated mitochondrial fission and mitoptosis during programmed cell death." Current biology : CB **15**(16332536): 2112-2118.

Ashkenazi, A. and V. M. Dixit (1998). "Death Receptors: Signaling and Modulation." Science (New York, NY) **281**: 1-4.

Bach, D., S. Pich, et al. (2003). "Mitofusin-2 determines mitochondrial network architecture and mitochondrial metabolism. A novel regulatory mechanism altered in obesity." THE JOURNAL OF BIoLoGiCaL CHEMISTRY **278**(12598526): 17190-17197.

Bakeeva, L., Y. Chentsov, et al. (1978). "MITOCHONDRIAL FRAMEWORK (RETICULUM MITOCHONDRIALE) IN RAT DIAPHRAGM MUSCLE." Biochimica et biophysica acta **501**: 1-21.

Bakeeva, L. E., S. Chentsov Yu, et al. (1983). "Intermitochondrial contacts in myocardiocytes." Journal of molecular and cellular cardiology **15**(6620393): 413-420.

Banks, W. (2003). "Linguistic Variables: Clear Thinking with Fuzzy Logic." 1-18.

Beal, M. F. (2005). "Mitochondria take center stage in aging and neurodegeneration." Annals of Neurology **58**(16178023): 495-505.

Benard, G., N. Bellance, et al. (2007). "Mitochondrial bioenergetics and structural network organization." Journal of Cell Science **120**(17298981): 838-848.

Benard, G. and R. Rossignol (2008). "Ultrastructure of the mitochondrion and its bearing on function and bioenergetics." Antioxidants & Redox Signaling **10**(18435594): 1313-1342.

Beraud, N., S. Pelloux, et al. (2009). "Mitochondrial dynamics in heart cells: very low amplitude high frequency fluctuations in adult cardiomyocytes and flow motion in non beating Hl-1 cells." Journal of bioenergetics and biomembranes **41**(19399598): 195-214.

Bereiter-Hahn, J. and M. Vöth (1994). "Dynamics of mitochondria in living cells: shape changes, dislocations, fusion, and fission of mitochondria." Microscopy research and technique **27**(8204911): 198-219.

Bernardi, P., V. Petronilli, et al. (2001). "A mitochondrial perspective on cell death." Trends in biochemical sciences **26**(11166569): 112-117.

Billen, L., C. Kokoski, et al. (2008). "Bcl-XL Inhibits Membrane Permeabilization by Competing with Bax." PLoS Biology **6**(6): e147.

Bosl, W. J. (2007). "Systems biology by the rules: hybrid intelligent systems for pathway modeling and discovery." BMC Syst Biol **1**: 13.

Bossy, B., A. Petrilli, et al. (2010). "S-Nitrosylation of DRP1 does not affect enzymatic activity and is not specific to Alzheimer's disease." Journal of Alzheimer's disease : JAD **20 Suppl 2**(20463395): S513-526.

Bossy-Wetzelz, E., M. J. Barsoum, et al. (2003). "Mitochondrial fission in apoptosis, neurodegeneration and aging." ELSEVIER: 1-11.

Bouchier-Hayes, L., C. Muñoz-Pinedo, et al. (2008). "Measuring apoptosis at the single cell level." Methods (San Diego, Calif) **44**(18314052): 222-228.

Bowser, D. N., T. Minamikawa, et al. (1998). "Role of mitochondria in calcium regulation of spontaneously contracting cardiac muscle cells." Biophysical Journal **75**(9746542): 2004-2014.

Bradham, C. A., T. Qian, et al. (1998). "The Mitochondrial Permeability Transition Is Required for Tumor Necrosis Factor Alpha-Mediated Apoptosis and Cytochrome c Release." MOLECULAR AND CELLULAR BIOLOGY **18**: 1-12.

Brady, N. R., S. P. Elmore, et al. (2004). "Coordinated behavior of mitochondria in both space and time: a reactive oxygen species-activated wave of mitochondrial depolarization." Biophys J **87**(3): 2022-2034.

Brady, N. R., A. Hamacher-Brady, et al. (2006). "Proapoptotic BCL-2 family members and mitochondrial dysfunction during ischemia/reperfusion injury, a study employing cardiac HL-1 cells and GFP biosensors." Biochimica et biophysica acta **1757**(16730326): 667-678.

Breiman, L. (1996). "Bagging Predictors." Technical Report N0421: 1-20.

Breiman, L. (2001). "Random Forests." Machine Learning **45**: 5-32.

Brini, M. (2003). "Ca(2+) signalling in mitochondria: mechanism and role in physiology and pathology." Cell Calcium **34**(12909084): 399-405.

Brown, G. C. (1992). "Control of respiration and ATP synthesis in mammalian mitochondria and cels." Biochem. J. **284**: 1-13.

Bulashevska, S. and R. Eils (2005). "Inferring genetic regulatory logic from expression data." Bioinformatics **21**(15784747): 2706-2713.

Bursch, W. (2001). "The autophagosomal ¬± lysosomal compartment in programmed cell death." Cell Death and Diferentiation **8**: 1-13.

Cabrera, I. P., P. Cordero, et al. (2009). "Fuzzy Logic, Soft Computing, and Applications‚ãÜ." 1-8.

Carpenter, A. E., T. R. Jones, et al. (2006). "CellProfiler: image analysis software for identifying and quantifying cell phenotypes." Genome biology **7**(17076895): R100.

Chakraborty, A., M. L. Dustin, et al. (2003). "In silico models for cellular and molecular immunology: sucesses, promises and challenges." Nature Immunology **4**: 1-4.

Chan, D. (2006). "Mitochondria: Dynamic Organelles in Disease, Aging, and Development." Cell **125**(7): 1241-1252.

Chan, D. C. (2006). "Mitochondrial fusion and fission in mammals." Annual review of cell and developmental biology **22**(16704336): 79-99.

Chang, D. T. and I. J. Reynolds (2006). "Mitochondrial trafficking and morphology in healthy and injured neurons." Progress in neurobiology **80**(17188795): 241-268.

Chen, H. (2005). "Emerging functions of mammalian mitochondrial fusion and fission." Human molecular genetics **14**(suppl_2): R283-R289.

Chen, H. and D. C. Chan (2009). "Mitochondrial dynamics--fusion, fission, movement, and mitophagy--in neurodegenerative diseases." Human molecular genetics **18**(19808793): R169-176.

Chen, H., A. Chomyn, et al. (2005). "Disruption of fusion results in mitochondrial heterogeneity and dysfunction." THE JOURNAL OF BIoLoGiCaL CHEMISTRY **280**(15899901): 26185-26192.

Chen, H., S. A. Detmer, et al. (2003). "Mitofusins Mfn1 and Mfn2 coordinately regulate mitochondrial fusion and are essential for embryonic development." The Journal of Cell Biology **160**(12527753): 189-200.

Chen, H., M. Vermulst, et al. (2010). "Mitochondrial fusion is required for mtDNA stability in skeletal muscle and tolerance of mtDNA mutations." Cell **141**(20403324): 280-289.

Chen, K. H., X. Guo, et al. (2004). "Dysregulation of HSG triggers vascular proliferative disorders." Nature cell biology **6**(15322553): 872-883.

Chen, Y., M. B. Azad, et al. (2009). "Superoxide is the major reactive oxygen species regulating autophagy." Cell Death and Differentiation **16**(19407826): 1040-1052.

Chen, Y., E. McMillan-Ward, et al. (2008). "Oxidative stress induces autophagic cell death independent of apoptosis in transformed and cancer cells." Cell Death and Differentiation **15**(17917680): 171-182.

Cheng, E. H., M. C. Wei, et al. (2001). "BCL-2, BCL-X(L) sequester BH3 domain-only molecules preventing BAX- and BAK-mediated mitochondrial apoptosis." Molecular Cell **8**(3): 705-711.

Cheung, E. C. C. (2005). "Apoptosis-Inducing Factor Is a Key Factor in Neuronal Cell Death Propagated by BAX-Dependent and BAX-Independent Mechanisms." The Journal of neuroscience : the official journal of the Society for Neuroscience **25**(6): 1324-1334.

Chinnaiyan, A. M., K. O. M. Tewari, et al. (1995). "FADD, a Novel Death Domain-Containing Protein, Interacts with the Death Domain of Fas and Initiates Apoptosis." Cell **81**: 1-8.

Cho, D.-H., T. Nakamura, et al. (2010). "Mitochondrial dynamics in cell death and neurodegeneration." Cell. Mol. Life Sci.: 1-13.

Cho, D. H., T. Nakamura, et al. (2009). "S-nitrosylation of Drp1 mediates beta-amyloid-related mitochondrial fission and neuronal injury." Science (New York, NY) **324**(19342591): 102-105.

Cho, D. H., T. Nakamura, et al. (2010). "Mitochondrial dynamics in cell death and neurodegeneration." Cellular and Molecular Life Sciences: 1-13.

Cipolat, S., O. Martins de Brito, et al. (2004). "OPA1 requires mitofusin 1 to promote mitochondrial fusion." Proceedings of the National Academy of Sciences of the United States of America **101**(15509649): 15927-15932.

Colca, J. R., W. G. McDonald, et al. (2004). "Identification of a novel mitochondrial protein ("mitoNEET") cross-linked specifically by a thiazolidinedione photoprobe." American journal of physiology Endocrinology and metabolism **286**(14570702): E252-260.

Collins, T. J., M. J. Berridge, et al. (2002). "Mitochondria are morphologically and functionally heterogeneous within cells." The EMBO Journal **21**(11927546): 1616-1627.

Collins, T. J. and M. D. Bootman (2003). "Mitochondria are morphologically heterogeneous within cells." The Journal of experimental biology **206**(12756281): 1993-2000.

Colombini, M. (1979). "A candidate for the permeability pathway of the outer mitochondrial membrane." Nature **279**(14): 1-3.

Conradt, B. (2006). "Cell biology: mitochondria shape up." Nature **443**(17035992): 646-647.

Cortassa, S., M. Aon, et al. (2004). "A mitochondrial oscillator dependent on reactive oxygen species." Biophysical Journal **87**(15345581): 2060-2073.

Cribbs, J. T. and S. Strack (2007). "Reversible phosphorylation of Drp1 by cyclic AMP-dependent protein kinase and calcineurin regulates mitochondrial fission and cell death." EMBO reports **8**(17721437): 939-944.

Crompton, M. (1999). "The mitochondrial permeability transition pore and its role in cell death." The Biochemical journal **341 (Pt 2)**(10393078): 233-249.

Cui, M., X. Tang, et al. (2010). "Perturbations in Mitochondrial Dynamics Induced by Human Mutant PINK1 Can Be Rescued by the Mitochondrial Division Inhibitor mdivi-1." JBC: 1-27.

Daido, S. (2004). "Pivotal Role of the Cell Death Factor BNIP3 in Ceramide-Induced Autophagic Cell Death in Malignant Glioma Cells." Cancer research **64**(12): 4286-4293.

Das, A. M. (1998). "Regulation of mitochondrial ATP synthase activity in human myocardium." Clinical science (London, England : 1979) **94**(9682672): 499-504.

Das, A. M. and D. J. Byrd (1996). "Regulation of the mitochondrial ATP-synthase in skeletal muscle from children--a new diagnostic tool." Journal of inherited metabolic disease **19**(8739949): 137-139.

De Brito, O. and L. Scorrano (2008). "Mitofusin 2 tethers endoplasmic reticulum to mitochondria." Nature **456**(7222): 605-610.

De Giorgi, F., L. Lartigue, et al. (2000). "Electrical coupling and plasticity of the mitochondrial network." Cell Calcium **28**(11115375): 365-370.

Delettre, C., J. M. Griffoin, et al. (2001). "Mutation spectrum and splicing variants in the OPA1 gene." Human Genetics **109**(11810270): 584-591.

Delettre, C., G. Lenaers, et al. (2000). "Nuclear gene OPA1, encoding a mitochondrial dynamin-related protein, is mutated in dominant optic atrophy." Nature Genetics **26**(11017079): 207-210.

Desagher, S. and J. C. Martinou (2000). "Mitochondria as the central control point of apoptosis." Trends in cell biology **10**(10932094): 369-377.

Detmer, S. A. and D. C. Chan (2007). "Functions and dysfunctions of mitochondrial dynamics." Nature reviews Molecular cell biology **8**(17928812): 870-879.

Dimauro, S. and G. Davidzon (2005). "Mitochondrial DNA and disease." Annals of Medicine **37**(16019721): 222-232.

Dimmer, K. S., S. Fritz, et al. (2002). "Genetic basis of mitochondrial function and morphology in Saccharomyces cerevisiae." Molecular biology of the cell **13**(11907266): 847-853.

Dinsdale, D., J. Zhuang, et al. (1999). "Redistribution of cytochrome c precedes the caspase-dependent formation of ultracondensed mitochondria, with a reduced inner membrane potential, in apoptotic monocytes." The American journal of pathology **155**(10433953): 607-618.

Duchen, M. R., A. Surin, et al. (2003). "Imaging mitochondrial function in intact cells." Methods in enzymology **361**(12624920): 353-389.

Dzeja, P. P., R. Bortolon, et al. (2002). "Energetic communication between mitochondria and nucleus directed by catalyzed phosphotransfer." Proceedings of the National Academy of Sciences of the United States of America **99**(12119406): 10156-10161.

Elmore, S. P., T. Qian, et al. (2001). "The mitochondrial permeability transition initiates autophagy in rat hepatocytes." The FASEB Journal **15**(11511528): 2286-2287.

Enriquez, J. A., J. Cabezas-Herrera, et al. (2000). "Very rare complementation between mitochondria carrying different mitochondrial DNA mutations points to intrinsic genetic autonomy of the organelles in cultured human cells." THE JOURNAL OF BIoLoGiCaL CHEMISTRY **275**(10753928): 11207-11215.

Eskes, R., B. Antonsson, et al. (1998). "Bax-induced cytochrome C release from mitochondria is independent of the permeability transition pore but highly dependent on Mg2+ ions." J Cell Biol **143**(1): 217-224.

Fontanillas, P., A. Depraz, et al. (2005). "Nonshivering thermogenesis capacity associated to mitochondrial DNA haplotypes and gender in the greater white-toothed shrew, Crocidura russula." Molecular Ecology **14**(15660955): 661-670.

Fosslien, E. (2001). "Mitochondrial medicine--molecular pathology of defective oxidative phosphorylation." Annals of clinical and laboratory science **31**(11314862): 25-67.

Frank, S., B. Gaume, et al. (2001). "The role of dynamin-related protein 1, a mediator of mitochondrial fission, in apoptosis." Developmental cell **1**(11703942): 515-525.

Frey, T. G. and C. A. Mannella (2000). "The internal structure of mitochondria." Trends in biochemical sciences **25**(10871882): 319-324.

Frey, T. G., C. W. Renken, et al. (2002). "Insight into mitochondrial structure and function from electron tomography." Biochimica et biophysica acta **1555**(12206915): 196-203.

Frieden, M., D. James, et al. (2004). "Ca(2+) homeostasis during mitochondrial fragmentation and perinuclear clustering induced by hFis1." THE JOURNAL OF BIoLoGiCaL CHEMISTRY **279**(15024001): 22704-22714.

Friedman, N. (2004). "Inferring cellular networks using probabilistic graphical models." Science (New York, NY) **303**(14764868): 799-805.

Frigault, M., J. Lacoste, et al. (2009). "Live-cell microscopy - tips and tools." Journal of cell science **122**(6): 753-767.

Ganote, C. E. and S. C. Armstrong (2003). "Effects of CCCP-induced mitochondrial uncoupling and cyclosporin A on cell volume, cell injury and preconditioning protection of isolated rabbit cardiomyocytes." J Mol Cell Cardiol **35**(7): 749-759.

Gao, W., Y. Pu, et al. (2001). "Temporal relationship between cytochrome c release and mitochondrial swelling during UV-induced apoptosis in living HeLa cells." Journal of cell science **114**(11683418): 2855-2862.

Gerlich, D., J. Beaudouin, et al. (2001). "Four-dimensional imaging and quantitative reconstruction to analyse complex spatiotemporal processes in live cells." Nature cell biology **3**(9): 852-855.

Gilkerson, R. W., D. H. Margineantu, et al. (2000). "Mitochondrial DNA depletion causes morphological changes in the mitochondrial reticulum of cultured human cells." FEBS LETTERS **474**(10828440): 1-4.

Gonzalez, R. C. and R. E. Woods (2001). "Digital Image Processing." Prentice-Hall: 1-11.

Gottlieb, E., S. M. Armour, et al. (2003). "Mitochondrial membrane potential regulates matrix configuration and cytochrome c release during apoptosis." Cell Death and Differentiation: 1-9.

Gottlieb, R. A. (2003). "Debatable contribution of mitochondrial swelling to cell swelling in ischemia." Journal of molecular and cellular cardiology **35**(12818563): 735-737.

Gray, M. W., G. Burger, et al. (2001). "The origin and early evolution of mitochondria." Genome biology: 1-5.

Green, C. John, et al. (1998). "Mitochondria and Apoptosis." Science (New York, NY) **281**(5381): 1309-1312.

Griffin, E. E. and D. C. Chan (2006). "Domain interactions within Fzo1 oligomers are essential for mitochondrial fusion." THE JOURNAL OF BIoLoGiCaL CHEMISTRY **281**(16624808): 16599-16606.

Griffin, E. E., J. Graumann, et al. (2005). "The WD40 protein Caf4p is a component of the mitochondrial fission machinery and recruits Dnm1p to mitochondria." The Journal of Cell Biology **170**(16009724): 237-248.

Gronowicz, G., H. Swift, et al. (1984). "Maturation of the Reticulocyte in vitro." J. Cell Sci **71**: 1-22.

Guo, X., K. H. Chen, et al. (2007). "Mitofusin 2 triggers vascular smooth muscle cell apoptosis via mitochondrial death pathway." Circulation Research **101**(17901359): 1113-1122.

Halestrap, A. and C. Brenner (2003). "The Adenine Nucleotide Translocase: A Central Component of the Mitochondrial Permeability Transition Pore and Key Player in Cell Death." Current Medicinal Chemistry **10**: 1-19.

Hamacher-Brady, A., N. Brady, et al. (2006). "The interplay between pro-death and pro-survival signaling pathways in myocardial ischemia/reperfusion injury: apoptosis meets autophagy." Cardiovascular Drugs and Therapy **20**(17149555): 445-462.

Hamacher-Brady, A., N. R. Brady, et al. (2007). "Response to myocardial ischemia/reperfusion injury involves Bnip3 and autophagy." Cell Death and Differentiation **14**(16645637): 146-157.

Hamacher-Brady, A., H. A. Stein, et al. (2010). "Artesunate activates mitochondrial apoptosis in breast cancer cells via iron-catalysed lysosomal reactive oxygen species production." THE JOURNAL OF BIoLoGiCaL CHEMISTRY(21149439).

Han, X. J., Y. F. Lu, et al. (2008). "CaM kinase I¬†-induced phosphorylation of Drp1 regulates mitochondrial morphology." The Journal of Cell Biology **182**(3): 573-585.

Harder, N., F. Mora-Bermudez, et al. (2009). "Automatic analysis of dividing cells in live cell movies to detect mitotic delays and correlate phenotypes in time." Genome Research **19**(11): 2113-2124.

Harder, Z., R. Zunino, et al. (2004). "Sumo1 conjugates mitochondrial substrates and participates in mitochondrial fission." Current biology : CB **14**(14972687): 340-345.

Held, M., M. H. A. Schmitz, et al. (2010). "CellCognition: time-resolved phenotype annotation in high-throughput live cell imaging." Nature Publishing Group **7**(9): 747-754.

Henry-Mowatt, J., C. Dive, et al. (2004). "Role of mitochondrial membrane permeabilization in apoptosis and cancer." Oncogene **23**(15077148): 2850-2860.

Herlan, M., F. Vogel, et al. (2003). "Processing of Mgm1 by the rhomboid-type protease Pcp1 is required for maintenance of mitochondrial morphology and of mitochondrial DNA." THE JOURNAL OF BIoLoGiCaL CHEMISTRY **278**(12707284): 27781-27788.

Hermann, G. J., J. W. Thatcher, et al. (1998). "Mitochondrial fusion in yeast requires the transmembrane GTPase Fzo1p." The Journal of Cell Biology **143**(9786948): 359-373.

Hlavacek, W. S., J. R. Faeder, et al. (2006). "Rules for modeling signal-transduction systems." Science's STKE : signal transduction knowledge environment **2006**(16849649): re6.

Hsu, Y. and R. J. Youle (1997). "Nonionic Detergents Induce Dimerization among Members of the Bcl-2 Family." THE JOURNAL OF BIoLoGiCaL CHEMISTRY **272**: 1-6.

Huang, D. C. and A. Strasser (2000). "BH3-Only proteins-essential initiators of apoptotic cell death." Cell **103**(11136969): 839-842.

Huang, H., S.-Y. Choi, et al. (2010). "A quantitative assay for mitochondrial fusion using Renilla luciferase complementation." Mitochondrion **10**(5): 559-566.

Huang, H. M., C. Fowler, et al. (2004). "Mitochondrial heterogeneity within and between different cell types." Neurochemical research **29**(15038612): 651-658.

Huang, K. and R. Murphy (2004). "Boosting accuracy of automated classification of fluorescence microscope images for location proteomics." BMC Bioinformatics **5**(15207009): 78.

Hüser, J., C. E. Rechenmacher, et al. (1998). "Imaging the Permeability Pore Transition in Single Mitochondria." Biophysical Journal **74**(4): 2129-2137.

Ishihara, N., Y. Eura, et al. (2004). "Mitofusin 1 and 2 play distinct roles in mitochondrial fusion reactions via GTPase activity." Journal of Cell Science **117**(15572413): 6535-6546.

Jahani-Asl, A., E. Cheung, et al. (2007). "Mitofusin 2 Protects Cerebellar Granule Neurons against Injury-induced Cell Death." Journal of Biological Chemistry **282**(33): 23788-23798.

Jakobs, S. (2006). "High resolution imaging of live mitochondria." Biochimica et Biophysica Acta (BBA) - Molecular Cell Research **1763**(5-6): 561-575.

James, D. I., P. A. Parone, et al. (2003). "hFis1, a novel component of the mammalian mitochondrial fission machinery." THE JOURNAL OF BIoLoGiCaL CHEMISTRY **278**(12783892): 36373-36379.

Janes, K. and M. Yaffe (2006). "Data-driven modelling of signal-transduction networks." Nature reviews Molecular cell biology **7**(17057752): 820-828.

Jänicke, R. U., M. L. Sprengart, et al. (1998). "Caspase-3 is required for DNA fragmentation and morphological changes associated with apoptosis." THE JOURNAL OF BIoLoGiCaL CHEMISTRY **273**(9545256): 9357-9360.

Jimenez, M., C. Yvon, et al. (2002). "Expression of uncoupling protein-3 in subsarcolemmal and intermyofibrillar mitochondria of various mouse muscle types and its modulation by fasting." European journal of biochemistry / FEBS **269**(12071950): 2878-2884.

Jofuku, A., N. Ishihara, et al. (2005). "Analysis of functional domains of rat mitochondrial Fis1, the mitochondrial fission-stimulating protein." Biochemical and Biophysical Research Communications **333**(15979461): 650-659.

Jones, B. and W. Fangman (1992). "Mitochondrial DNA maintenance in yeast requires a protein containing a region related to the GTP-binding domain of dynamin." Genes & development **6**(1532158): 380-389.

Jones, T. R., A. Carpenter, et al. (2009). "Scoring diverse cellular morphologies in image-based screens with iterative feedback and machine learning." Proceedings of the National Academy of Sciences of the United States of America **106**(19188593): 1826-1831.

Jouaville, L. S., P. Pinton, et al. (1999). "Regulation of mitochondrial ATP synthesis by calcium: evidence for a long-term metabolic priming." Proceedings of the National Academy of Sciences of the United States of America **96**(10570154): 13807-13812.

Joza, N., S. A. Susin, et al. (2001). "Essential role of the mitochondrial apoptosis-inducing factor in programmed cell death." Nature **410**(11279485): 549-554.

Jürgensmeier, J. M., Z. Xie, et al. (1998). "Bax directly induces release of cytochrome c from isolated mitochondria." Proceedings of the National Academy of Sciences of the United States of America **95**(9560217): 4997-5002.

Kane, L. and R. J. Youle (2010). "Mitochondrial fission and fusion and their roles in the heart." Journal of Molecular Medicine **88**(10): 971-979.

Kanzawa, T., L. Zhang, et al. (2004). "Arsenic trioxide induces autophagic cell death in malignant glioma cells by upregulation of mitochondrial cell death protein BNIP3." Oncogene **24**(6): 980-991.

Karbowski, M., D. Arnoult, et al. (2004). "Quantitation of mitochondrial dynamics by photolabeling of individual organelles shows that mitochondrial fusion is blocked during the Bax activation phase of apoptosis." The Journal of cell biology **164**(14769861): 493-499.

Karbowski, M., Y. Lee, et al. (2002). "Spatial and temporal association of Bax with mitochondrial fission sites, Drp1, and Mfn2 during apoptosis." The Journal of cell biology **159**(12499352): 931-938.

Karbowski, M., A. Neutzner, et al. (2007). "The mitochondrial E3 ubiquitin ligase MARCH5 is required for Drp1 dependent mitochondrial division." The Journal of Cell Biology **178**(17606867): 71-84.

Karbowski, M., K. L. Norris, et al. (2006). "Role of Bax and Bak in mitochondrial morphogenesis." Nature **443**(17035996): 658-662.

Karbowski, M. and R. J. Youle (2003). "Dynamics of mitochondrial morphology in healthy cells and during apoptosis." Cell Death and Differentiation **10**(12867994): 870-880.

Kennady, P. K., M. G. Ormerod, et al. (2004). "Variation of mitochondrial size during the cell cycle: A multiparameter flow cytometric and microscopic study." Cytometry **62A**(2): 97-108.

Kerr, J. F. R., A. H. Wyllie, et al. (1972). "APOPTOSIS: A Basic Biological Phenomenon with Wide-Ranging Implications in Tissue Kinetics. ." Br. J. Cancer **239**(26): 1-19.

Kieffer, L., T. Thalhammere, et al. (1992). "Isolation and Characterizationof a 40-kDa Cyclophilin-related Protein." THE JOURNAL OF BIOLOGICAL CHEMISTRY **267**(8): 1-5.

Kim, H., H. Tu, et al. (2009). "Stepwise activation of BAX and BAK by tBID, BIM, and PUMA initiates mitochondrial apoptosis." Molecular Cell **36**(19917256): 487-499.

Kim, I., S. Rodriguezenriquez, et al. (2007). "Selective degradation of mitochondria by mitophagy,òÜ." Archives of biochemistry and biophysics **462**(2): 245-253.

Kim, J. S., T. Qian, et al. (2003). "Mitochondrial permeability transition in the switch from necrotic to apoptotic cell death in ischemic rat hepatocytes." Gastroenterology **124**(12557154): 494-503.

Knight, M. M., S. R. Roberts, et al. (2003). "Live cell imaging using confocal microscopy induces intracellular calcium transients and cell death." American journal of physiology Cell physiology **284**(12661552): C1083-1089.

Koshiba, T., S. A. Detmer, et al. (2004). "Structural basis of mitochondrial tethering by mitofusin complexes." Science (New York, NY) **305**(15297672): 858-862.

Kristian, T., T. M. Weatherby, et al. (2002). "Heterogeneity of the calcium-induced permeability transition in isolated non-synaptic brain mitochondria." Journal of Neurochemistry **83**(12472884): 1297-1308.

Kroemer, G. and J. C. Reed (2000). "Mitochondrial control of cell death." Nature Medicine **6**(10802706): 513-519.

Kubasiak, L. A., O. M. Hernandez, et al. (2002). "Hypoxia and acidosis activate cardiac myocyte death through the Bcl-2 family protein BNIP3." Proceedings of the National Academy of Sciences of the United States of America **99**(20): 12825-12830.

Kubli, D. A., J. E. Ycaza, et al. (2007). "Bnip3 mediates mitochondrial dysfunction and cell death through Bax and Bak." The Biochemical journal **405**(17447897): 407-415.

Kuwana, T., L. Bouchier-Hayes, et al. (2005). "BH3 domains of BH3-only proteins differentially regulate Bax-mediated mitochondrial membrane permeabilization both directly and indirectly." Molecular Cell **17**(15721256): 525-535.

Kuwana, T., M. R. Mackey, et al. (2002). "Bid, Bax, and lipids cooperate to form supramolecular openings in the outer mitochondrial membrane." Cell **111**(12419244): 331-342.

Kuznetsov, A., M. Janakiraman, et al. (2004). "Regulating cell survival by controlling cellular energy production: novel functions for ancient signaling pathways?" FEBS LETTERS **577**(15527752): 1-4.

Kuznetsov, A. and R. Margreiter (2009). "Heterogeneity of Mitochondria and Mitochondrial Function within Cells as Another Level of Mitochondrial Complexity." International Journal of Molecular Sciences **10**(19468346): 1911-1929.

Kuznetsov, A., J. Smigelskaite, et al. (2008). "Survival signaling by C-RAF: mitochondrial reactive oxygen species and Ca2+ are critical targets." MOLECULAR AND CELLULAR BIOLOGY **28**(18212057): 2304-2313.

Kuznetsov, A., J. Troppmair, et al. (2006). "Mitochondrial subpopulations and heterogeneity revealed by confocal imaging: possible physiological role?" Biochimica et biophysica acta **1757**(16712778): 686-691.

Kuznetsov, A. V., O. Mayboroda, et al. (1998). "Functional imaging of mitochondria in saponin-permeabilized mice muscle fibers." The Journal of Cell Biology **140**(9490722): 1091-1099.

Kuznetsov, A. V., S. Schneeberger, et al. (2004). "Functional Heterogeneity of Mitochondria after Cardiac Cold Ischemia and Reperfusion revealed by Confocal Imaging. ." TRANSPLANTATION: 1-3.

Kuznetsov, A. V., Y. Usson, et al. (2004). "Subcellular heterogeneity of mitochondrial function and dysfunction: evidence obtained by confocal imaging." Molecular and cellular biochemistry **256-257**(14977194): 359-365.

Lamprecht, M. R., D. M. Sabatini, et al. (2007). "CellProfilerTM: free, versatile software for automated biological image analysis." BioTechniques **12**(112257): 379-382.

Lee, I., E. Bender, et al. (2002). "Control of mitochondrial membrane potential and ROS formation by reversible phosphorylation of cytochrome c oxidase." Molecular and cellular biochemistry **234-235**(12162461): 63-70.

Lee, Y., others, et al. (2004). "Roles of Mammalian Mitochondrial Fission and Fusion Mediators Fis1, Drp1, and Opa1 in Apoptosis." Moecular Biology of the Cell **15**: 5001-5011.

Legros, F., A. Lombes, et al. (2002). "Mitochondrial Fusion in Human Cells Is Efficient, Requires the Inner Membrane Potential, and Is Mediated by Mitofusins." Molecular biology of the cell: 1-12.

Lemasters, J. J. (2005). "Selective Mitochondrial Autophagy, or Mitophagy, as a Targeted Defense Against Oxidative Stress, Mitochondrial Dysfunction, and Aging." REJUVENATION RESEARCH **8**: 3.

Lesnefsky, E. J., B. Tandler, et al. (1997). "Myocardial ischemia decreases oxidative phosphorylation through cytochrome oxidase in subsarcolemmal mitochondria." The American journal of physiology **273**(9321848): H1544-1554.

Levchenko, A., J. Bruck, et al. (2000). "Scaffold proteins may biphasically affect the levels of mitogen-activated protein kinase signaling and reduce its threshold properties." Proceedings of the National Academy of Sciences of the United States of America **97**(10823939): 5818-5823.

Li, H., H. Zhu, et al. (1998). "Cleavage of BID by Caspase 8 Mediates the Mitochondrial Damage in the Fas Pathway of Apoptosis." Cell **94**: 1-11.

Liaw, A. and M. Wiener (2002). "Classification and Regression by randomForest." **2**(3): 1-5.

Lin, C. C., Y. S. Tsai, et al. (2007). "Boosting multiclass learning with repeating codes and weak detectors for protein subcellular localization." Bioinformatics **23**(17956879): 3374-3381.

Lin, Y. S., C. C. Lin, et al. (2010). "A spectral graph theoretic approach to quantification and calibration of collective morphological differences in cell images." Bioinformatics **26**(20529919): i29-37.

Lindsten, T. and C. B. Thompson (2006). "Cell death in the absence of Bax and Bak." Cell Death and Differentiation **13**(16676001): 1272-1276.

Lodish, H., A. Berk, et al. (2008). "Molecular Cell Biology." Freeman Chaps 17, 18(6th Edition).

Luo, X., I. Budihardjo, et al. (1998). "Bid, a Bcl2 interacting protein, mediates cytochrome c release from mitochondria in response to activation of cell surface death receptors." Cell **94**(9727491): 481-490.

Margineantu, D. H., W. Gregory Cox, et al. (2002). "Cell cycle dependent morphology changes and associated mitochondrial DNA redistribution in mitochondria of human cell lines." Mitochondrion **1**(16120295): 425-435.

Margolin, A., K. Wang, et al. (2006). "Reverse engineering cellular networks." Nature Protocols **1**(17406294): 662-671.

Martinou, I., S. Desagher, et al. (1999). "The release of cytochrome c from mitochondria during apoptosis of NGF-deprived sympathetic neurons is a reversible event." The Journal of Cell Biology **144**(10085288): 883-889.

Mattenberger, Y., D. I. James, et al. (2003). "Fusion of mitochondria in mammalian cells is dependent on the mitochondrial inner membrane potential and independent of microtubules or actin." FEBS LETTERS **538**: 1-7.

Mayer, B. and R. Oberbauer (2003). "Mitochondrial Regulation of Apoptosis." News Physiologic Sciences **18**: 1-6.

McBride, H. M., M. Neuspiel, et al. (2006). "Mitochondria: more than just a powerhouse." Current biology : CB **16**(16860735): R551-560.

McConnell, S. J., L. C. Stewart, et al. (1990). "Temperature-sensitive yeast mutants defective in mitochondrial inheritance." The Journal of Cell Biology **111**(2202739): 967-976.

Meeusen, S., R. DeVay, et al. (2006). "Mitochondrial inner-membrane fusion and crista maintenance requires the dynamin-related GTPase Mgm1." Cell **127**(17055438): 383-395.

Meeusen, S., J. M. McCaffery, et al. (2004). "Mitochondrial fusion intermediates revealed in vitro." Science **305**(15297626): 1747-1752.

Métivier, D., B. Dallaporta, et al. (1998). "Cytofluorometric detection of mitochondrial alterations in early CD95/Fas/APO-1-triggered apoptosis of Jurkat T lymphoma cells. Comparison of seven mitochondrion-specific fluorochromes." Immunology letters **61**(9657269): 157-163.

Minamikawa, T., D. A. Williams, et al. (1999). "Mitochondrial permeability transition and swelling can occur reversibly without inducing cell death in intact human cells." Experimental Cell Research **246**(9882512): 26-37.

Mitra, K., C. Wunder, et al. (2009). "A hyperfused mitochondrial state achieved at G1-S regulates cyclin E buildup and entry into S phase." Proceedings of the National Academy of Sciences of the United States of America **106**(19617534): 11960-11965.

Mouli, P. K., G. Twig, et al. (2009). "Frequency and selectivity of mitochondrial fusion are key to its quality maintenance function." Biophysical Journal **96**(19413957): 3509-3518.

Muchmore, S. W., M. Sattler, et al. (1996). "X-ray and NMR structure of human Bcl-XL, an inhibitor of programmed cell death." Nature **381**: 1-7.

Nakano, K. and K. H. Vousden (2001). "PUMA, a Novel Proapoptotic Gene, Is Induced by p53." Molecular Cell **7**: 1-12.

Nechushtan, A., C. L. Smith, et al. (2001). "Bax and Bak Coalesce into Novel Mitochondria-associated Clusters during Apoptosis." The Journal of Cell Biology **153**(6): 1-12.

Nedergaard, J., V. Golozoubova, et al. (2001). "UCP1: the only protein able to mediate adaptive non-shivering thermogenesis and metabolic ine¬§ciency." Biochimica et biophysica acta **1504**: 1-25.

Nedergaard, J., V. G. A. Matthias, et al. (2001). "Life without UCPI: mitochondrial, cellular and organismal characteristics of the UCPI-ablated mice." Biochemical Society Transactions **29**: 1-8.

Nelson, D. L. and M. M. Cox (2000). Lehninger Principles of Biochemistry, Third Edition, W. H. Freeman.

Neumann, B., T. Walter, et al. (2010). "Phenotypic profiling of the human genome by time-lapse microscopy reveals cell division genes." Nature **464**(7289): 721-727.

Neuspiel, M. (2005). "Activated Mitofusin 2 Signals Mitochondrial Fusion, Interferes with Bax Activation, and Reduces Susceptibility to Radical Induced Depolarization." Journal of Biological Chemistry **280**(26): 25060-25070.

Neuspiel, M., R. Zunino, et al. (2005). "Activated mitofusin 2 signals mitochondrial fusion, interferes with Bax activation, and reduces susceptibility to radical induced depolarization." The Journal of biological chemistry **280**(15878861): 25060-25070.

Newmeyer, D. D. and S. Ferguson-Miller (2003). "Mitochondria: Releasing Power for Life and Unleashing the Machineries of Death." Cell **112**: 1-10.

Nicastro, D. (2000). "Cryo-electron Tomography of Neurospora Mitochondria." Journal of Structural Biology **129**(1): 48-56.

Nicholls, D. G., and Ferguson, S. J. (2004). "Bioenergetics 3 " Biochemistry (Moscow) **69**(7): 818-819.

Novak, I. and I. Dikic (2011). "Autophagy receptors in developmental clearance of mitochondria." Autophagy **7**: 1-3.

Nunnari, J., t. Marshall, et al. (1997). "Mitochondrial Transmission during Mating in Saccharomyces cerevisiae Is Determined by Mitochondrial Fusion and Fission and the Intramitochondrial Segregation ofMitochondrial DNA." MolecularBiologyoftheCell **8**: 1-10.

O'Rourke, B. (2007). "Mitochondrial ion channels." Annual review of physiology **69**(17059356): 19-49.

Oda, E. (2000). "Noxa, a BH3-Only Member of the Bcl-2 Family and Candidate Mediator of p53-Induced Apoptosis." Science (New York, NY) **288**(5468): 1053-1058.

Olichon, A., L. Baricault, et al. (2003). "Loss of OPA1 perturbates the mitochondrial inner membrane structure and integrity, leading to cytochrome c release and apoptosis." THE JOURNAL OF BIoLoGiCaL CHEMISTRY **278**(12509422): 7743-7746.

Olichon, A., L. J. Emorine, et al. (2002). "The human dynamin-related protein OPA1 is anchored to the mitochondrial inner membrane facing the inter-membrane space." FEBS LETTERS **523**(12123827): 171-176.

Ong, S. B. and D. J. Hausenloy (2010). "Mitochondrial morphology and cardiovascular disease." Cardiovascular Research(20631158).

Ong, S. B., S. Subrayan, et al. (2010). "Inhibiting mitochondrial fission protects the heart against ischemia/reperfusion injury." Circulation **121**(20421521): 2012-2022.

Otsuga, D., B. R. Keegan, et al. (1998). "The Dynamin-related GTPase, Dnm1p, Controls Mitochondrial Morphology in Yeast." The Journal of Cell Biology **143**: 1-17.

Palmer, J. W., B. Tandler, et al. (1985). "Biochemical Differences between Subsarcolemmal and lntet-fibrillar Mitochondria from Rat Cardiac Muscle: Effects of Procedural Manipulations." ARCHIVES OF BIOCHEMISTRY AND BIOPHYSICS **236**: 1-12.

Park, M. K., M. C. Ashby, et al. (2001). "Perinuclear, perigranular and sub-plasmalemmal mitochondria have distinct functions in the regulation of cellular calcium transport." The EMBO Journal **20**(11296220): 1863-1874.

Parra, V., V. Eisner, et al. (2008). "Changes in mitochondrial dynamics during ceramide-induced cardiomyocyte early apoptosis." Cardiovascular Research **77**(18006463): 387-397.

Parra, V., V. Eisner, et al. (2008). "Changes in mitochondrial dynamics during ceramide-induced cardiomyocyte early apoptosis." Cardiovasc Res **77**(2): 387-397.

Parra, V., V. Eisner, et al. (2008). "Changes in mitochondrial dynamics during ceramide-induced cardiomyocyte early apoptosis." Cardiovascular Research **77**(18006463): 387-397.

Pastorino, J. G., S. T. Chen, et al. (1998). "The overexpression of Bax produces cell death upon induction of the mitochondrial permeability transition." THE JOURNAL OF BIoLoGiCaL CHEMISTRY **273**(9516487): 7770-7775.

Pastorino, J. G., M. Tafani, et al. (1999). "Functional consequences of the sustained or transient activation by Bax of the mitochondrial permeability transition pore." THE JOURNAL OF BIoLoGiCaL CHEMISTRY **274**(10531385): 31734-31739.

Pater, N. (2005). "Enhancing Random Forest Implementation in Weka." Machine Learning Conference Paper for ECE591Q. November 28, 2005: 1-5.

Pei, Y., D. Xing, et al. (2007). "Real-time monitoring full length bid interacting with Bax during TNF-alpha-induced apoptosis." Apoptosis **12**(17520191): 1681-1690.

Pelloux, S., J. Robillard, et al. (2006). "Non-beating HL-1 cells for confocal microscopy: application to mitochondrial functions during cardiac preconditioning." Progress in biophysics and molecular biology **90**(16140363): 270-298.

Penefsky, H. S. (1984). "Mechanism of inhibition of mitochondrial adenosine triphosphatase by dicyclohexyl carbodiimide and oligomycin:Relationship to ATP synthesis." Proc. Nati. Acad.: 1-5.

Peng, T. and M. Jou (2004). "Mitochondrial swelling and generation of reactive oxygen species induced by photoirradiation are heterogeneously distributed." Annals of the New York Academy of Sciences **1011**(15126289): 112-122.

Perez, D. and E. White (2000). "TNF-alpha signals apoptosis through a bid-dependent conformational change in Bax that is inhibited by E1B 19K." Molecular Cell **6**(10949027): 53-63.

Petit, P. X., M. Goubern, et al. (1998). "Disruption of the outer mitochondrial membrane as a result of large amplitude swelling: the impact of irreversible permeability transition." FEBS LETTERS **426**(9598989): 111-116.

Petronilli, V., G. Miotto, et al. (1999). "Transient and Long-Lasting Openings of the Mitochondrial Permeability Transition Pore Can Be Monitored Directly in Intact Cells by Changes in Mitochondrial Calcein Fluorescence." Biophysical Journal **76**(2): 725-734.

Pham, N.-A., T. Richardson, et al. (2004). "Altered Mitochondrial Structure and Motion Dynamics in Living Cells with Energy Metabolism Defects Revealed by Real Time Microscope Imaging." Microscopy and Microanalysis **10**(02): 247-260.

Pich, S., D. Bach, et al. (2005). "The Charcot-Marie-Tooth type 2A gene product, Mfn2, up-regulates fuel oxidation through expression of OXPHOS system." Human molecular genetics **14**(15829499): 1405-1415.

Pitts, K. R., Y. Yoon, et al. (1999). "The dynamin-like protein DLP1 is essential for normal distribution and morphology of the endoplasmic reticulum and mitochondria in mammalian cells." Molecular biology of the cell **10**(10588666): 4403-4417.

Polster, B. and G. Fiskum (2004). "Mitochondrial mechanisms of neural cell apoptosis." Journal of Neurochemistry **90**(6): 1281-1289.

Presley, A., K. Fuller, et al. (2003). "MitoTracker Green labeling of mitochondrial proteins and their subsequent analysis by capillary electrophoresis with laser-induced fluorescence detection." Journal of Chromatography B **793**(1): 141-150.

Price, N. D., J. Trent, et al. (2007). "Highly accurate two-gene classifier for differentiating gastrointestinal stromal tumors and leiomyosarcomas." Proceedings of the National Academy of Sciences of the United States of America **104**(17360660): 3414-3419.

Puthalakath, H., D. C. Huang, et al. (1999). "The Proapoptotic Activity of the Bcl-2 Family Member Bim Is Regulated by Interaction with the Dynein Motor Complex." Molecular Cell **3**: 1-10.

Puthalakath, H., L. A. O'Reilly, et al. (2007). "ER stress triggers apoptosis by activating BH3-only protein Bim." Cell **129**(17604722): 1337-1349.

Rizzuto, Dsandona, et al. (1990). "Nucleotide sequence ofthe cDNA encoding subunitV IIe of cytochrome c oxidase from the slime mold Dictyostelium discoideum." Nucleic Acids Research **18**(22): 1-1.

Rizzuto, Dsandona, et al. (2010). "Nucleotide sequence ofthe cDNA encoding subunitV IIe of cytochrome c oxidase from the slime mold Dictyostelium discoideum." Nucleic Acids Research **18**(22): 1-1.

Rizzuto, R. (1998). "Close Contacts with the Endoplasmic Reticulum as Determinants of Mitochondrial Ca2+ Responses." Science (New York, NY) **280**(5370): 1763-1766.

Rizzuto, R., P. Pinton, et al. (1998). "Close Contacts with the Endoplasmic Reticulum as Determinants of Mitochondrial Ca 2+ Responses." Science: 1-5.

Rodriguez-Enriquez, S., I. Kim, et al. (2006). "Tracker dyes to probe mitochondrial autophagy (mitophagy) in rat hepatocytes." Autophagy **2**(16874071): 39-46.

Romanello, V., E. Guadagnin, et al. (2010). "Mitochondrial fission and remodelling contributes to muscle atrophy." The EMBO Journal **29**(20400940): 1774-1785.

Romashko, D. N., E. Marban, et al. (1998). "Subcellular metabolic transients and mitochondrial redox waves in heart cells." Proceedings of the National Academy of Sciences of the United States of America **95**(9465065): 1618-1623.

Sachs, K., O. Perez, et al. (2005). "Causal protein-signaling networks derived from multiparameter single-cell data." Science (New York, NY) **308**(15845847): 523-529.

Said, M. R., A. V. Oppenheim, et al. (2003). "Modeling Cellular Signal Processing usin Interacting Markov Chains." IEEE: 1-4.

Saito, M., S. J. Korsmeyer, et al. (2000). "BAX-dependent transport of cytochrome c reconstituted in pure liposomes." Nature cell biology **2**(8): 553-555.

Saks, V., P. Dzeja, et al. (2006). "Cardiac system bioenergetics: metabolic basis of the Frank-Starling law." The Journal of physiology **571**(16410283): 253-273.

Saks, V. A., T. Kaambre, et al. (2001). "Intracellular energetic units in red muscle cells." The Biochemical journal **356**(11368796): 643-657.

Salvioli, S., J. Dobrucki, et al. (2000). "Mitochondrial heterogeneity during staurosporine-induced apoptosis in HL60 cells: analysis at the single cell and single organelle level." Cytometry **40**(10878561): 189-197.

Sambrook, J. and D. W. Russell (2001). "Molecular cloning: a laboratory manual."

Sandoval, H., P. Thiagarajan, et al. (2008). "Essential role for Nix in autophagic maturation of erythroid cells." Nature **454**(18454133): 232-235.

Santel, A. and M. T. Fuller (2001). "Control of mitochondrial morphology by a human mitofusin." Journal of cell science **114**(11181170): 867-874.

Saraste, M. (1999). "Oxidative phosphorylation at the fin de si√®cle." Science (New York, NY) **283**(10066163): 1488-1493.

Satoh, M., T. Hamamoto, et al. (2003). "Differential sublocalization of the dynamin-related protein OPA1 isoforms in mitochondria." Biochemical and Biophysical Research Communications **300**(12504110): 482-493.

Sattler, M., H. Liang, et al. (1997). "Structure of Bcl-xL-Bak peptide complex: recognition between regulators of apoptosis." Science (New York, NY) **275**(9020082): 983-986.

Sauvanet, C., S. Duvezin-Caubet, et al. (2010). "Energetic requirements and bioenergetic modulation of mitochondrial morphology and dynamics." Seminars in Cell and Developmental Biology: 1-8.

Scaffidi, C., S. Fulda, et al. (1998). "Two CD95 (APO-1/Fas) signaling pathways." The EMBO Journal **17**(9501089): 1675-1687.

Scarlett, J. L., P. W. Sheard, et al. (2000). "Changes in mitochondrial membrane potential during staurosporine-induced apoptosis in Jurkat cells." FEBS LETTERS **475**(10869569): 267-272.

Scatena, R., P. Bottoni, et al. (2007). "The role of mitochondria in pharmacotoxicology: a reevaluation of an old, newly emerging topic." AJP: Cell Physiology **293**(1): C12-C21.

Scherz-Shouval, R. and Z. Elazar (2007). "ROS, mitochondria and the regulation of autophagy." Trends in cell biology **17**(17804237): 422-427.

Scherz-Shouval, R., E. Shvets, et al. (2007). "Reactive oxygen species are essential for autophagy and specifically regulate the activity of Atg4." The EMBO Journal **26**(17347651): 1749-1760.

Schmitz, I., S. Kirchhoff, et al. (2000). "Regulation of death receptor-mediated apoptosis pathways." Elsevier Science **32**: 1-14.

Schweers, R. L., J. Zhang, et al. (2007). "NIX is required for programmed mitochondrial clearance during reticulocyte maturation." Proceedings of the National Academy of Sciences of the United States of America **104**(18048346): 19500-19505.

Scorrano, L., M. Ashiya, et al. (2002). "A distinct pathway remodels mitochondrial cristae and mobilizes cytochrome c during apoptosis." Developmental cell **2**(11782314): 55-67.

Scott, I. and D. C. Logan (2007). "Mitochondrial morphology transition is an early indicator of subsequent cell death in Arabidopsis." New Phytologist **0**(0): 071106233614001-???

Sesaki, H. and R. E. Jensen (1999). "Division versus Fusion: Dnm1p and Fzo1p Antagonistically Regulate Mitochondrial Shape." Journal of Cell Biology **147**(4): 1-8.

Seul, M., L. O´Gorman, et al. (2000). "Practical Algorithms for Image Analysis." Cambridge University Press: 1-22.

Sharpe, J. C., D. Arnoult, et al. (2004). "Control of mitochondrial permeability by Bcl-2 family members." Biochimica et biophysica acta **1644**(14996495): 107-113.

Sheridan, C., P. Delivani, et al. (2008). "Bax- or Bak-induced mitochondrial fission can be uncoupled from cytochrome C release." Molecular Cell **31**(18722181): 570-585.

Shi, Y. (2004). "Caspase activation, inhibition, and reactivation: a mechanistic view." Protein science : a publication of the Protein Society **13**(15273300): 1979-1987.

Shimizu, S., A. Konishi, et al. (2000). "BH4 domain of antiapoptotic Bcl-2 family members closes voltage-dependent anion channel and inhibits apoptotic mitochondrial changes and cell death." PNAS **97**(7): 1-7.

Shimizu, S. and M. N. Y. Tsujimoto (1999). "Bcl-2 family proteins regulate the release of apoptogenic cytochrome c by the mitochondrial channel VDAC." Nature **399**: 1-5.

Shimizu, T. and Y. Pommier (1997). "Camptothecin-induced apoptosis in p53-null human leukemia HL60 cells and their isolated nuclei: effects of the protease inhibitors Z-VAD-fmk and dichloroisocoumarin suggest an

involvement of both caspases and serine proteases." Leukemia : official journal of the Leukemia Society of America, Leukemia Research Fund, UK **11**(9264376): 1238-1244.

Sjoestrand, F. S. (1963). "A Comparison of Plasma Membrane, Cytomembranes, and Mitochondrial Membrane Elements with Respect to Ultrastructural Features. ." Journal of ultrastructure research **52**(14089000): 561-580.

Smaili, S., Y. Hsu, et al. (2001). "Bax translocation to mitochondria subsequent to a rapid loss of mitochondrial membrane potential." Cell Death and Differentiation **8**: 909-920.

Smirnova, E., L. Griparic, et al. (2001). "Dynamin-related protein Drp1 is required for mitochondrial division in mammalian cells." Molecular biology of the cell **12**(11514614): 2245-2256.

Song, Z., H. Chen, et al. (2007). "OPA1 processing controls mitochondrial fusion and is regulated by mRNA splicing, membrane potential, and Yme1L." The Journal of Cell Biology **178**(17709429): 749-755.

Soubannier, V. and H. M. McBride (2009). "Positioning mitochondrial plasticity within cellular signaling cascades." Biochimica et biophysica acta **1793**(18694785): 154-170.

Speakman, J. R. (2003). "Oxidative phosphorylation, mitochondrial proton cycling, free-radical production and aging." Advances in Cell Aging and Gerontology **14**: 1-34.

Sugeno, M. (1985
). "Industrial Applications of Fuzzy Control." Elsevier Science Inc(0444878297): 1-9.

Sugioka, R., S. Shimizu, et al. (2004). "Fzo1, a protein involved in mitochondrial fusion, inhibits apoptosis." THE JOURNAL OF BIoLoGiCaL CHEMISTRY **279**(15459195): 52726-52734.

Szabadkai, G., A. M. Simoni, et al. (2004). "Drp-1-dependent division of the mitochondrial network blocks intraorganellar Ca2+ waves and protects against Ca2+-mediated apoptosis." Molecular Cell **16**(15469822): 59-68.

Szeto, H. H. (2006). "Cell-permeable, mitochondrial-targeted, peptide antioxidants." The AAPS journal **8**(16796378): E277-283.

Taguchi, N., N. Ishihara, et al. (2007). "Mitotic phosphorylation of dynamin-related GTPase Drp1 participates in mitochondrial fission." The Journal of biological chemistry **282**(17301055): 11521-11529.

Tanaka, M., R. Bateman, et al. (2005). "An unbiased cell morphology-based screen for new, biologically active small molecules." PLoS Biology **3**(15799708): e128.

Tang, S., P. Le, et al. (2009). "Heterozygous mutation of Opa1 in Drosophila shortens lifespan mediated through increased reactive oxygen species production." PLoS One **4**(19221591): e4492.

Tartaglia, L. A. and D. V. Goeddel (1992). "Two TNF receptors." Trends **13**: 1-3.

Tatsuta, T. and T. Langer (2008). "Quality control of mitochondria: protection against neurodegeneration and ageing." The EMBO Journal **27**: 306-314.

Taylor, R., S. Cullen, et al. (2008). "Apoptosis: controlled demolition at the cellular level." Nature reviews Molecular cell biology **9**(18073771): 231-241.

Taylor, R. W. and D. M. Turnbull (2005). "Mitochondrial DNA mutations in human disease." Nature reviews Genetics **6**(15861210): 389-402.

Thornberry, N. A. and Y. Lazebnik (1998). "Caspases: enemies within." Science **281**(9721091): 1312-1316.

Tieu, Q., V. Okreglak, et al. (2002). "The WD repeat protein, Mdv1p, functions as a molecular adaptor by interacting with Dnm1p and Fis1p during mitochondrial fission." The Journal of Cell Biology **158**(12163467): 445-452.

Toescu, E. and A. Verkhratsky (2000). "Assessment of mitochondrial polarization status in living cells based on analysis of the spatial heterogeneity of rhodamine 123 fluorescence staining." Pflegers Archiv European Journal of Physiology **440**(6): 941-947.

Tondera, D., S. Grandemange, et al. (2009). "SLP-2 is required for stress-induced mitochondrial hyperfusion." The EMBO Journal **28**(11): 1589-1600.

Tondera, D., S. Grandemange, et al. (2009). "SLP-2 is required for stress-induced mitochondrial hyperfusion." The EMBO Journal **28**(11): 1589-1600.

Turrens, J. F. (2003). "Mitochondrial formation of reactive oxygen species." The Journal of physiology **552**(2): 335-344.

Twig, G., A. Elorza, et al. (2008). "Fission and selective fusion govern mitochondrial segregation and elimination by autophagy." The EMBO journal **27**(18200046): 433-446.

Twig, G., S. A. Graf, et al. (2006). "Tagging and tracking individual networks within a complex mitochondrial web with photoactivatable GFP." American journal of physiology Cell physiology **291**(16481372): C176-184.

Ubeyli, E. D. (2009). "Adaptive neuro-fuzzy inference system for classification of ECG signals using Lyapunov exponents." Comput Methods Programs Biomed **93**(3): 313-321.

Ubeyli, E. D. (2009). "Adaptive neuro-fuzzy inference systems for automatic detection of breast cancer." J Med Syst **33**(5): 353-358.

van der Bliek, A. M. (2000). "A mitochondrial division apparatus takes shape." The Journal of cell biology **151**(11038192): F1-4.

Vande Velde, C., J. Cizeau, et al. (2000). "BNIP3 and genetic control of necrosis-like cell death through the mitochondrial permeability transition pore." MOLECULAR AND CELLULAR BIOLOGY **20**(15): 5454-5468.

Vander Heiden, M. G., N. S. Chandel, et al. (1997). "Bcl-xL regulates the membrane potential and volume homeostasis of mitochondria." Cell **91**(9393856): 627-637.

Vendelin, M., N. Béraud, et al. (2005). "Mitochondrial regular arrangement in muscle cells: a "crystal-like" pattern." American journal of physiology Cell physiology **288**(15496480): C757-767.

Vokes, M. and A. Carpenter (2008). "Using CellProfiler for automatic identification and measurement of biological objects in images." Current protocols in molecular biology / edited by Frederick M Ausubel [et al] **Chapter 14**(18425761): Unit 14.17.

Wang, K., X. M. Yin, et al. (1996). "BID: a novel BH3 domain-only death agonist." Genes & development **10**(22): 2859-2869.

Wang, P. and S. Tan (1997). "Soft computing and fuzzy logic." Soft Computing **1**: 1-7.

Wang, W., H. Fang, et al. (2008). "Superoxide flashes in single mitochondria." Cell **134**(18662543): 279-290.

Wang, X. (2001). "The expanding role of mitochondria in apoptosis." Genes & development **15**(11711427): 2922-2933.

Wasiak, S., R. Zunino, et al. (2007). "Bax/Bak promote sumoylation of DRP1 and its stable association with mitochondria during apoptotic cell death." The Journal of Cell Biology **177**(17470634): 439-450.

Waterhouse, N. J., J. C. Goldstein, et al. (2001). "Cytochrome c Maintains Mitochondrial Transmembrane Potential and ATP Generation after Outer Mitochondrial Membrane Permeabilization during the Apoptotic Process." Journal of Cell Biology **153**(2): 1-10.

Wei, M. (2001). "Proapoptotic BAX and BAK: A Requisite Gateway to Mitochondrial Dysfunction and Death." Science (New York, NY) **292**(5517): 727-730.

Wei, M. C., T. Lindsten, et al. (2000). "tBID, a membrane-targeted death ligand, oligomerizes BAK to release cytochrome c." Genes & development **14**: 1-12.

Weng, G., U. S. Bhalla, et al. (1999). "Complexity in biological signaling systems." Science (New York, NY) **284**(10102825): 92-96.

Wiley, H. S., S. Y. Shvartsman, et al. (2003). "Computational modeling of the EGF-receptor system: a paradigm for systems biology." Trends in cell biology **13**(12480339): 43-50.

Wiley, S. E., A. N. Murphy, et al. (2007). "MitoNEET is an iron-containing outer mitochondrial membrane protein that regulates oxidative capacity." Proceedings of the National Academy of Sciences of the United States of America **104**(17376863): 5318-5323.

Wolter, K. G., Y. T. Hsu, et al. (1997). "Movement of Bax from the cytosol to mitochondria during apoptosis." The Journal of cell biology **139**(9382873): 1281-1292.

Xue, L., G. C. Fletcher, et al. (2001). "Mitochondria are selectively eliminated from eukaryotic cells after blockade of caspases during apoptosis." Current biology : CB **11**(11267874): 361-365.

Yarosh, W., J. Monserrate, et al. (2008). "The molecular mechanisms of OPA1-mediated optic atrophy in Drosophila model and prospects for antioxidant treatment." PLoS genetics **4**(18193945): e6.

Yasuda, M., P. Theodorakis, et al. (1998). "Adenovirus E1B-19K/BCL-2 interacting protein BNIP3 contains a BH3 domain and a mitochondrial targeting sequence." THE JOURNAL OF BIoLoGiCaL CHEMISTRY **273**(20): 12415-12421.

Yethon, J. (2003). "Interaction with a Membrane Surface Triggers a Reversible Conformational Change in Bax Normally Associated with Induction of Apoptosis." Journal of Biological Chemistry **278**(49): 48935-48941.

Yoon, Y., E. W. Krueger, et al. (2003). "The mitochondrial protein hFis1 regulates mitochondrial fission in mammalian cells through an interaction with the dynamin-like protein DLP1." MOLECULAR AND CELLULAR BIOLOGY **23**(12861026): 5409-5420.

Yoon, Y., K. R. Pitts, et al. (2001). "Mammalian dynamin-like protein DLP1 tubulates membranes." Molecular biology of the cell **12**(11553726): 2894-2905.

Yoon, Y., D. Yoon, et al. (2006). "Formation of elongated giant mitochondria in DFO-induced cellular senescence: involvement of enhanced fusion process through modulation of Fis1." Journal of Cellular Physiology **209**(16883569): 468-480.

Youle, R. J. (2005). "Morphology of mitochondria during apoptosis: worms-to-beetles in worms." Developmental cell **8**(15737923): 298-299.

Youle, R. J. (2007). "Cell biology. Cellular demolition and the rules of engagement." Science (New York, NY) **315**(17289967): 776-777.

Youle, R. J. and M. Karbowski (2005). "Mitochondrial fission in apoptosis." Nature reviews Molecular cell biology **6**(16025099): 657-663.

Yu, T., J. L. Robotham, et al. (2006). "Increased production of reactive oxygen species in hyperglycemic conditions requires dynamic change of mitochondrial morphology." Proceedings of the National Academy of Sciences of the United States of America **103**(16477035): 2653-2658.

Yuan, H., S. D. Williams, et al. (2003). "Cytochrome c dissociation and release from mitochondria by truncated Bid and ceramide." Mitochondrion **2**(4): 237-244.

Zadeh, L. (1965). "Fuzzy Sets." Information and Control **8**: 1-16.

Zeviani, M. and S. Di Donato (2004). "Mitochondrial disorders." Brain : a journal of neurology **127**(15358637): 2153-2172.

Zha, J., S. Weiler, et al. (2000). "Posttranslational N-myristoylation of BID as a molecular switch for targeting mitochondria and apoptosis." Science (New York, NY) **290**(5497): 1761-1765.

Zhou, W., K.-H. Chen, et al. (2010). "Mutation of the protein kinase A phosphorylation site influences the anti-proliferative activity of mitofusin 2." Atherosclerosis **211**(1): 216-223.

Zoratti, M. and I. Szabb (1995). "The mitochondrial permeability transition." Biochimica et biophysica acta **124**: 1-38.

Zorov, D. B., C. R. Filburn, et al. (2000). "Reactive oxygen species (ROS)-induced ROS release: a new phenomenon accompanying induction of the mitochondrial permeability transition in cardiac myocytes." The Journal of experimental medicine **192**(11015441): 1001-1014.

Zuechner, S., I. Mersiyanova, et al. (2004). "Mutations in the mitochondrial GTPase mitofusin 2 cause Charcot-Marie-Tooth neuropathy type 2A." Nature Genetics **36**(15064763): 449-451.

Zunino, R., A. Schauss, et al. (2007). "The SUMO protease SENP5 is required to maintain mitochondrial morphology and function." Journal of Cell Science **120**(17341580): 1178-1188.